UNIVERSITY OF OKLAHOMA

GRADUATE COLLEGE

SEISMIC AND QUASI-STATIC LATERAL LOAD BEHAVIOR OF PILE GROUPS IN IMPROVED SOFT CLAY: CENTRIFUGE AND NUMERICAL MODELING

A DISSERTATION

SUBMITTED TO THE GRADUATE FACULTY

in partial fulfillment of the requirements for the

Degree of

DOCTOR OF PHILOSOPHY

By

AMIRATA TAGHAVI
Norman, Oklahoma
2015

SEISMIC AND QUASI-STATIC LATERAL LOAD BEHAVIOR OF PILE GROUPS IN IMPROVED SOFT CLAY: CENTRIFUGE AND NUMERICAL MODELING

A DISSERTATION APPROVED FOR THE
SCHOOL OF CIVIL ENGINEERING AND ENVIRONMENTAL SCIENCE

BY

_____
Dr. Kanthasamy Muraleetharan, Chair

_____
Dr. Younane Abousleiman

_____
Dr. Amy Cerato

_____
Dr. Gerald Miller

_____
Dr. Sri Sritharan

To My Parents

Acknowledgements

I am grateful to my doctoral advisor, Professor K.K. “Muralee” Muraleetharan, for his invaluable guidance and support throughout the course of my studies and research at the University of Oklahoma (OU). He has served as a wonderful teacher and mentor to me and his continuous encouragement, trust, concern, and care, made my Ph.D. journey enjoyable and successful. His intuition, scientific curiosity, and comments during the thorough review of my work, has been truly invaluable and will guide my research in the future. It was a great pleasure for me to work with Professor Muraleetharan.

Professors Gerald A. Miller and Amy B. Cerato at the University of Oklahoma and Professor Sri Sritharan at Iowa State University have advised me on numerous occasions on the fundamentals of soil behavior, centrifuge testing, instrumentation, the design of centrifuge experiments, and understanding the test results. They have reviewed my works multiple times, and made valuable recommendations. Their technical advice and guidance helped develop my research and engineering skills. I am grateful for their advice and support throughout the years. I have always learned from Professor Younane N. Abousleiman’s lectures and talks. I greatly appreciate him for serving on my doctoral committee and letting me know his valuable comments on my research. I also gratefully acknowledge the useful suggestions and discussions during the development of the centrifuge tests by Juan Baez, Arul Arulmoli, and Steve Vukazich.

I would like to thank Allison Quiroga, Bo Zhang, and Karrthik Kirupakaran from the University of Oklahoma. The experimental program carried out in this

research could not have been executed without their able assistance. I would like to thank all the staff at the Center for Geotechnical Modeling at the University of California, Davis, especially Dan Wilson, Peter Rojas, Jenny Chen, Ray Gerhard, Lars Pedersen, Anatoliy Ganchenko, Chad Justice, and Tom Kohnke for their support and technical input during the experimental phase of this study. My special thanks go to Michael F. Schmitz, instrument shop supervisor at the Fears Structural Engineering laboratory at OU, for his help in fabricating equipment needed for the centrifuge tests.

I was extremely fortunate to have the friendship and support of Roozbeh Geraili Mikola, Peter Rojas, Gabriel Candia, Manny Hakhamaneshi, Mark Stringer, Bradley Fleming, Mani Razi, Zachary Thompson, Zachary Bright, Mohammad Darayi, Mortaza Saeidi, Hasan Manzour, and Rodney Collins during my Ph.D. study at OU and also while I was doing centrifuge tests at UC Davis. I thank them for providing such a friendly environment.

Finally, I would like to thank my family for supporting me through this period. They have sacrificed much to make sure that I follow my dreams and I owe them everything that I have ever done and will ever do. They have been a constant source of love, concern, support and strength all these years. I would like to express my heart-felt gratitude to my family.

The research reported herein is a part of the NEES-pilEs (The George E. Brown, Jr. Network for Earthquake Engineering Simulation – piles in low E soils) project to study the behavior of pile foundations in improved and unimproved soft clay using centrifuge model tests, field tests, and computational simulations. The NEES-pilEs project was supported by the National Science Foundation (NSF) under Grant No.

CMMI-0830328 and this support is gratefully acknowledged. Any opinions, findings, and conclusions or recommendations expressed in this paper are those of the author and do not necessarily reflect the views of the National Science Foundation.

Table of Contents

List of Tables

List of Figures

Abstract

In the design of pile foundations subjected to lateral loading, one of the objectives is to restrict the lateral displacements. Improving the soil surrounding the pile foundation is an innovative and cost-efficient solution to increase lateral resistance and restrict lateral displacements. This technique is, however, not widely used due to lack of fundamental understanding of the behavior of pile groups in improved weak soils. Due to the dearth of experimental data and lack of thorough understanding of their behavior, engineers are forced to design pile groups in improved soft clay in a conservative manner to mitigate the uncertainties.

To increase our understanding of the behavior of pile groups in improved and unimproved soft clays subjected to seismic and quasi-static lateral loads, two centrifuge models consisting of several pile groups were constructed and tested. The soil profile consisted of four lightly overconsolidated clay layers overlying a dense layer of sand. The pile groups had a symmetrical layout consisting of 2×2 piles spaced at 3.0 and 7.0 pile diameters (D). After improving the soft clay in situ using simulated Cement Deep Soil Mixing (CDSM), pile foundations were driven into the improved ground. Centrifuge tests revealed that CDSM is an effective method to increase the lateral resistance of pile foundations. The lateral resistance of the improved pile group at 7D spacing increased by 157%. Due to pile-soil-pile interactions, the lateral resistance in 3D pile group increased by only 112%. In both the improved and unimproved pile groups with 3D spacing, the leading row of piles carried larger loads and bending moments than the trailing row of piles. No group interaction effects were observed in all

pile groups with 7D spacing. At very large deflections (about 80 cm), cracks developed and tension failure occurred in the CDSM block of the improved 3D pile group.

The quasi-static lateral load behavior of pile groups were modeled using the concept of Beam on Nonlinear Winkler Foundation (BNWF) implemented in the Finite Difference computer codes GROUP and LPILE. Using the results of centrifuge tests, the computer codes were calibrated and analyses were performed to back-calculate the p-multipliers. The results revealed that increasing the clay stiffness and pile spacing in the direction of loading increased p-multipliers. The proposed set of p-multipliers for the soft clay is very close to the set suggested by FEMA (Federal Emergency Management Agency). US Army and AASHTO design guidelines appear to recommend relatively conservative values of p-multipliers for both soft and stiff clay (improved ground). The parametric study revealed that for CDSM block depths greater than 9D, increases in lateral resistance are practically negligible.

The second centrifuge model was subjected to seven different earthquake events with the peak base accelerations ranging from 0.03 to 0.66g. The acceleration amplitude of the foundation level motions of the improved pile groups reduced compared to the surface free-field motion. This reduction is mainly attributed to the kinematic interaction effects. The foundation level motion in the unimproved pile group was, however, identical to that in the free-field. Higher peak accelerations were observed in the pile cap with smaller CDSM block (GIS) compared to the unimproved pile cap (GU) and the pile cap with larger CDSM block (GIL). The period where the maximum spectral amplification occurred became smaller as the size of the ground improvement increased. Cement-Deep-Soil-Mixing was an effective method in reducing the peak

displacements of the GIL pile cap. The peak displacements of the GIS pile cap remained about the same as the GU pile cap. The cohesion between soft clay and CDSM blocks helped to reduce the soft clay settlement in the vicinity of CDSM blocks compared to the free-field and in the vicinity of the unimproved pile group. More residual excess pore water pressures were, however, generated in the vicinity of CDSM blocks compared to the free-field and the corresponding location in the unimproved pile group.

A two dimensional, plain strain, fully coupled, nonlinear, dynamic finite element method (FEM), implemented into the computer code TeraDysac, was used to analyze the seismic behavior of the pile groups in improved and unimproved soft clay. A bounding surface constitutive model was used to model the stress-strain behavior of the soft clay and CDSM blocks. A linear elastic model was utilized to model the stress-strain behavior of dense sand layer. The constitutive models were calibrated using the laboratory test results. There was a satisfactory agreement between the measured and TeraDysac computed responses. TeraDysac model was able to predict the peak values and trends in accelerations, displacements, and excess pore water pressures very well. TeraDysac analyses also revealed that stress concentration occurred within the CDSM block. The negative EPWP in the CDSM block predicted by TeraDysac was indication of the dilative behavior of stiff clay.

Chapter 1: Introduction

1.1 Overview

Pile foundations can be subjected to lateral loading under static (sustained), quasi-static (slow load reversals), and dynamic (fast load reversals) conditions. The behavior of pile foundations under dynamic loading conditions, especially during earthquakes, is the most complex among these. Because of the large investments from the petroleum industry in offshore exploration, most of the available analysis and design procedures for behavior of pile foundations were developed for quasi-static conditions. However, the considerable loss of life and property during large earthquakes has motivated funding agencies to invest in research related to seismic behavior of pile foundations.

During past earthquakes, cases of poor performance of pile foundations in weak soils (e.g., soft clays and liquefiable sands) as a result of low lateral resistance have been observed (Tokimatsu et al. 1996; Tokimatsu et al. 2012). Increasing the lateral resistance, to decrease the lateral deflections, is therefore one of the main objectives in the design of pile foundations. It is relatively easy to restrict the lateral deflections of pile foundations in competent soils. In case of weak soils (e.g. soft clay and liquefiable sands), however, large lateral deflections are mitigated by using an increased number of more ductile, larger diameter piles that are difficult to design and expensive to construct. An innovative, more cost-efficient solution to this problem is to improve the soil surrounding the pile foundation. Ohtsuka et al. (2004) analytically showed that soil improvement around a pile group in weak soil can reduce the foundation cost by 28%.

For structures undergoing retrofit with existing pile groups in weak soils, improving the soils may be the best option to increase the lateral resistance of the foundation.

Improving the soft clays surrounding pile foundations is of particular interest to geotechnical engineers considering the fact that these soils are quite prevalent in many parts of the world and piles in soft clays often exhibit low lateral resistance. There are several ground improvement techniques for pile foundations in soft clays. Popular techniques in geotechnical engineering practice include: (1) replacing surficial layers by a compacted granular material; (2) soil mixing to construct shallow soilcrete walls on either side of the embedded pile cap; (3) jet grouting underneath the pile cap and around the piles; and (4) improving the ground by deep mixing and then driving the piles. Studies on the behavior of pile groups in improved and unimproved soft clays are, however, very limited. Due to the dearth of experimental data and lack of thorough understanding of their behavior, engineers are forced to design pile groups in improved soft clay in a conservative manner to mitigate the uncertainties. The literature also reveals that the lateral load tests on pile groups in soft clay with more than five pile diameter (5D) spacing are rare.

To improve our understanding of the quasi-static and seismic lateral load behavior of pile groups in improved and unimproved soft clay, two series of centrifuge model tests were conducted on pile groups. Observations from quasi-static lateral load behavior are useful because analytical procedures can be developed based on the quasi-static response. The quasi-static response can also be considered as a baseline for other types of loading conditions. Dynamic centrifuge tests, on the other hand, make it possible to observe and characterize the complex behavior of pile groups under seismic

excitation. The pile groups tested in this study had a symmetrical plan layout of piles in a 2×2 arrangement, and had a center-to-center pile spacing of 3D and 7D; where D is outside pile diameter. Limited tests were also performed on single piles in improved and unimproved soft clay for comparison purposes. The effects of ground improvement, lateral extent of treated zone, pile spacing, the amplitude and frequency content of seismic base motions on the behavior of pile groups were studied in detail using the centrifuge test results and numerical modeling.

1.2 Dissertation Outline

The material presented in this dissertation is organized into eight chapters as follows:

- Chapter 2 presents a brief literature review of the current state of knowledge and practice in evaluating the quasi-static and seismic lateral load behavior of pile groups. A summary of results from available field case histories, physical model tests, and numerical models for both quasi-static and dynamic lateral loading is provided in this chapter in addition to the areas of uncertainty in previous studies.
- Chapter 3 provides an overview of the fundamentals of dynamic centrifuge testing in Geotechnical Earthquake Engineering and its advantages and short-comings in evaluating the lateral load behavior of pile groups. Details of the centrifuge tests carried out in this study are also provided in this chapter.
- Chapter 4 provides the centrifuge test results of quasi-static loading on six pile groups and the comparison with single piles.

- Chapter 5 reports the methods used to determine separate sets of p-multipliers for each row of the 2 × 2 pile groups as a function of pile spacing and clay stiffness. Measured and computed lateral load-deflection, maximum bending moment-load, and bending moment-depth responses of the pile groups are presented. The computed results were obtained by the finite difference computer code GROUP (Reese et al. 2010) using the p-multipliers developed during this study. The p-multipliers obtained in this study for stiff clay and soft clay are also compared with previously recommended values. GROUP is then utilized to study the effects of undrained shear strength of the improved soils and the depth of improvement on the lateral resistance of pile groups in small and large deflections.
- Chapter 6 presents the results of seismic centrifuge tests on pile groups. The transient acceleration and lateral displacement responses of the structural models, their settlement, and the effect of pile groups on the dissipation of excess pore water pressure (EPWP) are presented and discussed in detail.
- Chapter 7 presents the results of two dimensional, plain strain, fully coupled, nonlinear, dynamic finite element analyses performed using the computer code TeraDysac (Muraleetharan et al. 2003) to study the seismic behavior of the pile groups in more detail. Spectral acceleration responses as well as acceleration-time, displacement-time, and EPWP-time histories in free-field and those for the pile groups are computed and compared with the measured values.

- Chapter 8 presents main conclusions from this study. This chapter also provides recommendations for practicing engineers and discusses future research needs in assessing the quasi-static and dynamic behavior of pile foundations.

Chapter 2: Literature Review

2.1 Overview

There is an abundance of research on the behavior of pile foundations under sustained, axial, lateral, and uplift loading. These studies have been done at full-scale or in model-scale in shaking tables or geotechnical centrifuges. Many computational methods have been also used to study pile foundations. The literature review presented here, therefore, is only limited to general behavioral features in quasi-static and dynamic lateral loading of pile groups in both improved and unimproved clays.

2.2 Quasi-Static Behavior in Unimproved Ground

2.2.1 Full-Scale Field Tests

Several full-scale field tests have been conducted to study the behavior of pile groups under lateral loads. Field tests have the advantage of closely modeling the in-situ conditions. These include studies of piles in sand (Alizadeh and Davisson 1970; Brown et al. 1988; Morrison and Reese 1988; Ruesta and Townsend 1997), clay (Brown et al. 1987; Lemnitzer et al. 2010; Matlock et al. 1980; Meimon et al. 1986; Rollins et al. 2006; Rollins et al. 1998), and silt (Brown et al. 2001). The full-scale tests on pile groups in clay are briefly described below.

Matlock et al. (1980) investigated the lateral load behavior of two pile groups in very soft clay at a site in Harvey, Louisiana. The first pile group consisted of five piles arranged in a circular layout with a center-to-center spacing of 3.4D. The second pile group had ten piles arranged in a circular layout with a center-to-center spacing of 1.8D. Six series of lateral load tests were performed and surprisingly small variations in shear

and bending moment among the piles in each group were observed. Reducing pile spacing moderately increased bending moment and the average lateral load per pile. For a given lateral load per pile, the lateral deflections also increased with decreased pile spacing. Their test results emphasized the highly inelastic response of the soft clay and, for such soils, discouraged using concepts of elastic interaction among piles in a group.

Meimon et al. (1986) performed two experiments on a 2 (rows) × 3 (columns) pile group driven into a low plastic clay layer overlying a silty sand layer. The center-to-center spacing of piles was 3D and pile had hinged end condition. Five cyclic tests from 1000 to 10000 cycles were carried out for each experiment. A large group effect characterized by different row by row behavior was observed. A soil reaction breakdown was observed near the soil surface while the soil reaction increased at lower levels.

Brown et al. (1987) performed cyclic lateral load tests on a group of piles in a 3 × 3 arrangement with a nominal spacing of 3D on centers and hinged end condition. The test was done in a stiff overconsolidated clay site in Houston, Texas. Their results emphasized the highly nonlinear nature of the pile-soil-pile interaction and group effects. The deflection of a single pile under a load equal to the average load per pile was substantially less than that of the piles in the group. The bending moments in the piles of the group were larger than bending moments in single piles. They showed that the front row pile in a group carries more loads than the piles in the following rows.

Rollins et al. (1998) performed quasi-static lateral load tests on a 3 × 3 pile group driven into a profile consisting of soft to medium-stiff clays and silts underlain by sand. The center-to-center spacing of piles was 3D and piles had hinged end condition.

Quasi-static tests on a single pile were also conducted for comparison. Their test results revealed that under the same average load, the piles in the group deflected over two times more than the single pile. For a given deflection, the first row of piles carried the maximum loads, followed by the second and third row of piles. Maximum bending moments were higher in the group piles than in the single pile.

Rollins et al. (2006) performed full-scale cyclic lateral load tests on pile groups in stiff clay spaced at 3.3D, 4.4D, and 5.65D with as many as five rows of piles. The piles had hinged end condition. Their test results revealed that for a given deflection, the leading row of piles carried the greatest load, while the second and third row of piles carried successively smaller amount of loads. The loads carried by fourth and fifth row of piles were almost the same as the third row of piles. Increasing pile spacing from 3.3D to 5.65D decreased group interaction effects.

Lemnitzer et al. (2010) performed cyclic lateral load tests on a 3 × 3 RC bored pile group to investigate group interaction effects. The piles were driven in clay with thin silty sand layers and were spaced at 3D. The piles had a fixed end condition. The group efficiency was defined as the average lateral load per pile divided by the lateral load on a single pile at the same pile head deflection. Group efficiencies were found to range from unity at very small lateral displacements (0.004D) to 0.9 at failure (0.04D), illustrating the dependency of group efficiency on the level of nonlinearity in the foundation system.

2.2.2 Model-Scale Tests

Full-scale tests have been supplemented by small-scale model testing in a geotechnical centrifuge and by models under normal gravity (at 1 g). Most of the centrifuge model studies on laterally loaded pile groups were performed in sand (McVay et al. 1995; McVay et al. 1998; Remaud et al. 1998). Small-scale testing of pile groups in clays involved mostly 1 g models (Chandrasekaran et al. 2010; Cox et al. 1984; Rao et al. 1998) with limited centrifuge studies (Ilyas et al. 2004). The model-scale tests on pile groups in clay are briefly described below.

Cox et al. (1984) conducted quasi-static lateral load tests on pile groups in very soft clay with undrained shear strength of 2 kPa. The tests were performed at 1 g. The piles had a center-to-center spacing ranging from 1.5D to 6D and number of piles in a group was 3 or 5. The piles had a fixed end condition. The average efficiency of three-pile groups with a spacing of 1.5D was found to be 60% and 80% in the direction of loading (in-line) and perpendicular to the direction of loading (side-by-side), respectively. Increasing the number of piles in a group or decreasing the spacing decreased the efficiency of these pile groups.

Rao et al. (1998) performed lateral load tests at 1 g on pile groups embedded in a marine clayey bed. The center-to-center spacing of piles varied between 3D and 8D and the piles were tested for embedment to diameter ratios (L/D) of 20, 30, and 40. The pile head conditions could be considered closer to free end condition. Their test results indicated that the lateral load capacity of a pile group mainly depends on the rigidity of pile-soil system for different arrangements of piles within a group. They verified this finding by performing a simplified finite element analysis and pointed out that the

differences in passive resistance in different pile arrangements influence the efficiency of a pile group.

Ilyas et al. (2004) performed centrifuge tests to investigate the response of pile groups in normally consolidated and overconsolidated kaolin clays subjected to quasi-static lateral loading. The piles were tightly secured through openings in the pile cap using screws. Different pile groups with center-to-center spacings of 3D or 5D were tested. Test results revealed that increasing the number of piles in a group significantly reduces the pile group efficiency. Shadowing effects caused the leading row of piles to experience larger loads and bending moments. The shadowing effects were more significant in the leading row of piles than the trailing rows.

Chandrasekaran et al. (2010) performed quasi-static lateral load tests at 1 g on different pile groups. The pile groups were installed in soft clay and had length to diameter ratios of 15, 30, and 40 and 3D to 9D spacing. Their results reveled that group interaction caused the lateral capacity of a pile in a 3 × 3 pile group with 3D spacing to be about 40% less than that of a single pile. Group interaction also increased the maximum bending moments of a pile in a group with 3D spacing by 20% compared to that of a single pile.

2.2.3 Numerical Models

There are different methods for predicting the behavior of pile groups under lateral loading. Fully coupled, nonlinear, computational methods can be used to model pile groups in improved or unimproved ground under lateral loading. While these nonlinear analyses can provide useful insights, they are typically time consuming and

are not practical in day-to-day design applications. Several researchers and agencies have therefore proposed simpler methods to analyze closely-spaced piles under lateral loading.

Poulos (1971) used the theory of elasticity to take into account the effect of a pile on other piles of a group. He used a linear elastic model for soil and piles and assumed that soil around piles behave as elastic half-space. However, the real soil and pile behavior, especially near the ground surface, is elastoplastic and cannot be accurately modeled using linear elastic models.

Focht and Koch (1973) combined the nonlinear p-y model for an isolated single pile with elastic continuum model of Poulos (1971) to predict the behavior of laterally loaded pile groups. The p-y model was used to predict the nonlinear soil behavior occurring close to each pile and elastic model was used for predicting the cumulative group deformation occurring farther from the piles. In p-y models, p is the soil reaction per unit length of the pile and y is the horizontal relative displacement between the pile and the soil. By obtaining the group deflection, the p-y curves of each single pile was modified by multiplying them by a y-factor. They also recommended applying a p-factor in cases where shadowing effects occur.

Davisson (1970) considered the group effects by selecting an appropriate variation of subgrade modulus, "k", by depth. Group action and cyclic loading can cause a reduction in effective subgrade modulus, "k_{eff}". That is, when both of these factors are available together, the effective modulus can reduce to 10 percent of that applicable to an isolated pile in the first cycle of loading. Provided that the side-by-side distance of piles in a group is equal or greater than 2.5D, the k_{eff} can be assumed to vary

linearly from 1k to 0.25k for the pile spacings from 8D to 3D, respectively. k_{eff} values were linearly interpolated between these two values for other spacings. These observations were deduced based on Prakash (1962) model tests on pile groups in sand. The Canadian Geotechnical Society (1978) recommended the same method to analyze pile groups under lateral loading. The Japan Road Association (1976) also used the subgrade modulus reduction procedure, but was less conservative in computing reduction factor for closely spaced pile groups.

Ooi and Duncan (1994) used the group amplification procedure to estimate deflections and maximum bending moments of pile groups. This simple procedure was based on the theories of Poulos (1971) and Focht and Koch (1973) and used amplification factors to multiply lateral deflections and maximum bending moments of single piles. However, like subgrade modulus reduction procedure, this method was not able to predict load distribution between piles in a group.

Brown et al. (1988) used p-multipliers (f_m) to modify the p-y curve of a single pile and obtain these curves for piles of a group in sand. Single piles were modeled as beam elements interacting with surrounding soil through p-y springs. These p-y springs can be made nonlinear to account for nonlinear behavior of soils. A p-y curve of a single pile can then be "squashed" to account for the reduced soil resistance of a pile in a pile group. Figure 2.1 illustrates the concept of using a p-multiplier to squash a single pile p-y curve and obtain that for a pile in a group. Brown et al. (1988) pointed out that more research is needed to establish a methodology for predicting the variation of p-multipliers with soil properties, pile spacing and stiffness, depth, cyclic loading, etc.

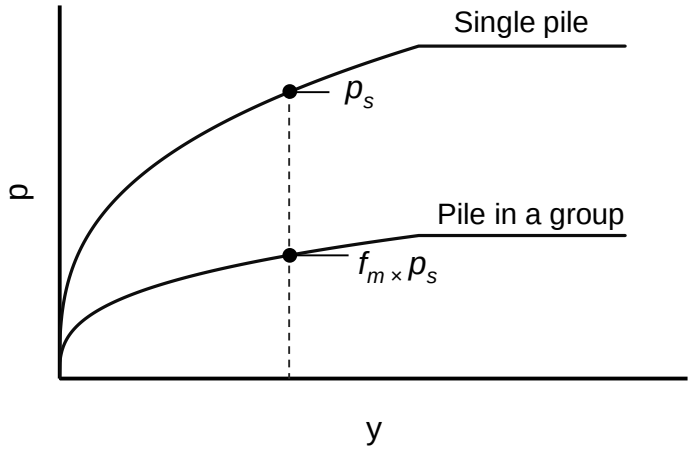

Figure 2-1. Applying a p-Multiplier (f_m) to a Single Pile p-y Curve to obtain that for a Pile in a Group.

The literature review reveals that due to lack of experimental data, analyzing pile groups in soft clay under quasi-static lateral loading still involves uncertainty. Lateral load tests on pile groups with center-to-center spacing greater than 5D are rare as well. Test results and analyses presented in this dissertation will provide valuable insight into the quasi-static lateral load behavior of pile groups in soft clays including those with spacing greater than 5D.

2.3 Dynamic Behavior in Unimproved Ground

Deep foundations can be subjected to lateral loadings under dynamic conditions. Dynamic loads can be produced by ocean waves, traffic, machine foundations, and earthquakes (Hadjian et al. 1992). The main components to consider in analyzing the seismic behavior of pile groups are: 1) kinematic interaction between soil and piles; 2) inertial forces imposed by the superstructure; 3) pile-soil-pile interaction; and 4) nonlinear coupled soil (solid skeleton and pore water) response as a result of a strong

ground motion. These components constitute a complex pile group behavior known as Soil-Pile-Structure Interaction (SPSI). SPSI can be studied under the following main categories: analytical and semi-analytical, numerical, and experimental methods. A detailed literature review of this subject is beyond the scope of this study and interested readers are referred to Finn (2005), Gazetas and Mylonakis (1998), Novak (1991), and Pender (1993). A brief review of literature is provided below.

2.3.1 Full-Scale Field Tests

A few dynamic loading tests have been performed on pile foundations with loading applied at the pile head (Blaney and O'Neill 1986; Blaney and O'Neill 1989; Burr et al. 1997; El-Marsafawi et al. 1992; Fleming et al. 2015; Han and Novak 1988; Nikolaou et al. 2001; Novak and Grigg 1976). There are also studies on the behavior of pile foundations under blast induced liquefaction (Ashford et al. 2000; Ashford et al. 2004; Weaver et al. 2005). The results from dynamic pile head load tests can be adapted to the seismic loading by using response spectra and making assumptions about the frequency of significant response. The main drawback of these tests is that dynamic loading at top only produces disturbances in the soil adjacent to the pile. Therefore, the pore water pressures will only be generated closer to the piles and dissipate faster than the case for seismic base (bed rock) shaking. A similar discussion is also applicable to the stiffness and strength degradation of the soil. Furthermore, there will be no kinematic interactions between soil and piles in pile head load tests.

2.3.2 Model-Scale Tests

Shaking table tests have been widely used to model SPSI. Large scale shaking table tests have the advantage of modeling SPSI with dimensions equal or comparable to the prototype scale. These shaking tables make it possible to construct soil profiles, compact soils, and easily instrument soil-pile systems (Nakagawa et al. 2000; Tokimatsu et al. 2004). However, it is difficult to account for high gravitational stresses (associated with deep soil profiles) in shaking table tests and constructing large models can be time consuming. Most shaking table tests have studied dynamic SPSI in sand during liquefaction or under lateral spreading (Chau et al. 2009; Dobry et al. 2011; Tang and Ling 2014; Yasuda et al. 2000). There are a few dynamic shaking table tests for pile foundations in clay (Meymand 1998; Meymand et al. 2000).

Meymand (1998) and Meymand et al. (2000) used a large shaking table to perform quasi-static and dynamic lateral load tests on single piles and pile groups in soft clay. Experimental p-y curves were successfully derived from quasi-static and dynamic tests. These curves compared reasonably with the API (2007) recommended p-y curves. Resistance degradation was observed due to hysteresis and gapping, illustrating gapping as an important analytical feature to model. The quasi-static lateral load test results were also in very good agreement with the results predicted by COM624P (Wang and Reese 1993).

Geotechnical centrifuge experiments have been used to investigate the complex seismic SPSI. Compared to field experiments, soil profiles can be well defined in centrifuge tests. In centrifuge tests, the stress condition at any point of the model and also the overall model behavior (e.g. acceleration, displacement, and failure

mechanisms) is identical to that in the full-scale prototype. The main drawback of model tests is the fact that because different scaling laws apply to different phenomena (e.g. dynamics and consolidation), similitude may not be provided simultaneously between all parameters. Furthermore, boundary effects are usually present due to the model containers used in the tests (Kutter 1995; Zeng and Schofield 1996). Like shaking table tests, most studies in geotechnical centrifuges have dealt with the behavior of pile foundations in sand during liquefaction or lateral speeding (Abdoun et al. 2003; Abdoun et al. 2013; Brandenberg et al. 2005; Brandenberg et al. 2007; Brandenberg et al. 2007; González et al. 2009; Sharp et al. 2003; Sharp et al. 2010; Taboada-Urtuzuástegui and Dobry 1998; Wilson et al. 2000). Preparing and consolidating clay and the long time often required to reach the desired degree of consolidation are some of the difficulties in centrifuge modeling of pile foundations in clay. Geotechnical centrifuge models studying SPSI in soft clay are rare and there are only limited results and observations (Banerjee et al. 2008; Wilson 1998). These two studies have been summarized below.

Wilson (1998) performed dynamic centrifuge tests on single piles and pile groups in soft clay and liquefying sand. These tests constituted a solid framework for future research and included detailed procedures for signal processing, data reduction, and data interpretation of dynamic centrifuge tests on pile foundations. The model layout used for seismic tests is shown in Figure 2.2. Wilson (1998) only presented single pile test results in detail. The test results in soft clay revealed that the bending moments and lateral displacements of piles in soft clay were strongly depended on the superstructure acceleration. For the first load cycles, the back-calculated p-y curves in

soft clays were in a reasonable agreement with the API (2007) recommended static p-y curves.

Banerjee et al. (2008) carried out dynamic centrifuge tests on 2 × 2 pile-raft systems. The piles had a clear spacing of 4.5D and were connected to a rigid steel base plate. Their results revealed that the pile-clay system behavior is affected by the stiffness degradation of clay during earthquakes, which changes the natural period of the pile-clay system.

The series of centrifuge tests performed in this study, to the author's knowledge, represent the first attempt to well characterize nonlinear dynamic SPSI effects of pile groups in soft clay.

2.3.3 Analytical or Semi-Analytical Models

Analytical or semi-analytical solutions are based on mechanics and give an insight into the physical mechanisms involved in SPSI. However, because of the considerable difficulties that arise in the exact prediction of the seismic SPSI, simplifying assumptions are made to obtain closed-form expressions. Solving the SPSI problem for the incidence of SH, SV, or Rayleigh waves or incidence of a combination of these waves, considering an elastic homogenous half-space, and accounting for just the kinematic interaction component are some of these assumptions made by researchers (Dezi et al. 2010; Di Laora et al. 2012; Di Laora et al. 2013; Kaynia and Kausel 1991; Kaynia and Novak 1992; Makris 1994; Mylonakis 2001; Saitoh 2005; Tajimi 1969). Because of these assumptions, it is often not possible to compare the results from analytical solutions with well-documented case histories or physical

models. The results from analytical studies; however, can be compared with those obtained from numerical models with the same assumptions (Dezi et al. 2010; Elgamal and Lu 2009) and constitute a valuable source for validating numerical models.

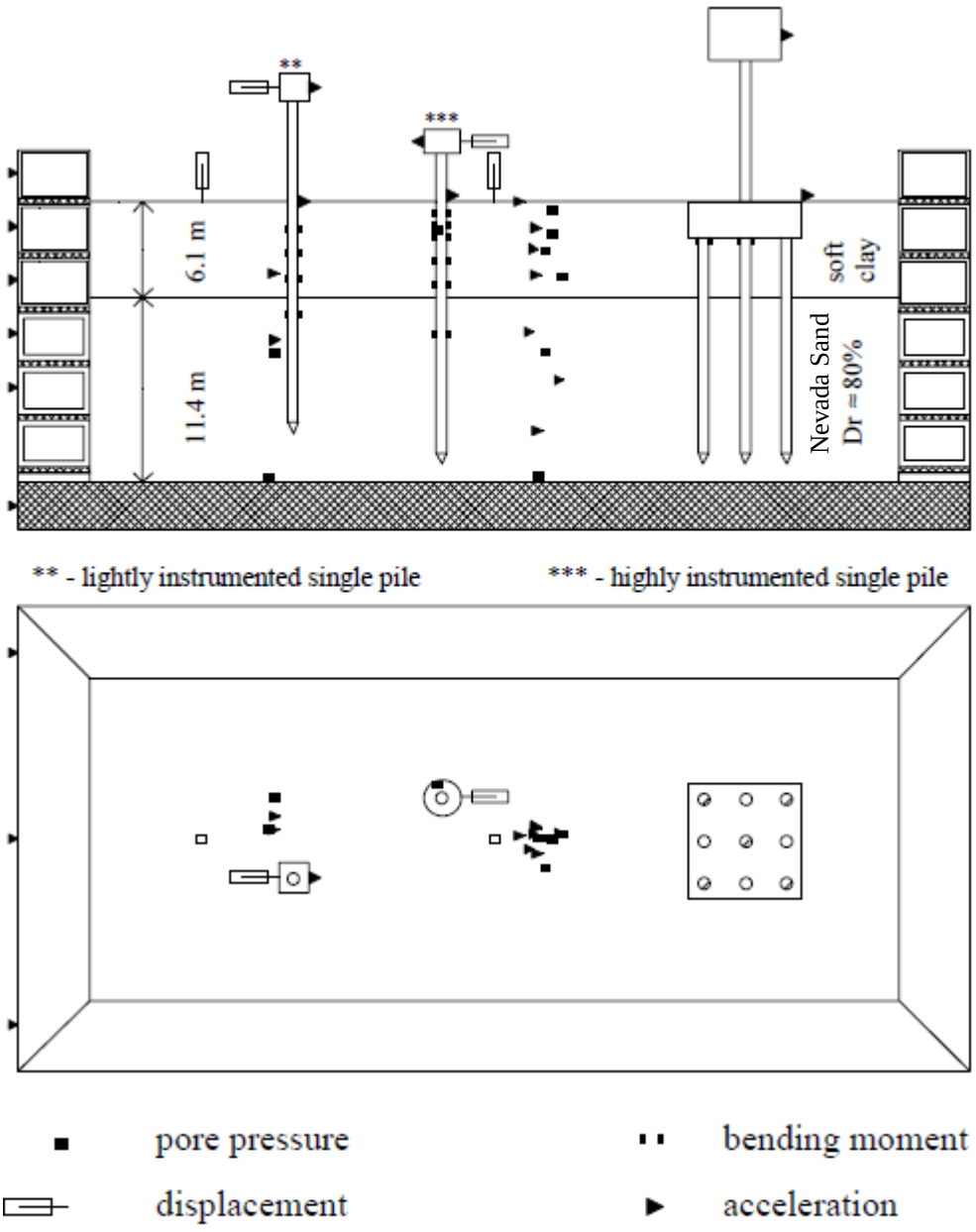

Figure 2-2. Model Layout for Seismic Tests in Soft Clay (Wilson 1998)

2.3.4 Numerical Models

Different numerical methods [e.g. Finite Element Method (FEM), Boundary Element Method (BEM), and Finite Difference Method (FDM)] have also been used to study SPSI. Each of these numerical techniques have their own advantages and disadvantages. FEM and FDM have proven effective in solving problems with bounded domains, particularly when inhomogeneities and nonlinear effects should be treated (Anandarajah et al. 1995; Bentley and Naggar 2000; Cai et al. 2000; Jeremić et al. 2009; Kirupakaran et al. 2010; Maheshwari et al. 2004; Sadek and Isam 2004; Uzuoka et al. 2007; Wu and Finn 1997). For domains of infinite extensions, however, standard finite element discretization leads to wave reflections at the boundaries of the finite element mesh, which can be only partially eliminated for some cases, by using so-called transmitting, silent and nonreflecting viscous boundaries. BEM has shown to be a very powerful numerical technique for linear and homogeneous materials for both bounded and unbounded domains, and does not require domain discretization, which can be an advantage in many practical applications (Kaynia 1982; Kaynia and Kausel 1991; Maeso et al. 2005; Sen et al. 1985). Since this method automatically satisfies the radiation conditions at infinity, there is no need to model the far field in problems with semi-infinite or infinite domains. To utilize the advantages of both FEM and BEM, a combination of these techniques seems ideal (Küçükarslan and Banerjee 2003; Millán and Domínguez 2009; Padrón et al. 2008). These models generally consider both the soil volume and the structures in the same model and analyze them in a single step; which is so called the direct method (Wolf 1985). However, the discretization of a three-dimensional continuum generates a multitude of degrees of freedom, causing

these methods to be somewhat impractical for the design of soil-pile-structure (SPS) systems. A simpler substructure procedure can also be adopted (Wolf 1985). In this method, pile foundation impedances are determined by performing soil-pile interaction analyses considering group interaction effects (Emani and Maheshwari 2009). The superstructure model is then analyzed using these impedances and input motions obtained from free-field. It is assumed that these motions are not affected by pile foundation itself. In substructure method the SPS system behavior is obtained by assuming linearity and superposition of forces from different substructures. However, same results will be obtained, if direct and substructure methods are implemented consistently. The Beam on Nonlinear Winkler Foundation (BNWF) model is a powerful tool capable of accurate analyzing the soil–pile interaction and has been used by several researchers producing results with less computational efforts than rigorous continuum models (Boulanger et al. 1999; Dezi et al. 2010; Di Laora et al. 2013; Kavvadas and Gazetas 1993; Maiorano et al. 2009; Mylonakis 2001; Mylonakis et al. 1997; Nikolaou et al. 2001; Wang et al. 1998). The piles are modeled as beam elements interacting with surrounding soil using p-y springs. An ideal p-y spring should consist of different components including elastic, plastic, and gap components. Dashpots are usually used to model radiation damping. For seismic loadings, the response of the soil profile is analyzed separately using equivalent-linear or nonlinear site response programs and is applied as displacement-time histories to the p-y elements. Compared to fully coupled continuum models, it is easier to perform parametric studies using this method. The drawback of this method is that the behavior of beam is uncoupled from the behavior of soil, shear transferring between adjacent soil layers is ignored, and the parameters for p-

y springs are difficult to obtain. In order to obtain reliable results from numerical models, they should be calibrated and validated by means of experimental results (Lok 1999; Makris et al. 1996; Manna and Baidya 2010; Tasiopoulou et al. 2013; Thavaraj et al. 2010).

2.4 Piles in Improved Ground

There are only a few existing experimental studies or case histories that have focused on the quasi-static or dynamic lateral loading behavior of pile groups in improved weak soils.

Fleming et al. (2015) performed full-scale tests to investigate the dynamic and quasi-static lateral load behavior of single piles in unimproved and CDSM improved soft clay. The tests were performed at a site in Miami, Oklahoma. The site consisted of a 4.4 m layer of soft clay overlying a 2.0 m layer of sandy gravel and limestone bedrock (Taghavi et al. 2010). A 3D rendering of their test configuration is shown in Figure 2-3.

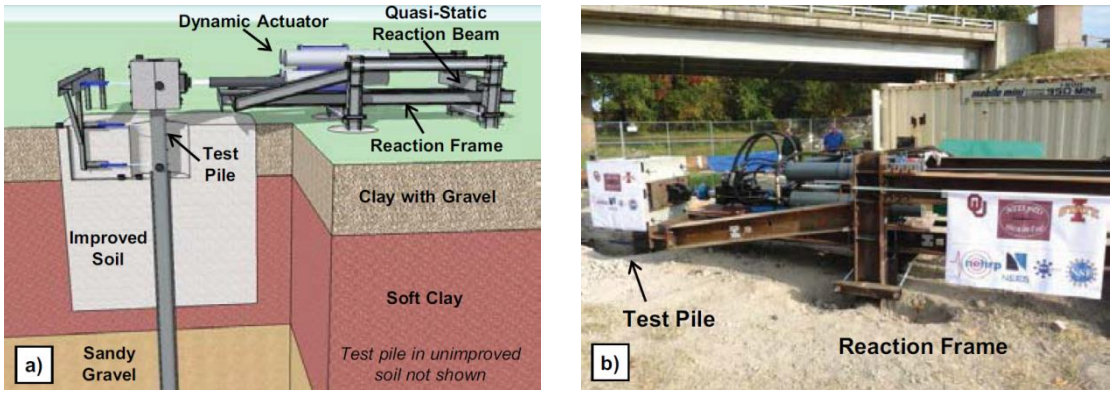

Figure 2-3. (a) Soil Profile and Test Configuration and (b) Full-Scale Testing Set-up of the Improved Pile (Fleming et al. 2015)

Their test results revealed that, compared to the unimproved pile, the lateral strength, effective elastic stiffness, and average equivalent damping ratio of the improved pile increased by 42%, 600%, and 650%, respectively. At a head displacement of 0.1 m, the improved pile reached its lateral capacity. At this point, the critical region at the base of the pile above the improved ground experienced buckling and subsequent fracture due to low cycle fatigue.

Rollins and Brown (2011), Rollins et al. (2010), and Rollins and Sparks (2002) performed full-scale quasi-static lateral load tests to evaluate the performance of pile groups in improved ground. The ground improvement methods included soil mixing, jet grouting, and replacement with compacted sand. While soil mixing was only possible on both sides of the embedded pile cap, jet grouting reached the soil underneath the pile cap. For increasing the lateral resistance and initial stiffness, the jet grouting technique was more effective than soil mixing outside the pile caps. Jet grouting below a pile cap (see Figure 2.3) increased the lateral resistance by 160%. By extending ground improvement to the sides of an embeded pile cap, the passive resistance against cap movements increased. In this case, soilcrete walls produced by jet grouting and soil mixing increased the lateral resistance by 185% and 60%, respectively, relative to untreated conditions (Figure 2.3). Excavating soft clay and replacing it with compacted granular fill was another ground improvement technique used and this technique increased lateral resistance by 10% to 50%, with the highest increases occurring when the contrast in strength is the greatest. To obtain the full lateral resistance of the granular soil, the compacted granular fill had to extend 5D below the ground surface and 10D beyond the face of the piles. Compacting a gravel backfill in place on the sides

of the cap also increased the lateral resistance. Passive cap resistance in this case contributed to the total increase in lateral resistance by 40-60%.

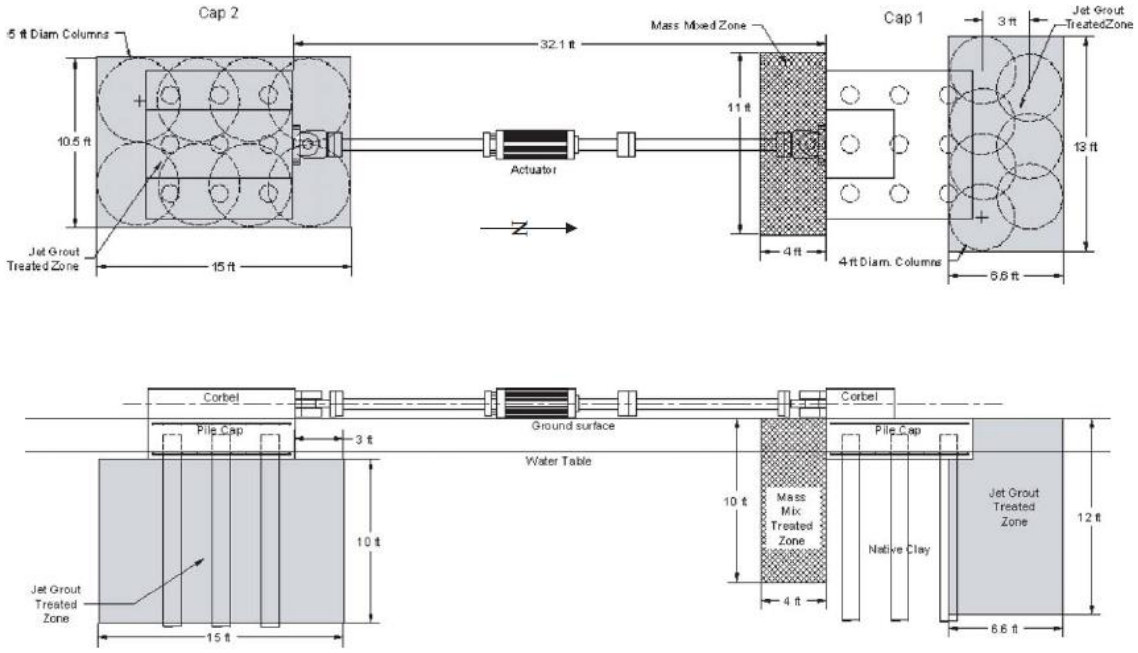

Figure 2-4. Plan and Profile Views of Pile Groups after Treatment with Jet Grouting (Rollins and Brown 2011)

Tokimatsu et al. (1996) performed field observations of building damage in the 1995 Hyogoken-Nambu (Kobe) earthquake. The observations revealed the effectiveness of ground improvement in enhancing the overall performance of buildings on improved foundations (mostly shallow foundation) compared to similar unimproved foundations in the region. The building founded on soils improved by either sand drains or preloading did not show serious foundation problems. Less settlement and tilt was observed in these buildings.

Ashford et al. (2000) tested full-scale pile groups in liquefiable sands improved with stone columns. They used controlled blasting to liquefy the soil surrounding pile

foundations. Their test set-up is presented in Figure 2.4. Their results showed that the stone columns significantly increased the stiffness of the foundation system, by more than 2.5 to 3.5 times than that in the liquefied soil. It was found that in the liquefied soil, pile groups in the treated ground performed better than the pile groups improved by doubling the number of piles or increasing shaft diameters by 50 percent.

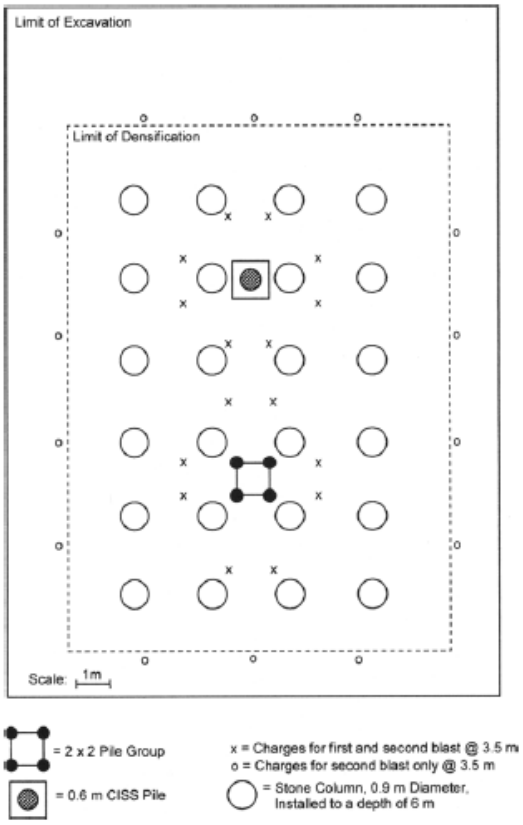

Figure 2-5. Plan View of Test Set-up (Ashford et al. 2000)

Yamashita et al. (2012) monitored the seismic behavior of a piled raft foundation supporting a 12-story base-isolated building in Tokyo, before and after the 2011 Tohoku Earthquake (see Figure 2.5). The building was located on loose silty sand, underlain by soft cohesive soil. Cement-Deep-Soil-Mixing was used to cope with the

liquefiable sand as well as to improve the bearing capacity of the raft foundation. The results show that the improved piled raft was quite stable in the soft ground during and after the earthquake. It was found that the horizontal accelerations of the superstructure were reduced to approximately 30% of those of the ground surface. This acceleration reduction was contributed to the input losses due to the kinematic soil–foundation interaction in addition to the base isolation system.

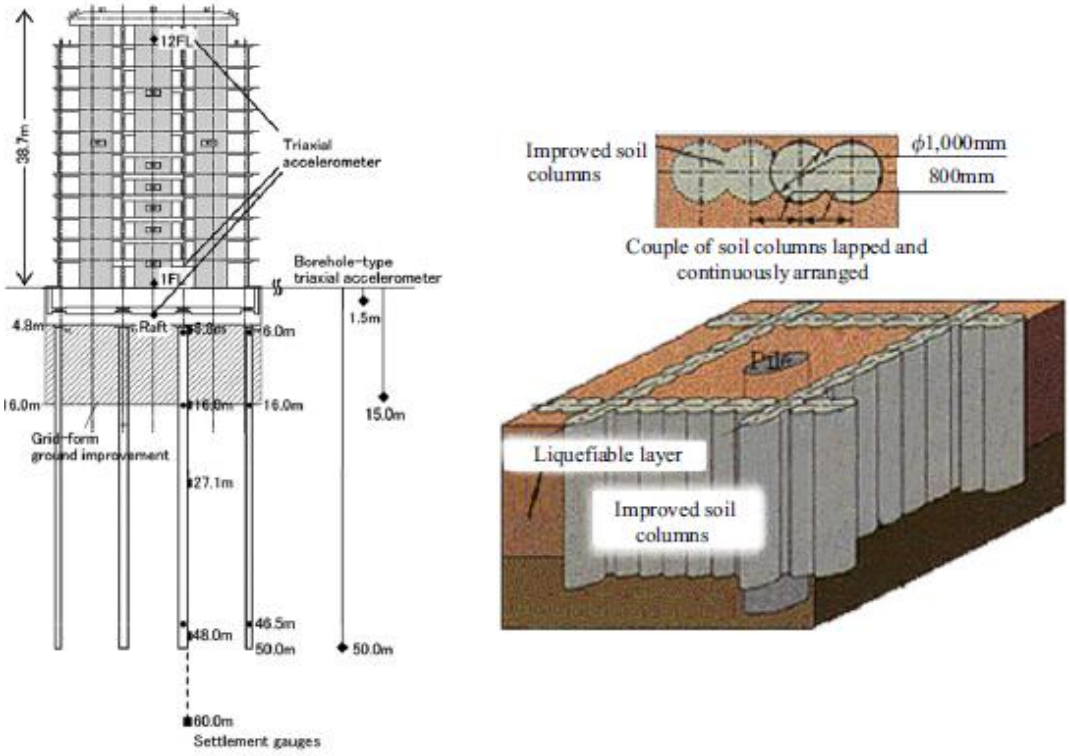

Figure 2-6. Schematic View of Building and Foundation and Grid-Form Deep Cement Mixing Walls (Yamashita et. al 2012)

This literature review reveals that well-documented case histories and physical model tests able to characterize the seismic and quasi-static behavior of pile groups in improved soft clay are very rare. The series of centrifuge tests performed in this study,

to the author's knowledge, represent the first attempt to characterize nonlinear dynamic and quasi-static soil-structure interaction effects of pile groups in improved soft clay.

2.4.1 Cost Comparisons

Simple cost comparisons performed by Rollins and Brown (2011) and Ohtsuka et al. (2004) indicated that almost all ground improvement techniques have the potential of reducing deep foundation system costs compared to common structural solutions (e.g. increasing the number of piles in a group, extending the cap, or increasing the diameter of the piles). The costs basically depend on the ground improvement technique and also vary with locality.

Chapter 3: Seismic and Quasi-static Centrifuge Testing of Pile Groups in Improved Soft Clay

3.1 Overview of Geotechnical Centrifuge Testing

Centrifuge testing allows the investigation of system-level, complex problems that would otherwise only be possible by full-scale testing. An important aspect to be considered in testing reduced-scale centrifuge models is their similitude with field-scale prototypes. Because the strength, stiffness, deformation, and volume change in soils is stress-dependent, the key objective of a centrifuge model is to keep the stresses identical to that of a prototype. The geotechnical centrifuge used in this study is shown in Figure 3.1. Centrifuge testing includes several key steps. After constructing the reduced-scale centrifuge model, it sits inside a bucket located at one end of the centrifuge arm with its long dimension parallel to the direction of shaking (Figure 3.2). Adjustable counterweights on the other end balance the weight on the model side (Figure 3.3). The container gradually rotates 90^{o} from a horizontal position as the centrifuge is spun-up. This step takes about 30-40 minutes and allows for a gradual transition of stresses. After reaching the target centrifugal acceleration, the model is tested.

3.1.1 Scaling Laws

In centrifuge modeling, the scale factor for length may be expressed as L* = 1/N. L* is the ratio of length in the model to length in the prototype. The scaling laws for centrifuge model tests can be found in Schofield (1981), Kutter (1992), and Garnier et al. (2007). A list of the main scaling factors used to convert the measured data to prototype-scale units is provided in Table 3.1.

Figure 3-1. The 9-m radius Centrifuge at the Center for Geotechnical Modeling (CGM) at University of California, Davis (UC Davis)

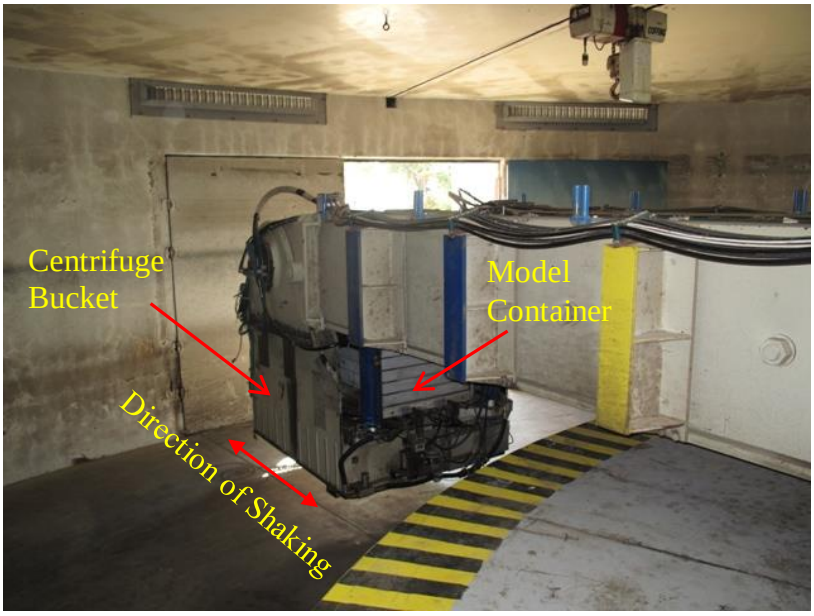

Figure 3-2. The Model Container inside the Centrifuge Bucket

Figure 3-3. Balancing Counterweights on the Centrifuge Arm

Table 3-1. Centrifuge Scaling Factors

Quantity	Symbol	Scale Factor
Gravity	g	N
Length	l	N^{-1}
Volume	v	N^{-3}
Mass	m	N^{-3}
Force	F	N^{-2}
Stress	σ	1
Strength	s	1
Moduli	E	1
Acceleration	a	N
Time (dynamic)	t_{dyn}	N^{-1}
Frequency	f	N
Time (diffusion)	t_{dif}	N^{-2}

3.1.2 Advantages of Centrifuge Testing

Analyzing a structure such as a bridge or an improved deep foundation as a system is a highly complex undertaking; however, with advances in computer hardware, mechanics, and computational techniques, huge leaps in our ability to digitally simulate these systems have been made. In fact, our ability to computationally model civil infrastructure has outstripped our ability to physically model these complex systems. Physical models are, however, necessary to validate computational simulations as well as understand failure mechanisms of complex structures. Creating full-scale physical models (e.g. instrumenting a real structure as it is built) is very costly and time consuming. Furthermore, field conditions such as subsurface soil profiles are often unknown, it is difficult to take a real structure to the failure state, and only limited

loading conditions can be studied. In seismic testing, there is no guaranty that an earthquake will strike an instrumented structure. Small-scale centrifuge models can solve all of these problems and make it possible to study geotechnical systems under variety of conditions. A geotechnical centrifuge makes it possible to accurately model deep deposits with realistic stress conditions; control the repeatability of test results; directly observe failure mechanism; apply a wide range of dynamic or quasi-static loads; validate numerical and empirical models, and use in consulting (Mitchell 1991). The centrifuge tests are also time and cost effective compared to full-scale tests.

3.1.3 Limitations of Centrifuge Testing

Propagation of 1D shear waves in a soil layer of infinite lateral extent and finite depth should be simulated in a container used in centrifuge tests. A well-designed container can reasonably satisfy the concerns regarding the boundary effects created by artificial boundaries of a model container. The important boundary effects in a model container include (1) distortion of the overall stress field and soil rocking relative to the base plane as a result of frictionless smooth end walls; (2) strain dissimilarity and soil deformation restriction as a result of a rigid end wall; (3) generation and propagation of unwanted P waves as a result of rigid end walls and their interaction with the model soil; and (4) destroying K_0 conditions due to the deflection of side walls. Many of these boundary effects can be minimized in specially designed model containers as discussed in the next section.

3.2 UC-Davis Centrifuge, Shaking Table, and Model Container

The centrifuge model tests in this study were carried out at a centrifuge acceleration of 30 g (at the center of mass of the model) in a flexible shear beam container. The maximum payload for the UC Davis centrifuge is 4,500 kg and the available bucket area is approximately 4 m^2. The maximum centrifugal acceleration is 75 g. The maximum payload for the shaking table is 2,700 kg. The 9-m radius UC Davis centrifuge has the largest radius of any centrifuge with a shake table in the world. One key advantage of a large centrifuge is that large models with holistic system-level complexities can be constructed and tested.

The Flexible Shear Beam (FSB) container (Kutter 1995) used in our tests had internal dimensions of 1722 mm (length) × 686 mm (width) × 700 mm (height). The model container is shown in Figure 3.4. This container made it possible to reduce the boundary effects and reasonably simulate 1-D propagation of shear waves in an infinite half space. The FSB container consists of six hollow aluminum rings separated by 12 mm thick layers of neoprene (rubber). The rubber thickness and stiffness are designed in such a way that to make the natural frequency of the container softer than the initial natural frequency of the soil. To provide complimentary shear stresses, flexible and inextensible shear rods were installed near both end walls. This container also made it possible to perform centrifuge tests with large payloads. The large inner dimension of the container allowed placing structures and instrumentation far from the boundaries and from each other.

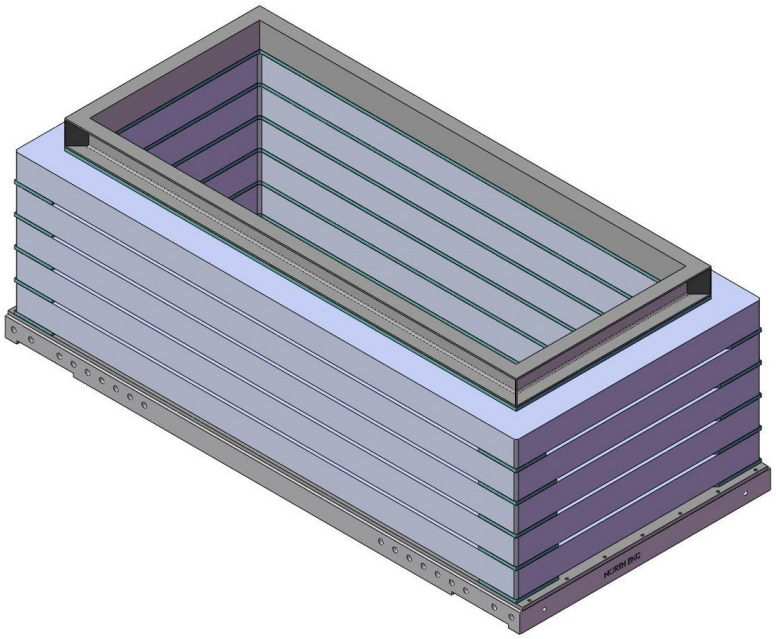

Figure 3-4. NEES at UC Davis Flexible Shear Beam Container (FSB1) used in This Study (Lars Pedersen, Personal Communication, 2012)

A servo-hydraulic shaker (Kutter 1995) was used to replicate key features of earthquake motions (see Figure 3.5). The shaker actuators were controlled by a conventional closed-loop feedback control system and in model scale could produce between 14 and 30 g shaking accelerations at frequencies of up to 200 Hz. The maximum peak to peak absolute shaking velocity was about 1 m/s and the stroke was 2.5 cm. Earthquake motions were recorded at different locations on the baseplate of the model container and also at the very bottom of soil profile (see Figure 3.6). All recorded motions were in excellent agreement with each other both in terms of time histories and frequency content and the differences were negligible.

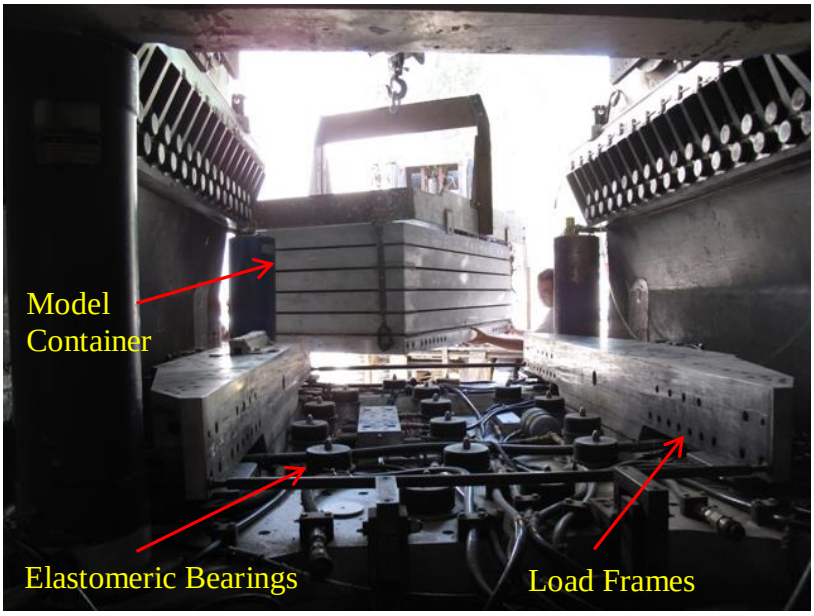

Figure 3-5. U.C. Davis Servo-hydraulic Shaker

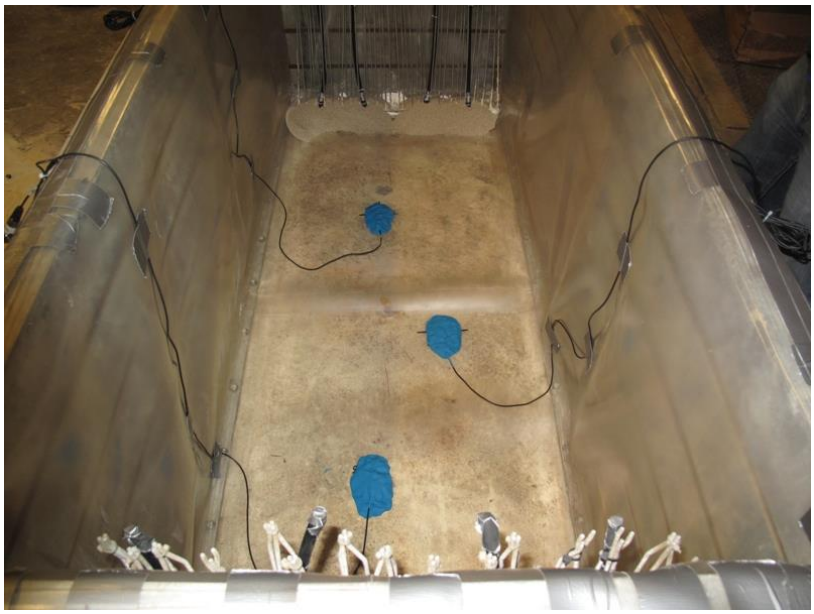

Figure 3-6. Accelerometers at the Bottom of FSB1 Container

3.3 Centrifuge Test Set-up

From this point onwards, all the results are presented in prototype scale unless otherwise stated. The soil profile in both centrifuge models consisted of four overconsolidated clay layers overlaying a dense sand layer (Figure 3.7). The total depth of clay layers in both tests was 9.6 m. The sand layer depth in the first (s=7D - ATA01) and second (s=3D - ATA02) series of tests was 8.0 m and 8.1 m, respectively. The water table was maintained above the soil surface. Generally, the clay layers were lightly overconsolidated (OCR≈1.1 to 2) except for the top layer with OCR varying from about 1.1 to 10 near the ground surface (Figure 3.8a). To prepare the dense sand layer, the Nevada sand was air pluviated to achieve a relative density of 84%, and a void ratio of 0.57. The sand density was controlled by maintaining a nearly constant drop height and rate. Sand was pluviated into the model container in successive layers, with each layer followed by leveling of the surface using a vacuum. Each lift corresponded to the elevation of a horizontal instrument array. Key properties of Nevada sand are summarized in Table 3.2 (Arulmoli et al. 1992). The sand layer was subjected to a vacuum of about 90 kPa and then flushed with carbon dioxide. After repeating this procedure twice, the sand layer was saturated under a vacuum. Figures 3.9 through 3.14 present photographs of the calibration, pluviation, instrumentation, and saturation processes.

Table 3-2. Properties of Nevada Sand (Arulmoli et al. 1992)

Property	Value
Grain size, D_{10}	0.09 mm
Grain size, D_{50}	0.15 mm
Specific gravity, G_s	2.67
Maximum void ratio, e_{max}	0.887
Minimum void ratio, e_{min}	0.511
Permeability at 1 g for D_r = 91%	2.3×10^{-5} m/s

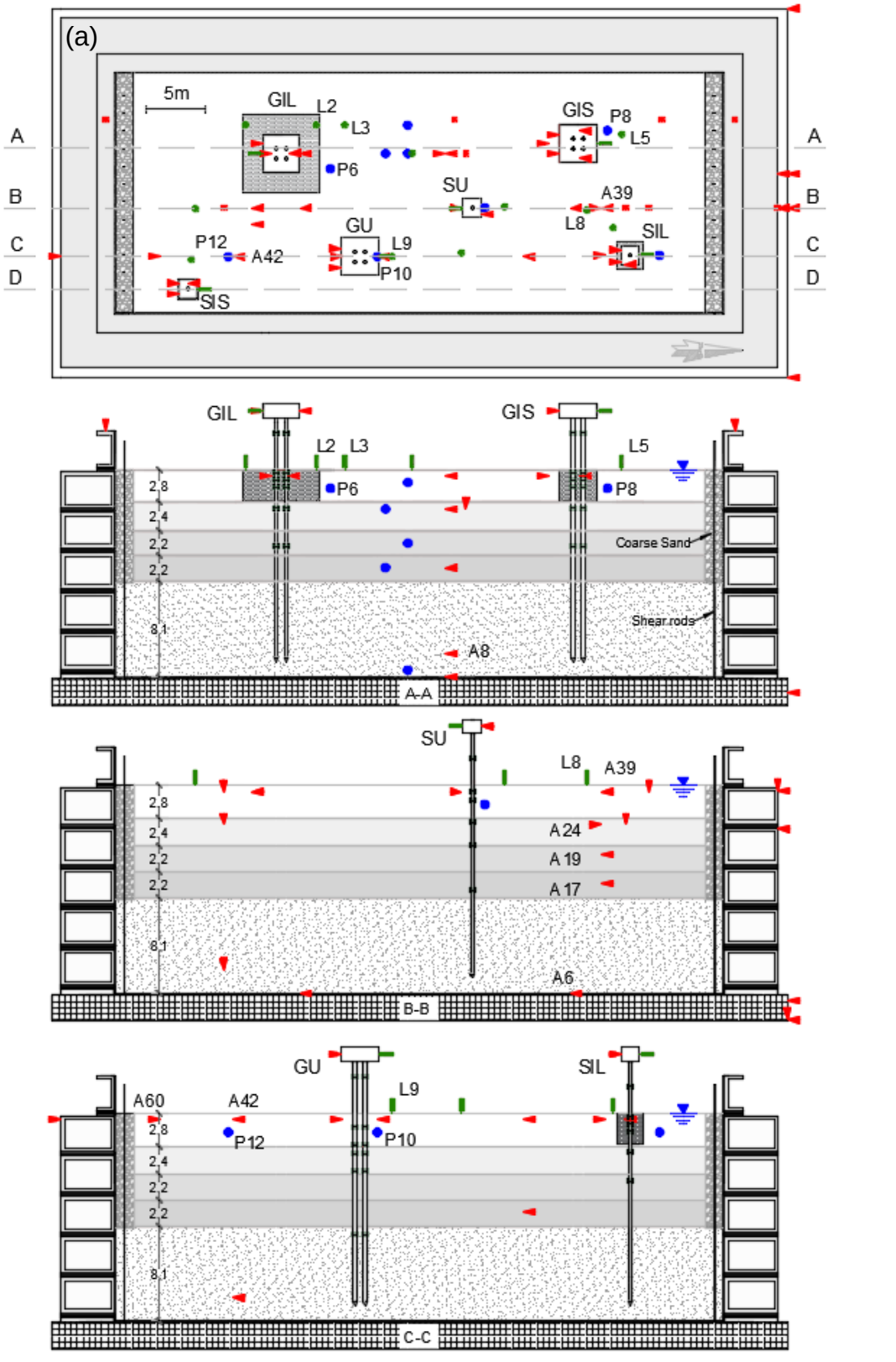
(a)
5m
GIL
L2
L3
P6
GIS
P8
L5
SU
A39
L8
SIL
GU
L9
P10
P12
A42
SIS
A
B
C
D
Coarse Sand
Shear rods
A8
A-A
A24
A19
A17
A6
B-B
A60
C-C
Horizontal Acc
Vertical Acc
Horizontal LP
Vertical LP
PPT

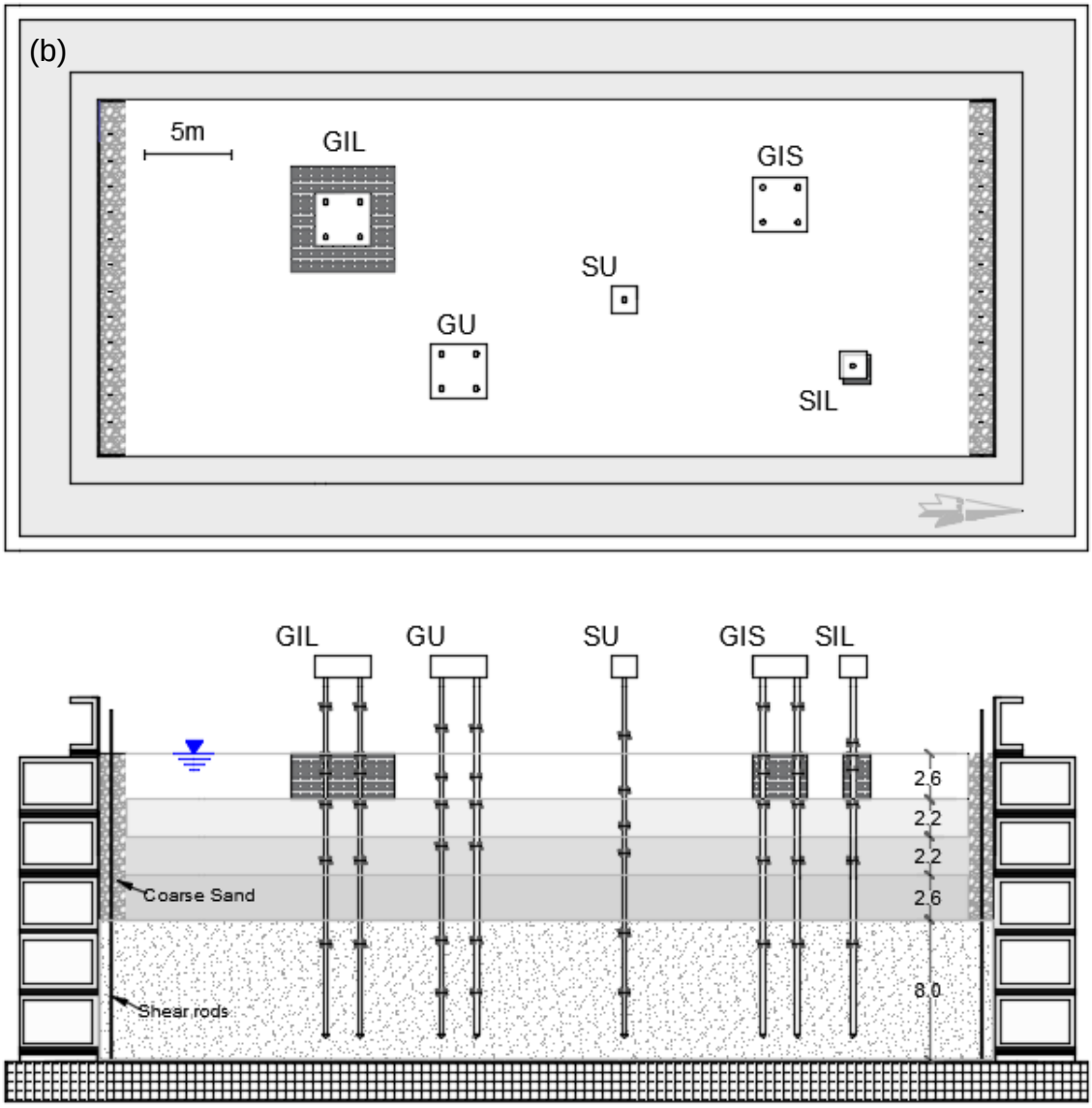

Figure 3-7. Cross Sections and Plan View of the Centrifuge Model Set-Up for Single Piles and 2×2 Pile Groups with (a) 3D Spacing-ATA02; and (b) 7D Spacing-ATA01 (All Dimensions are in m)

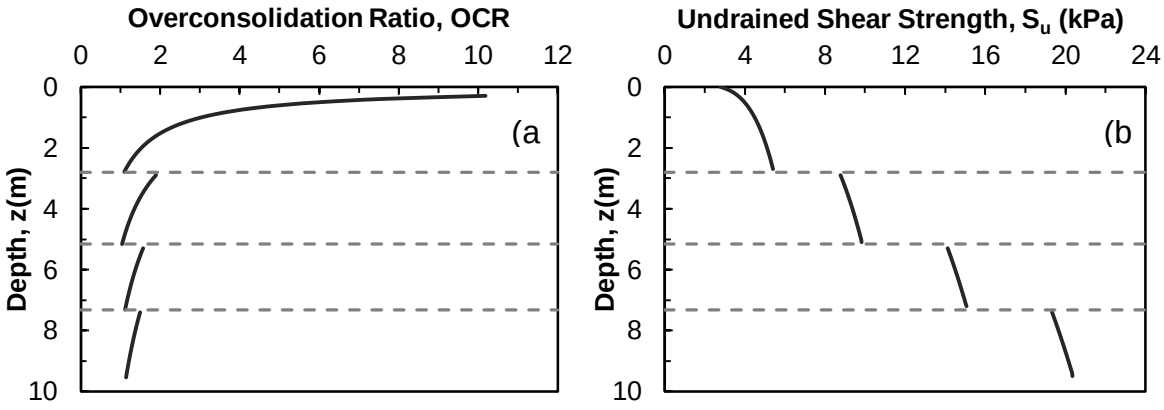

Figure 3-8. (a) Overconsolidation Ratio and; and (b) Undrained Shear Strength Profiles for the Second Centifuge Test-ATA02

Figure 3-9. Sand Pluviator

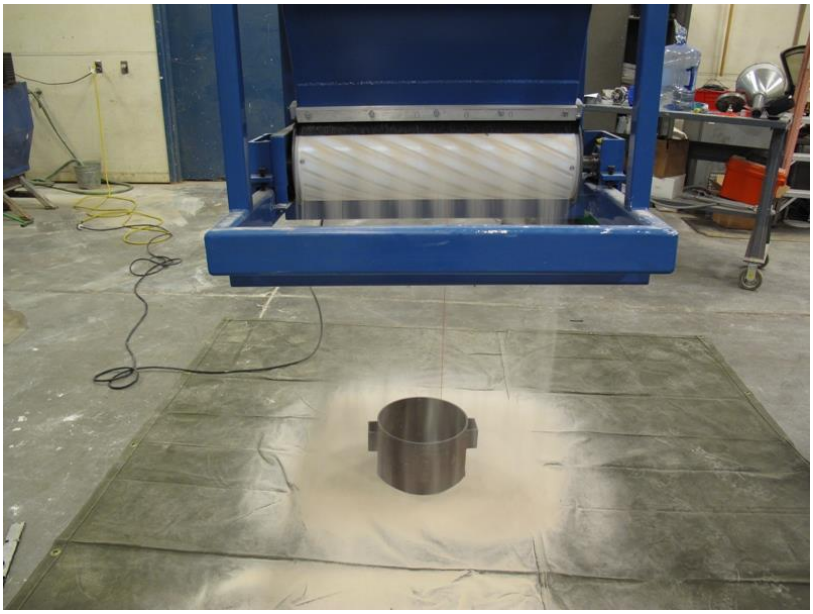

Figure 3-10. Calibrating the Sand Pluviator

Figure 3-11. Nevada Sand Pluviation

Figure 3-12. Dense Nevada Sand Layer Graded using a Vacuum

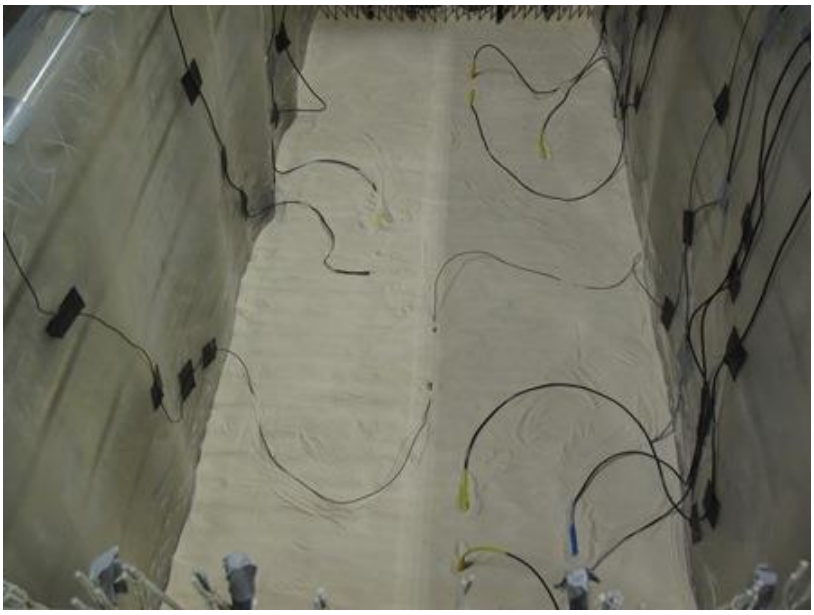

Figure 3-13. Placement of Instruments in Dense Nevada Sand Layer

Figure 3-14. Saturation of Sand Layer

In order to prepare soft clay layers and satisfy the requirements of the testing soil, i.e., low strength and acceptable permeability, a commercially available Kaolin (No. 1 Glaze Clay from Old Hickory Clay Company in Hickory, Kentucky) and a fine sand (D_{50} = 0.14 mm) from George Townsend Co., Inc. in Oklahoma City, Oklahoma (Quikrete Commercial Grade Fine White Sand, No. 1961-55) were selected for mixing. The mixture consisted of 1:1 Kaolin/sand by weight. Mixing was carried out under vacuum with an initial water content of 64% (twice the Liquid Limit). Key properties of the mixed soil (USCS classification CL) are given in Table 3.3. The soft clay slurry was then placed in the model container to a predetermined initial height and consolidated in a hydraulic press at 1 g with the specific consolidation pressures. The consolidation was accelerated through filter papers placed on top and the bottom of each layer and the coarse loose sand at both ends of the container (see Figures 3.7 and 3.12). Settlements

and pore water pressures in the clay were measured to monitor the progress of consolidation. In general, 4 days of consolidation time was required for each clay layer to achieve an average degree of consolidation of at least 98% resulting in a final clay thickness of about 9.6 m (320 mm in model). Figures 3.15 through 3.20 present photographs of the soft clay preparation and instrumentation process.

Table 3-3. Properties of Soft Clay

Property	Parameter	Value
Specific Gravity	G_s	2.7
Liquid limit	LL	32
Plastic limit	PL	15
Normally consolidated strength ratio	$(S_u/\sigma'_{v0})_{NC}$	0.22
Plastic volumetric strain ratio	Λ	0.80
Compression index	C_c	0.42
Swelling Index	C_s	0.04

Figure 3-15. Soil Mixer used for Preparing Soft Clay

Figure 3-16. Gentle Pouring of Soft Clay on Filter Papers

Figure 3-17. Leveling Soft Clay Surface

Figure 3-18. Soft Clay Layer under Hydraulic Press

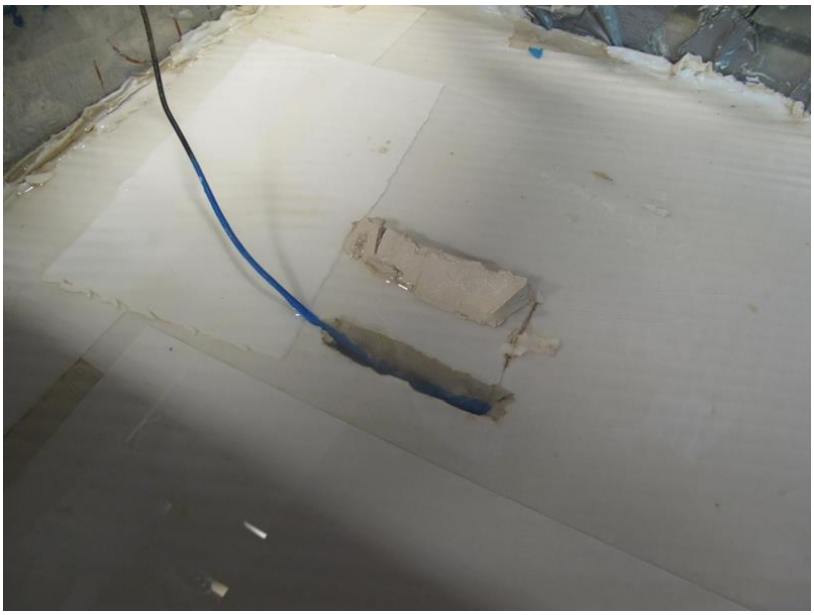

Figure 3-19. Placement of a Pore Pressure Transducer inside Soft Clay

Figure 3-20. Final Soil Profile

To obtain the desired overconsolidation ratio (OCR≈1.1) at the bottom of each soft clay layer, the model was reconsolidated under its self-weight in the centrifuge at 30 g. The resulting OCR profile is shown in Figure 3.8a; the discontinuous nature of the OCR profile is the result of using different successively lower hydraulic press pressures during slurry consolidation of each layer at 1 g. Linear potentiometers and pore pressure transducers were used to monitor the degree of consolidation in the centrifuge. Testing of the piles began after the average degree of consolidation reached about 95%. On average, it took about 8 hours of spinning to reach the desired overconsolidation ratio and degree of consolidation during each test.

3.3.1 Deep Mixing with Cement

Following consolidation in the hydraulic press and prior to reconsolidation at 30 g, a laboratory equivalent of Cement Deep Soil Mixing (CDSM) was used to improve

the manufactured soft clay at 1 g. CDSM has proven useful in increasing the stiffness and strength of soil (Bruce et al. 2013; Kitazume and Terashi 2013; Mitchell 2008; Puppala et al. 2008). Equal amounts (by weight) of Kaolin and fine sand were mixed together with deionized water (pH=7.0) to obtain a water content of 34%. This water content was the average water content after soft clay consolidation occurred in the hydraulic press.

Once the soil was mixed using a kitchen dough mixer for 10 minutes, equal (by weight) amounts of water and Type I Portland cement to obtain 10% cement content were mixed separately and transferred to the mixer and mixed with unimproved soil for 10 minutes. The goal was to obtain a uniformly treated cementitious soil matrix (commonly called soilcrete) with no lumps of soil or slurry and with uniform moisture content and a uniform distribution of binder throughout the soilcrete. The kitchen dough mixer was found to be useful in obtaining a uniform soilcrete in the laboratory. The properties of CDSM based on standardized definitions (Bruce et al. 2013; Filz et al. 2005) are given in Table 3.4.

Table 3-4. CDSM Properties Based on Standardized Definitions

	Water-to-cement ratio of the slurry	Cement factor (kg/m^3)	Cement factor in-place (kg/m^3)	Volume ratio	Cement content on dry weight basis (%)	Total-water-to-cement ratio
Definition	$w{:}c=\frac{w_{w,slurry}}{w_c}$	$\alpha=\frac{w_c}{v_{soil}}$	$\alpha_{in\text{-}place}=\frac{w_c}{v_{mix}}$	$VR=\frac{v_{slurry}}{v_{soil}}$	$a_w=\frac{w_c}{w_s}$	$w_T{:}c=\frac{w_{w,mix}}{w_c}$
Value	1.0	138	101	18.5	10	4.4

Right before the preparation of the soilcrete, soft clay in the centrifuge model was excavated from the top. Rectangular, bottomless aluminum molds were used as

guides and excavation support at predetermined locations to facilitate removal of clay and reach the desired dimensions (Figure 3.21). The soilcrete was then added in layers and lightly tamped and compacted to avoid any large voids or honeycombs within the CDSM blocks (see Figure 3.22). After placing the soilcrete, the top surface of the blocks were graded and the aluminum molds were removed. The soilcrete was placed for all the blocks at a temperature of about 25^{o} C. All the CDSM blocks cured in situ under water for 28 days before any tests were conducted. A similar procedure was used to prepare and cure improved clay samples in laboratory for Unconfined Compressive Strength testing. Several samples were tested and the 28-day compressive strength of samples was found to be 760 kPa. Figure 3.23 shows the stress-strain (q- ε_1) behavior of unimproved and cement-improved soft clay obtained from isotropically-consolidated undrained compression (CIUC) triaxial tests, where q is the deviatoric stress and ε_1 is the axial strain (Thompson 2011). Initial effective confining pressure values (p') for each sample prior to shearing is also shown in Figure 3.23. As expected, the unimproved soil shows the influence of initial confining pressure, while the behavior of the improved soil is essentially independent of the confining pressure.

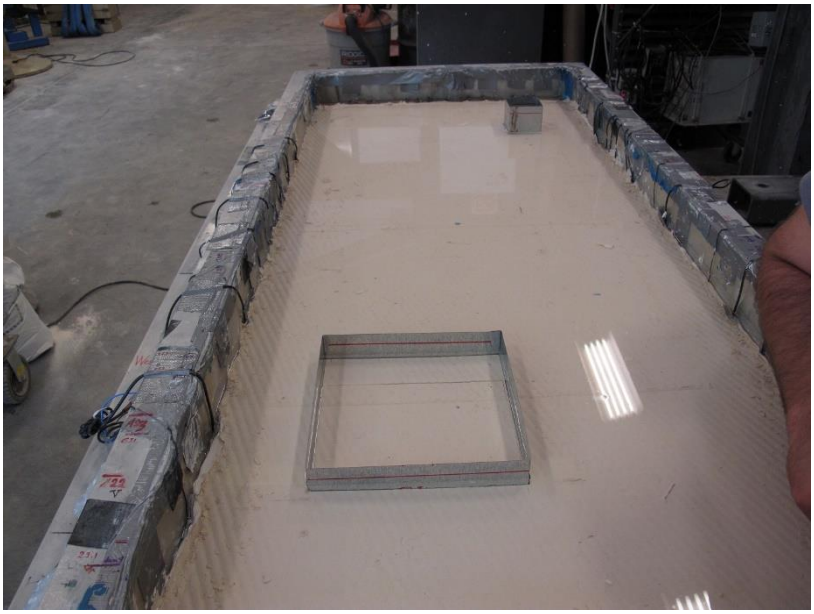

Figure 3-21. Molds as Guides and Excavation Support

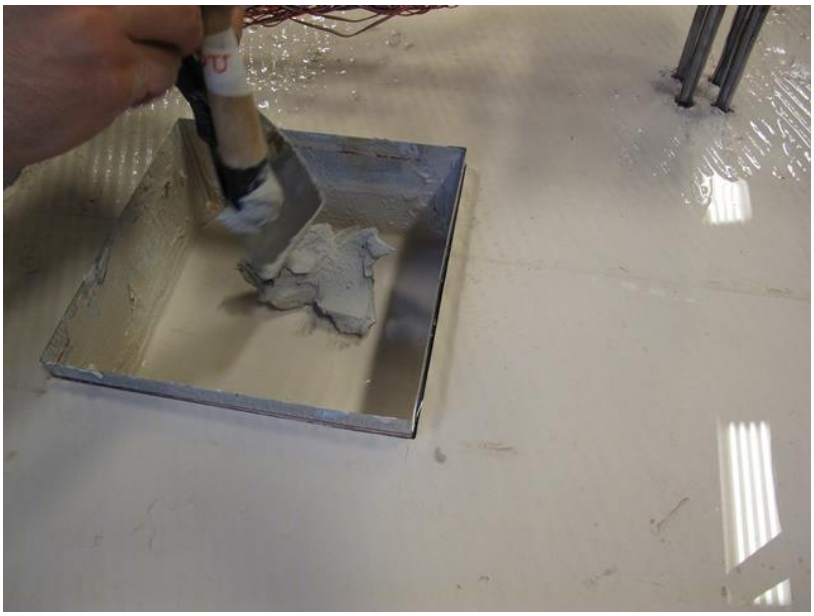

Figure 3-22. Improving Soft Clay in Predetermined Locations

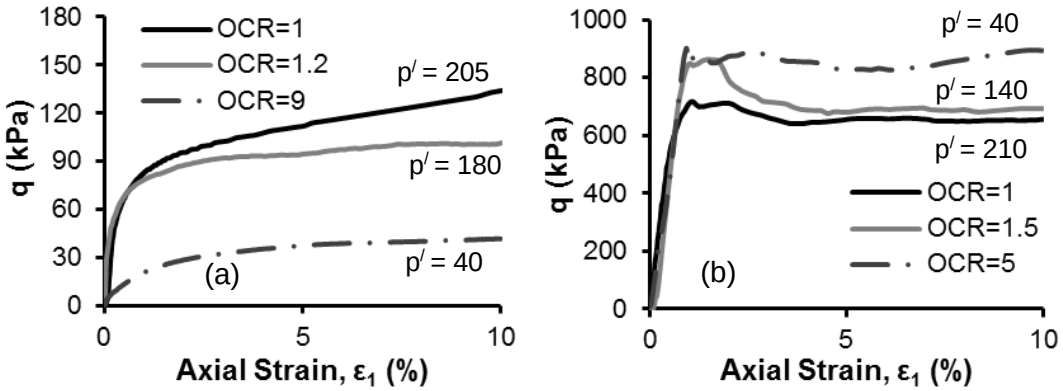

Figure 3-23. The Stress-Strain Behavior obtained from Isotropically-Consolidated Undrained Compression (CIUC) Triaxial Tests an (a) Unimproved Clay; and (b) Cement Improved Clay; p' Values are in kPa (Thompson 2011)

Two separate centrifuge models were tested for 7D and 3D pile spacings. The CDSM block dimensions and locations used in both the tests are given in Table 3.5 and shown in Figure 3.7. Note that the CDSM block dimensions for single piles used in both tests represent the corresponding tributary areas of a pile in the corresponding GIS pile groups. The CDSM procedure used in the centrifuge tests models field cases where wet soil mixing is used to improve the ground prior to installation of new pile foundations (Bruce et al. 2013; Kawasaki et al. 1981; Kitazume and Terashi 2013; Lorenzo and Bergado 2006; Maher et al. 2006; Porbaha 2006; Puppala et al. 2008). It is obvious that Deep Mixing Method (DMM) or CDSM cannot be used for existing pile foundations. Jet grouting (Burke 2004; Burke 2012; Clemente et al. ; Essler ; Shibazaki 2003; Yoshida 2012) is one of the most commonly used techniques to improve existing pile foundations because the grout can be pumped between the piles. The ultimate objective of all of these techniques is to improve the strength and stiffness of a weak soil and

therefore the results of the centrifuge tests presented in this study should be applicable to variety of ground improvement techniques.

Table 3-5. CDSM Block Dimensions for Different Pile Foundations

	First Series of Tests (s=7D)	Second Series of Tests (s=3D)
GIS	11D×11D×9D	11D×11D×9D
GIL	23D×23D×9D	23D×23D×9D
SI	5.5D×5.5D×9D	8D×8D×9D

3.3.2 Soil and Pile Characteristics

The undrained shear strength profile of unimproved clay was calculated based on the assumption of normalized behavior implied by the following function (Ladd et al. 1977; Wroth 1984):

$$S_u/\sigma'_{v0} = (S_u/\sigma'_{v0})_{NC} \times (OCR)^{\Lambda} \quad (3.1)$$

where σ'_{v0} is in situ vertical effective stress; $(S_u/\sigma'_{v0})_{NC}$ is normally consolidated strength ratio; OCR = overconsolidation ratio; and Λ = plastic volumetric strain ratio. The OCR profile of the centrifuge clay layer is shown in Figure 3.8(a) and the values of other parameters in Equation (3.1) are given in Table 3.3. These parameters were obtained using isotropically consolidated undrained compression (CIUC) triaxial tests (Thompson 2011) and verified by a bounding surface elastoplastic constitutive model (Dafalias and Herrmann 1986). The undrained shear strength profile calculated using Equation (3.1) is shown in Figure 3.8(b). Zhang et al. (2011), Afacan et al. (2014), and Boulanger et al. (1999) showed there is a good agreement between undrained shear

strength values obtained from this equation and directly measured values obtained from T-bar tests in soft clay profiles.

The model piles were fabricated from a hollow steel tube instrumented with six pairs of strain gauges at different levels to enable bending moment determinations through flexural strain measurements along the pile. The prototype values of the yield and ultimate flexural moments of the steel tube closely matched those of the Caltrans (California Department of Transportation) steel pipe pile PP14. The steel conformed to ASTM A513 Grade 1010 specifications and had an average yield stress of 260 MPa based on the 0.2% offset criteria. At each level, two active strain gauges were glued onto the opposite sides of the model pile to form a Wheatstone half bridge circuit. The instrumented pile was protected by a very thin layer of plastic shrink wrap.

The calibrated factors for strain gauges were obtained using two different procedures. In the first method, each pile was cantilevered from the pile cap and a known weight was hanged from a location near the pile tip. The advantage of this method of calibration is that it eliminates the problem of deviations from the alignment of the piles in the cap which can lower the sensitivity of the gauges. The drawback is that the gauges located near pile tip receive lower amount of bending moments, thus decreasing the sensitivity of the gauges in this area. In the second method, the strain gauges were calibrated using a simply supported beam configuration. Three different amounts of vertical loads were applied to the beam (pile) and the gauge readings were recorded at each time. In both methods, bending moments were calculated at the locations of gauges and the calibration factors were obtained as the average slope between calculated bending moment and gauge readings in voltage.

The outside diameter (D) of the piles was 0.29 m and the wall thickness (t) was 0.027 m. The cross sectional area (A) of the pile was 2.17×10^{-2} m^2 and the second moment of area (I) was 1.84×10^{-4} m^4. The Young's modulus (E) obtained from coupon tests was 182 GPa. The yield bending moment obtained for the piles based on the moment-curvature analysis was 305 kN.m. The piles were 20.4 m long with the lower 16.0 m inserted into the soil. The pile caps were made of thick solid aluminum and placed at 4.4 m above the ground level (free length). The piles were tightly fixed through openings in the pile cap using screws. The mass of all pile caps was 30.5 kg. Single piles also had caps with a mass almost equal to ¼ the mass of pile group caps (7.5 kg). Once the ground was improved at the predetermined locations, the piles were driven into the profile at 1 g. A pile driving system consisting of a hammer and a guide rod was used for this purpose (see Figure 3.24). By dropping the hammer on the cushion from a constant height, all piles were driven to the desired depth. Although driving piles at 1 g instead of 30 g may alter the bearing capacity and the behavior of pile foundations, Craig (1985) showed that this difference would not be significant in clays because the volume change in clays during pile driving is small compared to sands. The final centrifuge model, before going on the centrifuge arm, is shown in Figure 3.25.

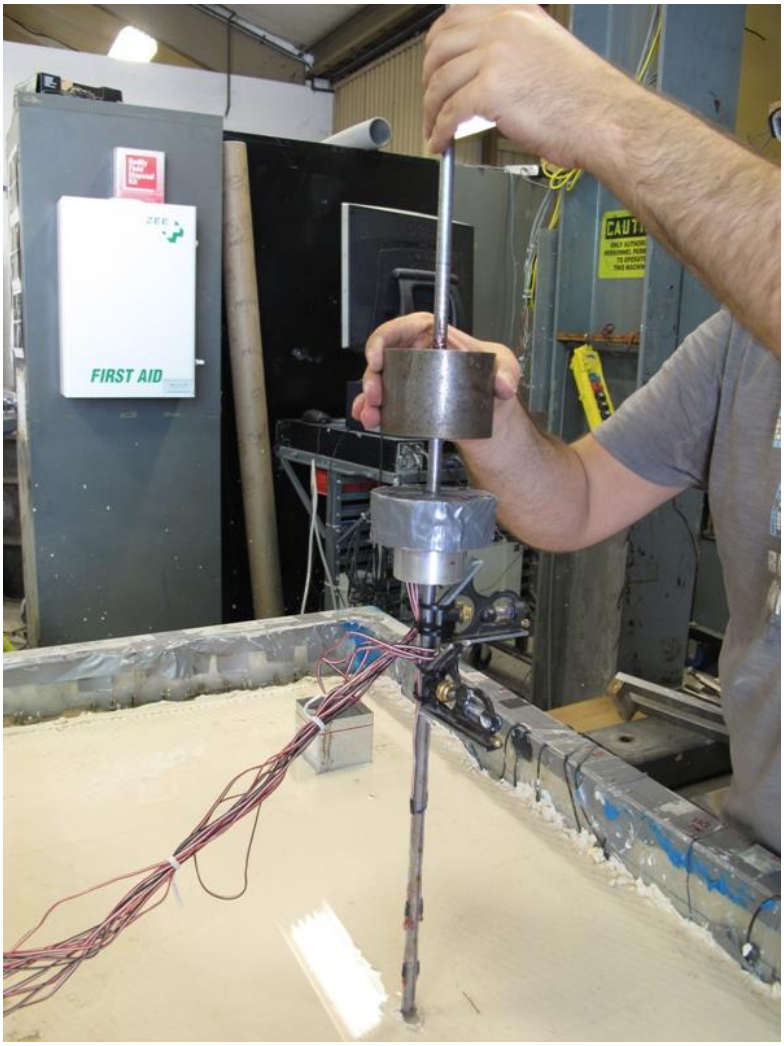

Figure 3-24. Driving Model Piles at 1 g

Figure 3-25. Centrifuge Model before Going on the Centrifuge Arm

The relative stiffness between the pile and the soil plays an important role in determining the behavior of pile foundations under lateral loading. The results of the current study are directly applicable to the foundation systems with similar relative stiffness values. A dimensionless parameter, $(E.I/A.t) / S_u.D$, can be used to capture the relative stiffness of the pile-soil system. The dimensionless parameter values for pile-soft clay and pile-CDSM were 248×10^5 and 5×10^5, respectively. The undrained shear strength ratio of improved to unimproved soft clay was 47 (380 kPa/8.17 kPa). Judgement and additional analyses are warranted in extrapolating the results presented in this study for other values of relative stiffness and undrained shear strength ratio.

3.4 Instrumentation

The model was instrumented with Micro-Electro-Mechanical Systems (MEMS) accelerometers, piezoelectric accelerometers, linear potentiometers (LPs), and pore pressure transducers (PPT). The instrumentation layout is shown in Figure 3.7(a). The detailed instrumentation layout and coordinates of the instruments are presented in Appendix A. The instrumented model on the centrifuge arm is shown in Figure 3.26. MEMS accelerometers were attached to the pile caps and piezoelectric accelerometers were placed in the CDSM blocks and also in soil to record acceleration responses. The base and container accelerations were also recorded using piezoelectric accelerometers. LPs were used to measure the soil profile and CDSM blocks settlement and also to record the transient and permanent horizontal displacements of the pile caps. PPTs were placed around the CDSM blocks and in the soil profile to record the excess pore water pressure (EPWP) generated during the seismic events. PPTs and LPs were also used to check the degree of consolidation before and during the tests.

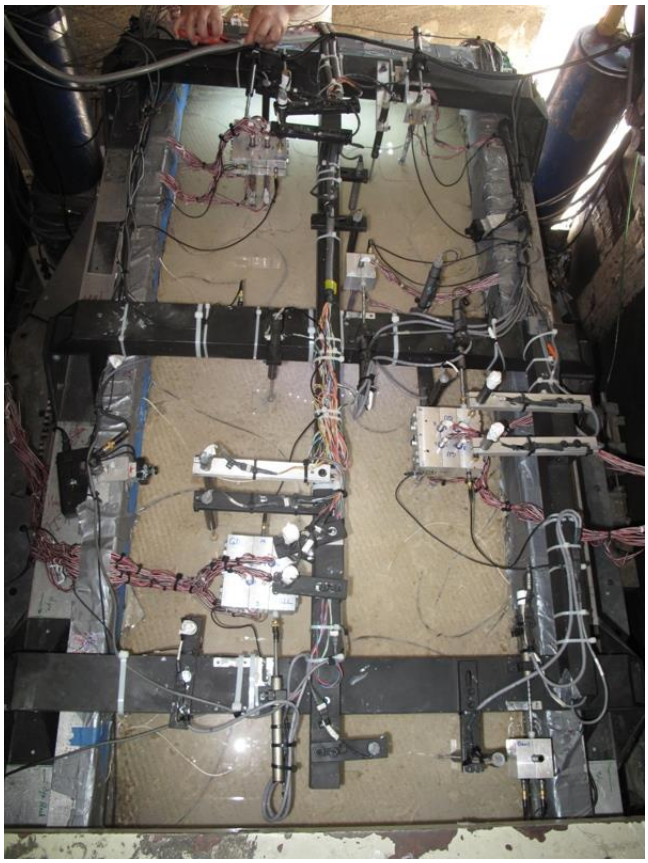

Figure 3-26. Instrumented Model on the Centrifuge Arm

3.5 Loading Sequence

After a minimum of 28 days of curing of the CDSM blocks, the clay was reconsolidated at 30 g as described previously and then two series of quasi-static tests were performed on the 7D and 3D pile groups in two separate centrifuge models. Similar lateral load tests were also performed on single piles for comparison purposes. Each lateral load test took several hours. Between each test, the centrifuge was stopped, the loading setup relocated to the next pile/pile group, the centrifuge was spun up, and soil reconsolidated before the next loading sequence. The first series of tests (7D tests) took about 6 days to complete and the second series of tests (3D) took about 12 days. Because an accident destroyed the 7D centrifuge model soon after initial lateral load

tests, only small amplitude tests were performed in the first series of tests. In the second series of tests (3D spacing), the pile foundations were first subjected to small amplitude quasi-static lateral loads, then to the earthquake base motions, and finally to large amplitude quasi-static lateral loads with deflections larger than the deflections experienced during seismic events. In both the series of tests, two different CDSM configurations were used for improved pile groups. Table 3.5 shows the dimensions of CDSM blocks with respect to the outside diameter of a single pile (D). Because the soil within the upper five to ten pile diameters dictate the lateral load response (Brown et al. 1988; Taghavi and Muraleetharan 2015c), soft clay was improved to a depth of 9D. Selecting this depth for ground improvement was also based on the parametric study performed during this study (see the Section CDSM Block Depth Effect in Chapter 5). GIL and GIS denote the Large and Small Improved pile Groups, respectively. SI and SU similarly represent the Single piles in Improved and Unimproved soil, respectively. Schematics of the first and second experimental models are provided in Figure 3.7, which includes important dimensions and the locations of selected instrumentation.

3.5.1 Quasi-static Loads

All tests were conducted under displacement control with a loading rate of 0.05 mm/s applied using a hydraulic actuator above the pile cap (see Figure 3.27). The loads and displacements were measured using a load cell and a linear variable differential transformer (LVDT), respectively. A single sine shaped displacement-time history (loading and unloading) was given as an input motion command to the actuator and the load was measured using a load cell. By multiplying displacement values by a constant

factor, the displacement amplitudes were changed to obtain the response at different deflection values. The results in chapters 4 and 5, however, are just presented for peak responses obtained during the loading part.

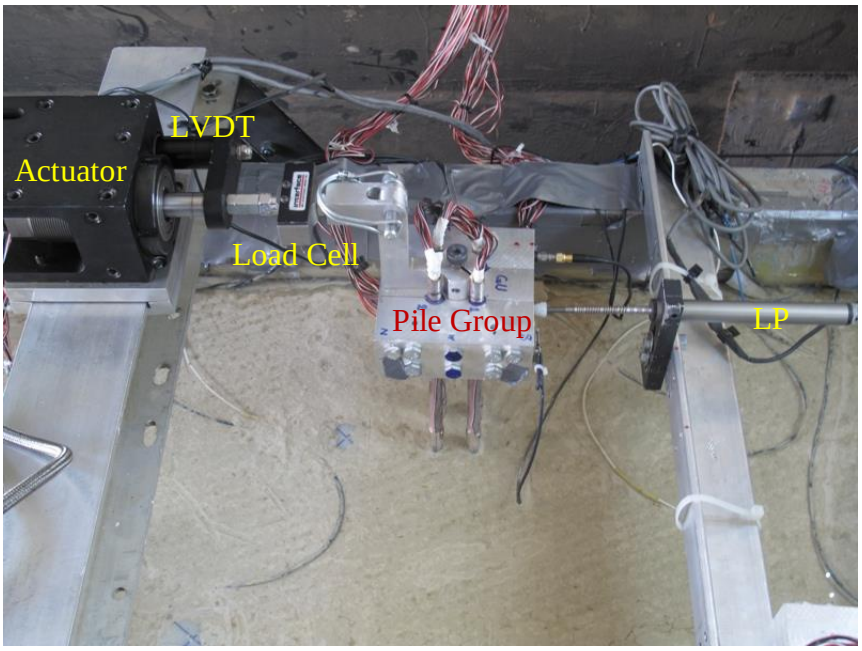

Figure 3-27. Loading Set-up for Quasi-static Lateral Load Tests

3.5.2 Earthquake Motions

The earthquake motions were applied to the model base over two days. On the first day, the model was subjected to different scaled versions of the recording from Port Island in the 1995 Hyogoken-Nambu (Kobe) earthquake (Events A-D). On the second day, the earthquake motions were different scaled versions of the recording from Santa Cruz in the 1989 Loma Prieta earthquake (Events E-G). A few very small amplitude step waves were applied before earthquake motions to check the functionality of the instruments. Earthquake motions were passed through a high-pass filter to remove low-frequency displacements that were outside the capacity range of the

centrifuge shaking table. Intensity variations (scaling) were performed by applying a linear scale factor to the acceleration–time history of the motion. Table 3.6 shows the order and characteristics of earthquake motions applied, which includes the peak acceleration (a_{max}), peak velocity (v_{max}), peak displacement (d_{max}), and Arias intensity (I_a). Figure 3.27 depicts response spectra of the motions. Each earthquake event was separated by sufficient time for dissipation of any shaking-induced EPWP. All response spectra in this study are obtained by applying 5% damping.

Table 3-6. Earthquake Input Motions Order Applied to the Base of the Container

Event	Motion	a_{max} (g)	v_{max} (cm/s)	d_{max} (cm)	I_a (m/s)
A	Kobe	0.026	4.01	0.98	0.009
B	Kobe	0.066	9.26	1.84	0.074
C	Kobe	0.160	22.23	4.66	0.489
D	Kobe	0.273	32.62	7.20	1.226
E	Santa Cruz	0.208	13.04	1.41	0.245
F	Santa Cruz	0.423	22.62	3.38	1.097
G	Santa Cruz	0.660	29.77	4.45	2.825

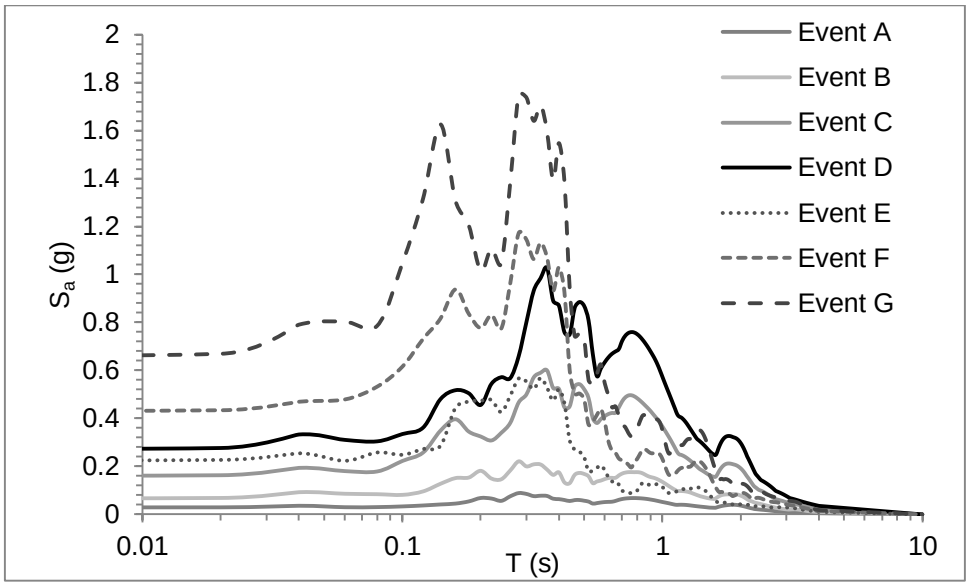

Figure 3-28. Acceleration Response Spectra (5% Damping) of Earthquake Motions Applied to the Base of the Container.

3.6 Signal Processing

A signal processing and double integration procedure was developed to obtain displacement-time histories from acceleration-time histories. A reliable double integration method was also needed for investigating container effects and uniformity of motions. Displacement-time histories tend to be dominated by low frequencies. However, acceleration-time histories cannot capture very low frequencies. Most piezoelectric accelerometers have an in-built high-pass filter to prevent signal drift. This high-pass filter in the analog circuit of the accelerometer; however, corrupts the amplitude and phase of signal near the corner frequency. A non-casual digital high-pass filter is; therefore, needed to remove the corrupted low frequency motion. Because typical earthquake records are band-limited below approximately 25 Hz, a Butterworth

filter with cut-off frequencies of 0.15 Hz and 25 Hz and an order of 4 was used for filtration. The selection of corner frequency and filter order was based on applying smallest possible amount of filtering while obtaining realistic displacement and velocity time series. By using this frequency range, reliable transient displacement-time and velocity-time histories were obtained. The high-pass cut-off frequency of 0.15 Hz was also recommended by Wilson (1998) for the same container and similar soil profile and earthquake motions. Considering the high number of acceleration records (about 1000 records), and because acceleration data had similar noise characteristics and was recorded and passed through similar instruments and electronic components, same signal processing and double integration method was used for all signals.

Figure 3.29 shows the displacement-time history for the pile cap of the GIL pile group recorded using a Linear Potentiometer (LP). The displacement-time history obtained by double integrating the acceleration using the aforementioned signal processing methodology is also depicted. There is a good agreement between both displacement-time histories.

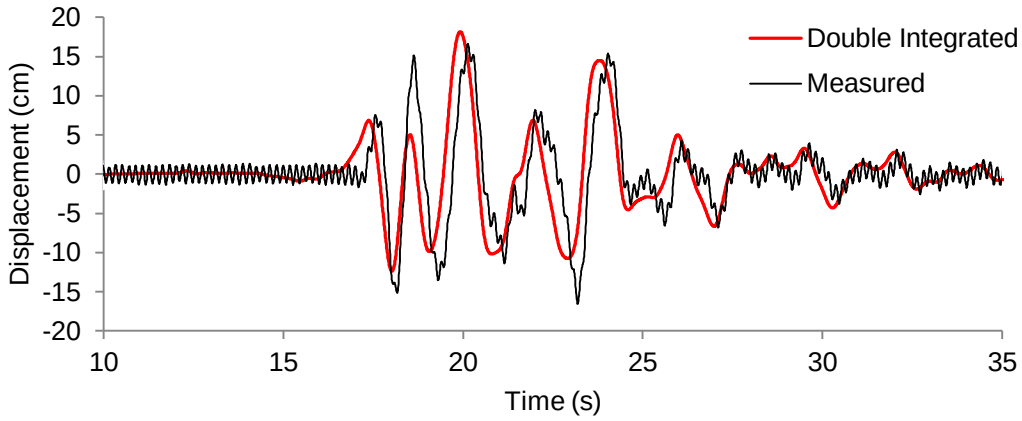

Figure 3-29. Displacement-Time History of the GIL Pile Cap obtained from Direct Measurement by a LP and by Conditioning and Double Integrating the Acceleration-Time History during Event D

3.7 Flexible Shear Beam Container - Soil Column Interaction

In order to reliably interpret the dynamic centrifuge tests, the behavior of the container and soil column system must be understood. Whitman and Lambe (1986), Van Laak et al. (1994), and Fiegel et al. (1994) are among the researchers who have looked into the interaction between a container and the soil column. Here we compare the horizontal motions of the soil column and the adjacent container ring.

Accelerometers were attached to the rings of the container at different levels. An accelerometer was also installed on the clay surface near the top ring (A60 in Figure 3.7a). Figure 3.30 shows the horizontal acceleration and displacement-time histories of the top ring and clay surface close to the top ring. This figure shows that the ring and clay surface acceleration waveforms are similar and the displacement-time histories are in good agreement. This confirms that the motion is uniform in the container-soil system. This illustrates that the shear rods at both ends of the container have provided

complementary shear stress at the soil-container interfaces and the soil column is deforming in shear as opposed to column bending (Taghavi et al. 2015a).

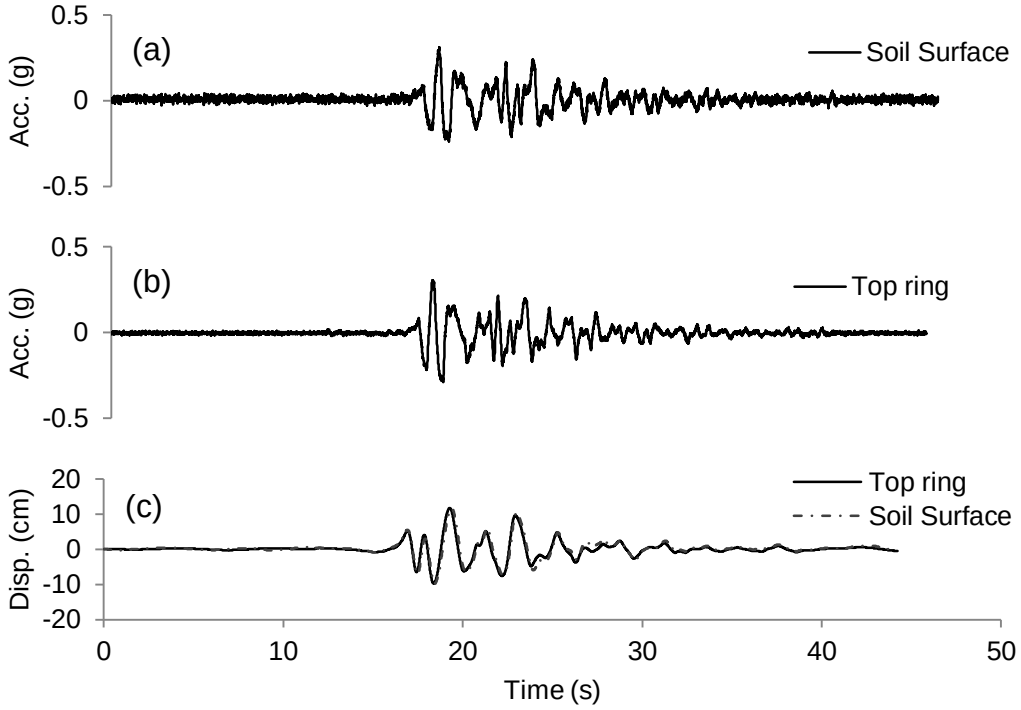

Figure 3-30. Horizontal Acceleration-Time Histories For: (a) Clay Surface Near the Top Ring; (b) The Top Ring; and (c) Displacement-Time Histories for the Top Ring and Clay Surface Near the Top Ring.

Chapter 4: Quasi-static Lateral Load Behavior of Pile Groups in Soft Clay Improved by Cement-Deep-Soil-Mixing: Centrifuge Tests

4.1 Overview

This chapter presents the results of quasi-static lateral load behavior of pile groups in unimproved and improved soft clay. The centrifuge test results revealed that the lateral resistance of the improved pile group at 7D spacing increased by 157%. Due to pile-soil-pile interactions, the lateral resistance in 3D pile group increased by only 112%. In both improved and unimproved pile groups with 3D spacing, the leading row of piles carried larger loads and bending moments than the trailing row of piles. No group interaction effects were observed in all pile groups with 7D spacing. At very large deflections, cracks developed and tension failure occurred in the CDSM block of the improved 3D pile group. Some results in this chapter are also reported in Taghavi et al. (2015b).

4.2 Load versus Deflection Responses

In order to study the failure mechanism of the improved pile foundations, the pile foundations in the second series of tests (3D spacing) were laterally loaded in small deflections as well as very large deflections. Because of the highly nonlinear elastoplastic behavior of soft clay in large strains, which significantly differs from the behavior in small deflections, load-deflection curves of pile groups are presented in both small and large deflection amplitudes. The peak total load versus deflection curves from the tests on the single piles and pile groups are shown in Figures 4.1 and 4.2,

respectively. All deflections represent the pile cap deflections at 3.5 m above the pile heads. Figure 4.1 shows, with the ground improvement, the improved single pile SI-1 has resisted 15.1 kN (at a deflection of 7.0 cm) compared to 9.3 kN for the single pile in unimproved soft clay. This represents an increase in lateral resistance of 62%. By increasing the lateral dimensions of the improvement zone from 5.5D to 8D in SI-2, the lateral resistance has increased by 19% with respect to the SI-1. The load-deflection curves of the unimproved single piles of first series of tests (SU-1) and second series of tests (SU-2) are in good agreement. This agreement validates the assumption that the soil profiles in both the tests were the same.

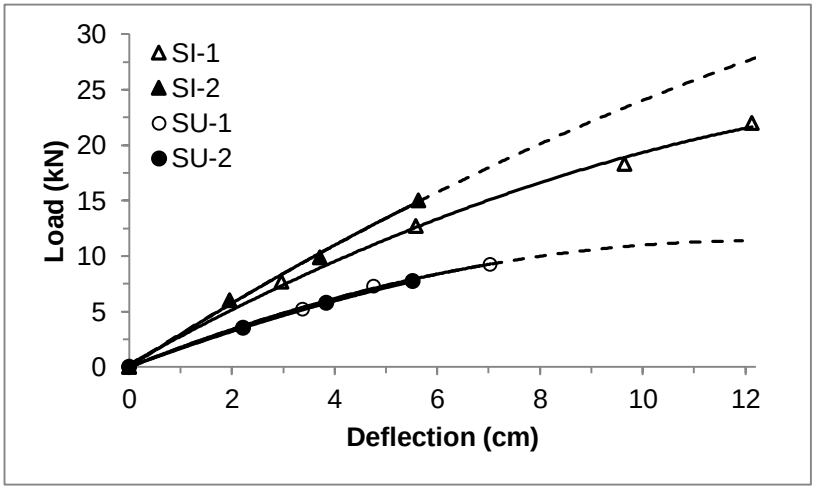

Figure 4-1. Load–Deflection Curves for the Unimproved and Improved Single Piles

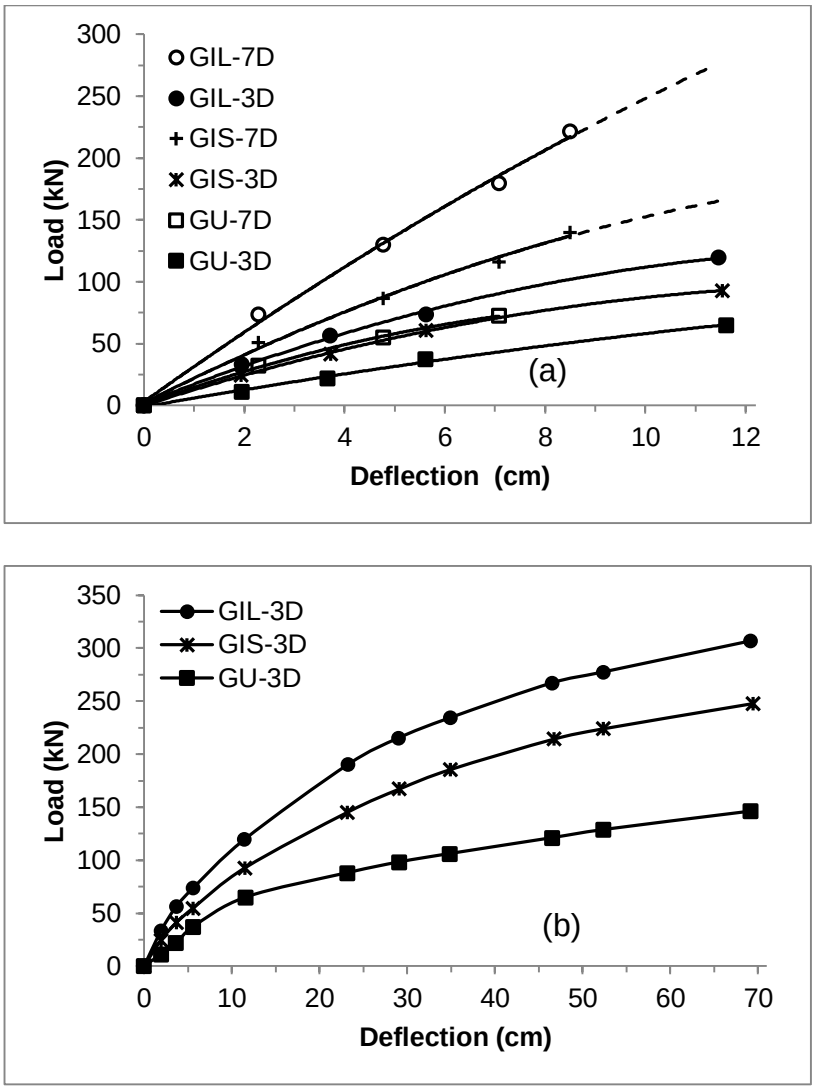

Figure 4-2. Load–Deflection Curves for the Unimproved and Improved Pile Groups at 3D and 7D Spacing: (a) Small Deflection; and (b) Large Deflection.

Similarly, CDSM blocks increased the lateral resistance of the pile groups. Figure 4.2(a) depicts load-deflection relationships for all pile groups in small deflections. In pile groups with 7D spacing, ground improvement increased the lateral resistance of the GIL and the GIS by 157% and 66%, respectively, in comparison to the unimproved case (at a deflection of 7.0 cm). In pile groups with 3D spacing, the lateral

resistance of the GIL and the GIS pile groups increased by 112%, and 65%, respectively. Increasing the dimensions of the improvement zone increased the lateral resistance. It is likely that pile-soil-pile interactions led to less increase in lateral resistance for 3D pile spacing. This phenomenon will be investigated further in subsequent sections. The load-deflection curves for pile groups at 3D spacing in very large deflections are shown in in Figure 4.2(b). At a deflection of 69 cm, the lateral resistance of the GIL and the GIS increased by 110% and 70%, respectively, in comparison to the unimproved case.

4.3 Maximum Bending Moment versus Load Responses

The maximum bending moment is the largest moment along the length of leading piles in each group and the load is the total load carried by that pile group. Maximum bending moment-load curves for all the piles are shown in Figure 4.3. In all three cases (GU, GIS, and GIL), the maximum bending moment increased as the spacing between piles decreased from 7D to 3D, indicating larger loads were carried by leading piles in 3D spacing. These curves suggest possible pile-soil-pile interactions at 3D spacing. When the piles are spaced closely in a pile group, the resistance provided by the soil adjacent to piles is reduced due to overlapping failure zones. This effect is more pronounced for trailing piles since soil in front of the leading piles is less disturbed and therefore, in closely spaced pile groups, leading piles carry more loads. This phenomenon is referred to as pile-soil-pile interaction and leads to shadow-effect and edge-effect reductions in pile group capacities. More interaction occurs in pile

groups with 3D spacing than the 7D spacing; thus, leading piles in 3D groups carry larger loads that results in larger bending moments as seen in Figure 4.3.

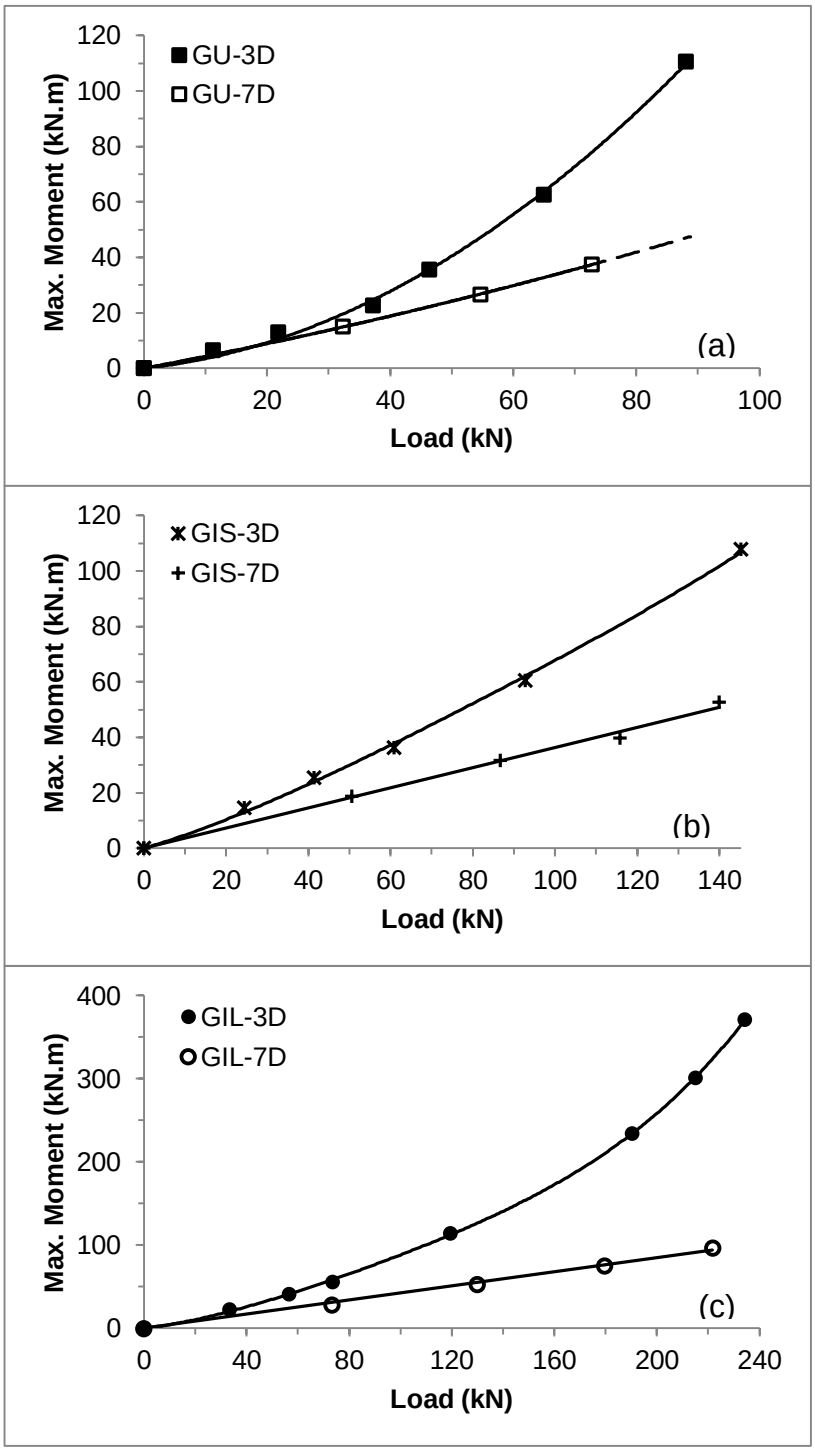

Figure 4-3. Variation of maximum leading pile bending moment with applied load for: (a) the GU pile group at 3D and 7D spacings; (b) the GIS pile group at 3D and 7D spacings; and (c) the GIL pile group at 3D and 7D spacings.

When the applied load increases, overlapping between the failure zones also increases, and consequently the difference between the maximum bending moments at 3D and 7D spacings also increases as seen in Figure 4.3. This effect is further investigated by calculating load distributions between piles in a group in Section 4.5.

4.4 Bending Moment versus Depth Curves

Bending moment versus depth curves are shown for the GIL and GU pile groups in Figures 4.4–4.6. Because some of the strain gage data from the GIS pile groups were deemed unreliable, these results are not presented. Curves are shown for leading and trailing piles of each group at different deflection levels. The maximum bending moments in both the leading and trailing piles in GIL-3D exceeded the yield bending moment of 305 kN.m at a deflection of 1.6 D. For the GIL and GU pile groups with the largest spacing (7D), the maximum moments for both leading and trailing piles are close to one another for a given deflection (see Figure 4.4). Figures 4.5 and 4.6 show bending moment profiles for leading and trailing piles at various deflection values for pile groups in unimproved (GU-3D) and improved (GIL-3D) soft clay, respectively. These profiles show that the depth to the maximum bending moment for GU-3D and GIL-3D piles are about 9 – 10D and 1– 2D below the ground surface, respectively. The bending moment increases with the applied deflection for both pile groups. For the same deflection, the piles in improved clay experienced higher bending moments than those in unimproved clay. This is as expected as the pile in unimproved clay would resist considerably less load as compared to the pile in improved clay at the same deflection, as illustrated in Figure 4.2. Both Figures 4.5 and 4.6 illustrate that a

reduction in the pile spacing from 7D to 3D leads to larger bending moments being mobilized in the leading row of piles at the same amount of deflection. Although this effect is more pronounced at larger deflections, it can be seen even at smaller deflections for 3D spacing. This once again points to pile-soil-pile interactions resulting in trailing row of piles carrying lower loads than the leading row of piles for 3D spacing.

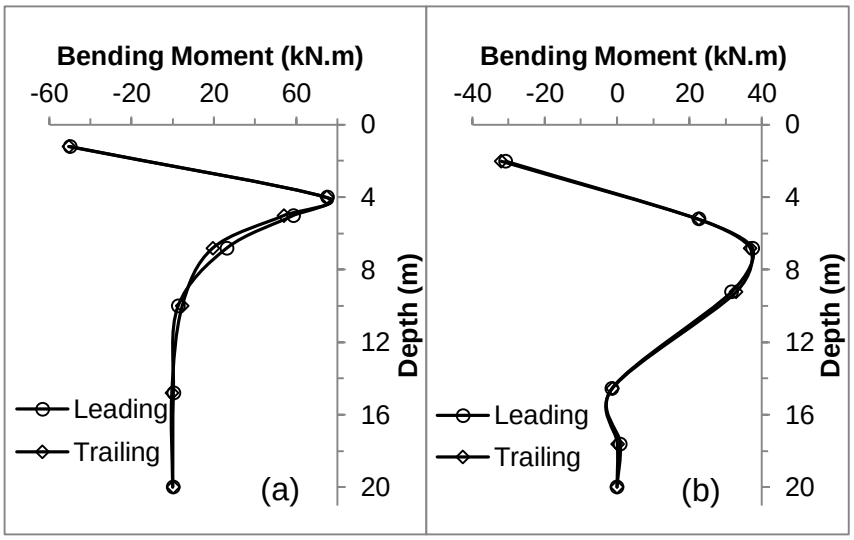

Figure 4-4. Bending Moment Distribution along Piles in 7D Group at a Deflection of 0.3D: (a) Improved Pile Group (GIL-7D); and (b) Unimproved Pile Group (GU-7D)

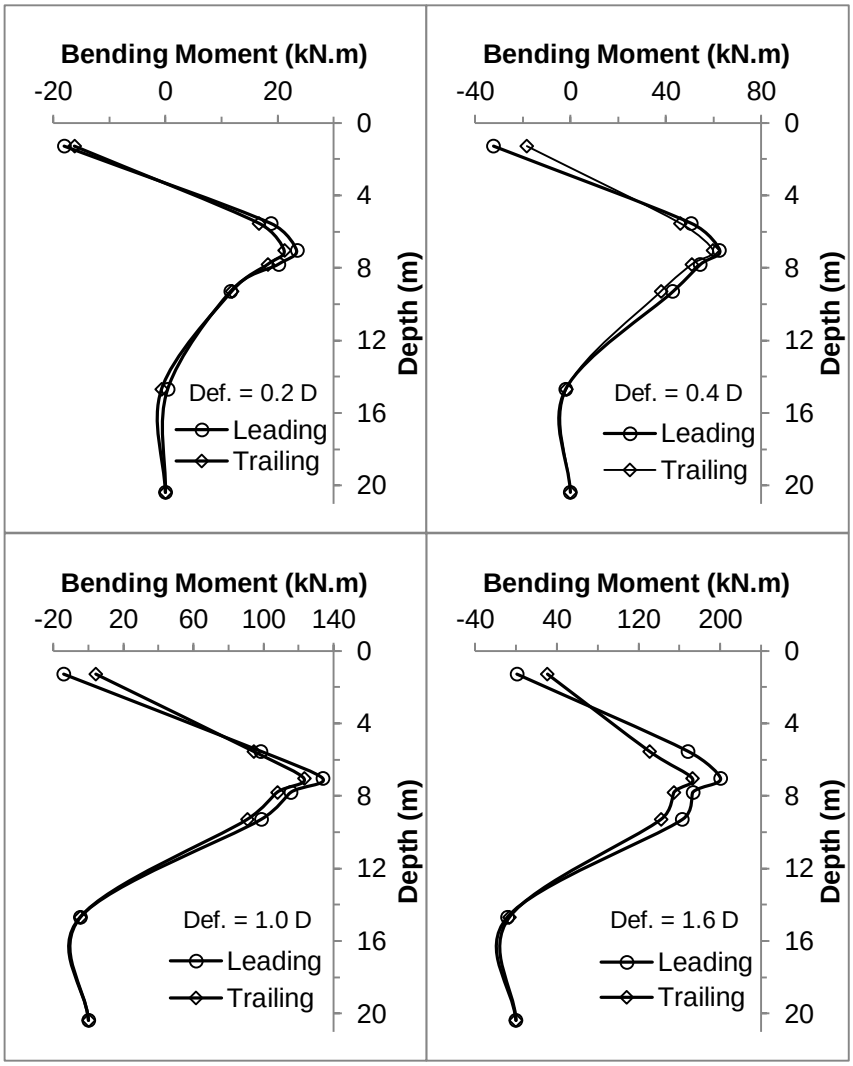

Figure 4-5. Bending Moment Distribution along the Piles in Unimproved Pile Group GU-3D at Various Deflection Values

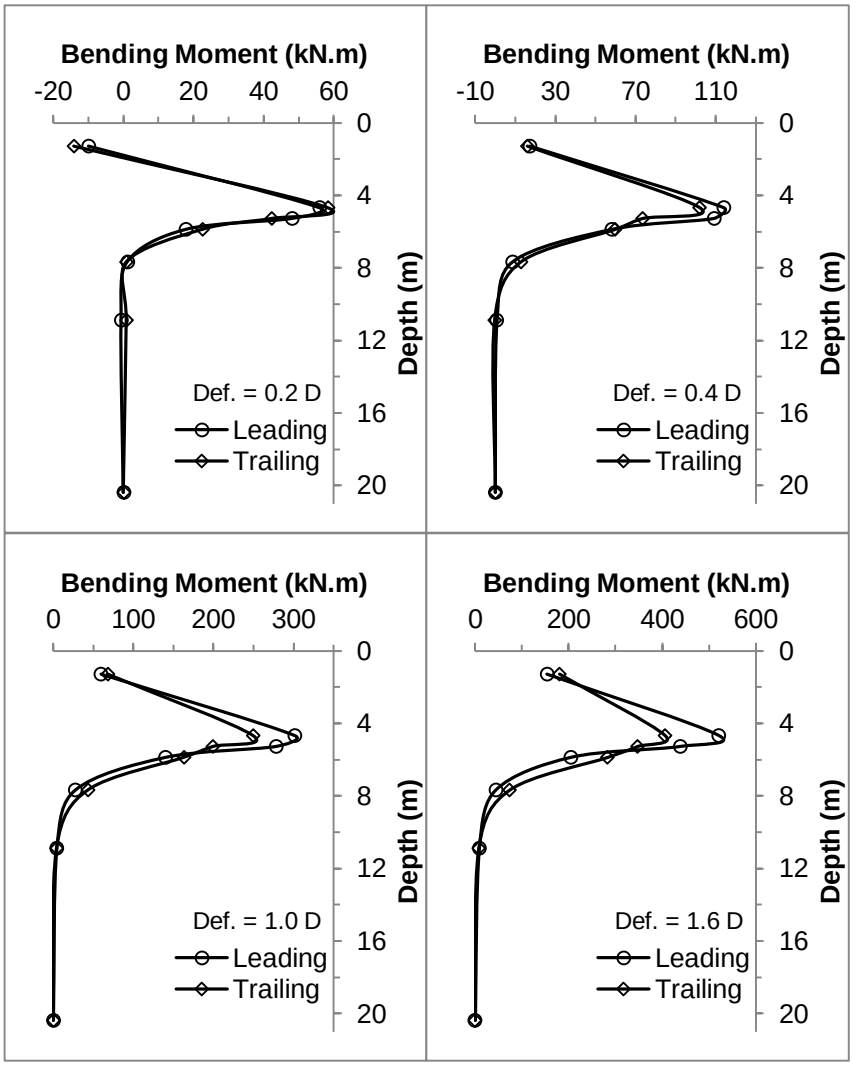

Figure 4-6. Bending Moment Distribution along the Piles in the Pile Group GIL-3D at Various Deflection Values

4.5 Load Distribution between Piles

Soil reaction (p) can be obtained by double differentiating the bending moment given by:

$$p = \frac{d^2}{dz^2} M(z) \tag{2}$$

A weighted residual approach is used for differentiating bending moment profiles. This method is proven to capture the second derivative of bending moment

more accurately than polynomial regressions in layered soils with nonlinear pile behavior (Brandenberg et al. 2010; Wilson 1998). Readers are referred to Brandenberg et al. (2010) and Wilson (1998) for details on applying this method to double differentiate discrete bending moment profiles. Figures 4.7(a) and (b) depict soil reaction profiles of the leading piles in GIL-3D and GIL-7D pile groups at 0.4D and 0.3D deflections, respectively. In both cases, significant amount of soil reaction can be observed in the improved zone indicating high resistance to piles against deflection within the improved zone. Soil reaction within unimproved soil layers is negligible. Even for smaller deflections, more soil reaction is seen in the GIL-7D group than the GIL-3D. This is again the reflection of the reduced soil resistance in the GIL-3D due to pile-soil-pile interactions for a given displacement.

By integrating soil reaction profiles, lateral loads carried by each pile can be deduced. Figures 4.8 and 4.9 show the lateral loads carried by the leading and trailing piles of the GU and GIL pile groups at 7D and 3D spacings, respectively. The average loads obtained by dividing the total loads by the number of piles in a group (4) are also depicted in these figures. In all pile groups, sum of the loads carried by each pile is equal to the total load of the group. In the GIL-7D and GU-7D groups, both leading and trailing piles carried approximately the same amount of loads at a given deflection. This indicates there are no group interaction effects in GU-7D and GIL-7D pile groups. However, at 3D spacing, leading row of piles in GIL-3D and GU-3D carried larger loads than the trailing row of piles. Difference between lateral loads carried by trailing and leading piles is small in small deflections and gets larger as the deflections get larger. This indicates pile-soil-pile interactions increases as the deflection increases.

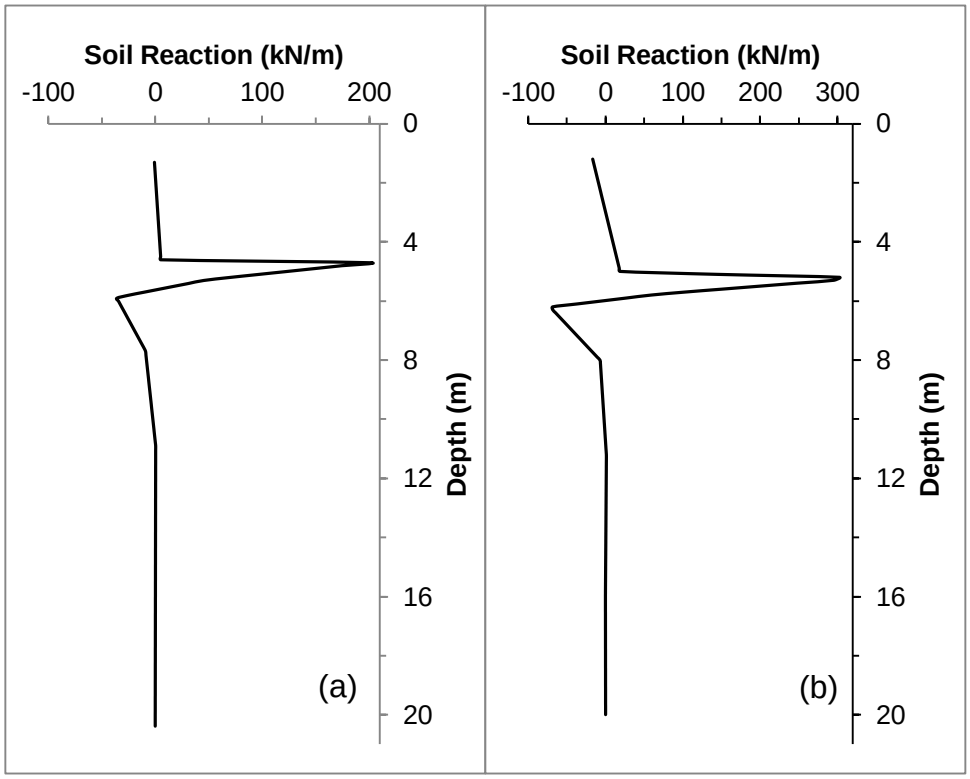

Figure 4-7. Soil Reaction Profiles obtained by Differentiating Bending Moment Data of Leading Piles using Weighted-Residual Method for (a) GIL-3D at 0.4 D Deflection, and (b) GIL-7D at 0.3 D Deflection

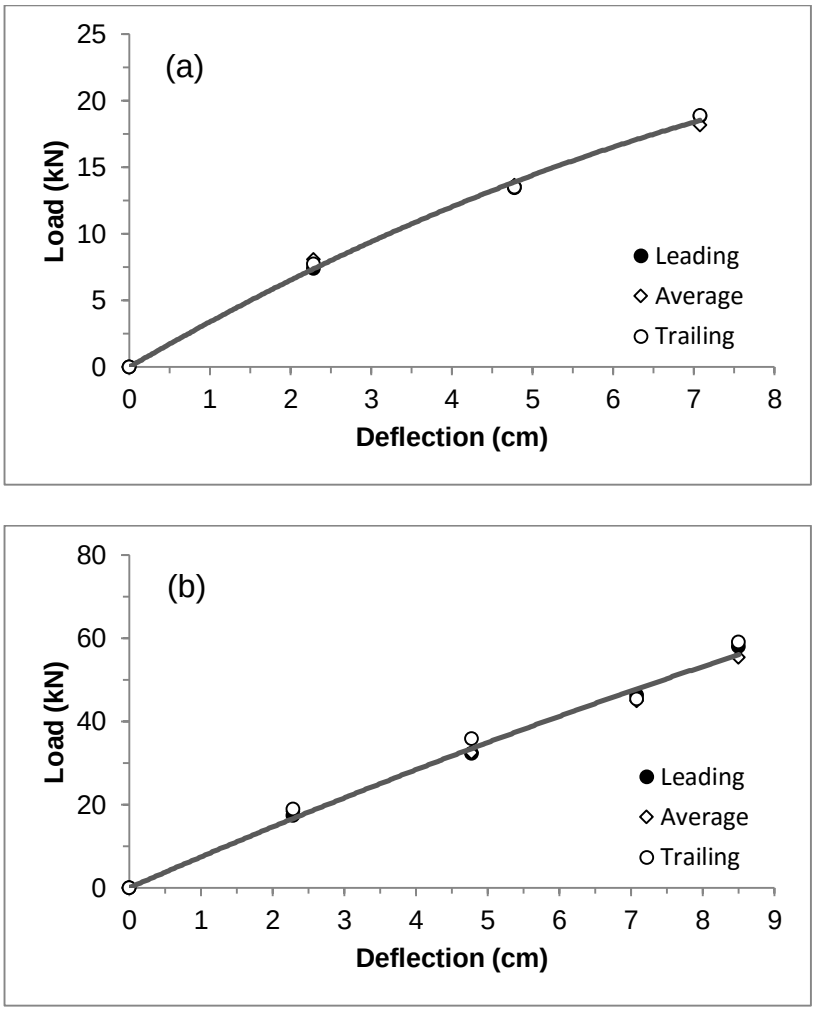

Figure 4-8. Load-Deflection Curves for Leading and Trailing Piles: (a) Unimproved Pile Group with 7D Spacing (GU-7D) and; (b) Improved Pile Group With 7D Spacing (GIL-7D)

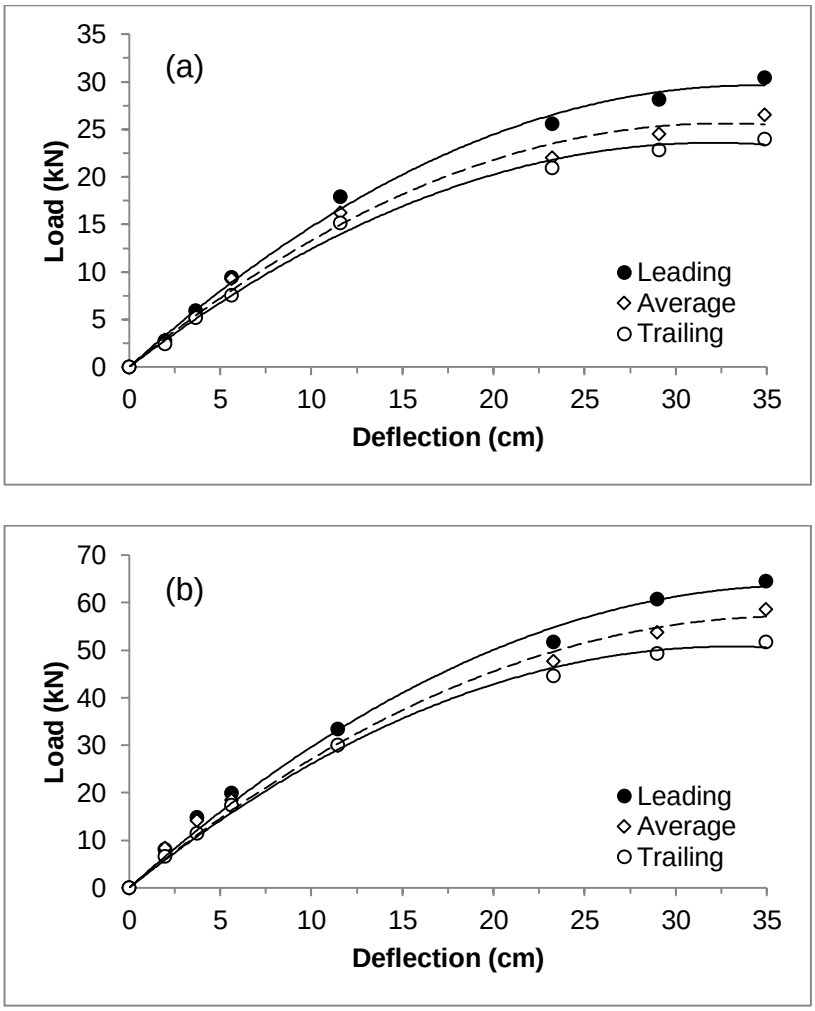

Figure 4-9. Load-Deflection Curves for Leading and Trailing Piles: (a) Unimproved Pile Group with 3D Spacing (GU-3D) and; (b) Improved Pile Group with 3D Spacing (GIL-3D)

4.6 Failure Mechanism of CDSM Blocks

The CDSM block failed in tension during lateral loading of the GIL-3D pile group at a deflection of about 80 cm. The failure is manifested in the load-deflection curve shown in Figure 4.10. As the deflection increased the load reached its maximum value and then reduced. Figure 4.11 shows the cracks developed in the failed CDSM block. The cracks are perpendicular to the direction of loading. The cracks initially formed at the interface between the piles and the CDSM block and then propagated to

the outside edges. As the deflection increased the cracks also propagated through the depth until a fracture occurred. The gaps formed between the piles and the CDSM block can also be seen in Figure 4.11. This is a classical tension failure where the failure plane is perpendicular to the direction of loading. When the horizontal loads transmitted to the CDSM block exceed the tensile strength of the improved soil, the CDSM block cracked. The tensile cracks will naturally form near the surface where the confining pressure from the soil that prolongs the CDSM block going into tension is the lowest. This failure mechanism should be considered in designing pile groups in CDSM improved soft clay subjected to large lateral deflections.

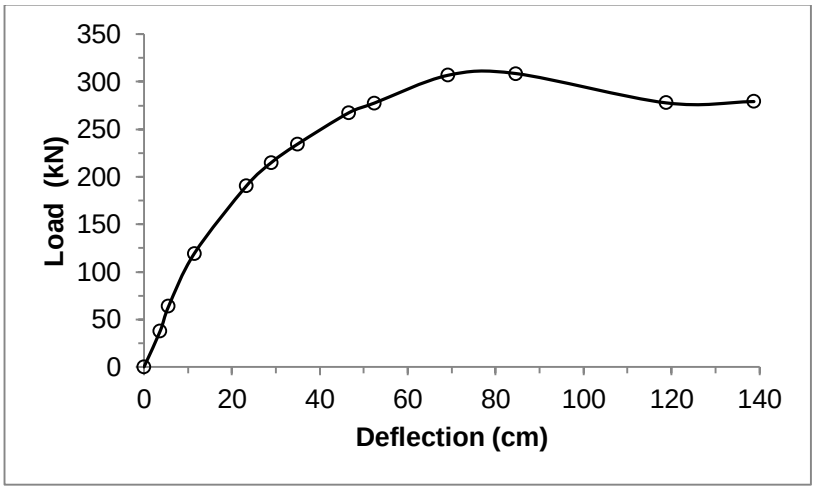

Figure 4-10. Load–Deflection Response of the GIL-3D Pile Group Showing the Failure Manifestation

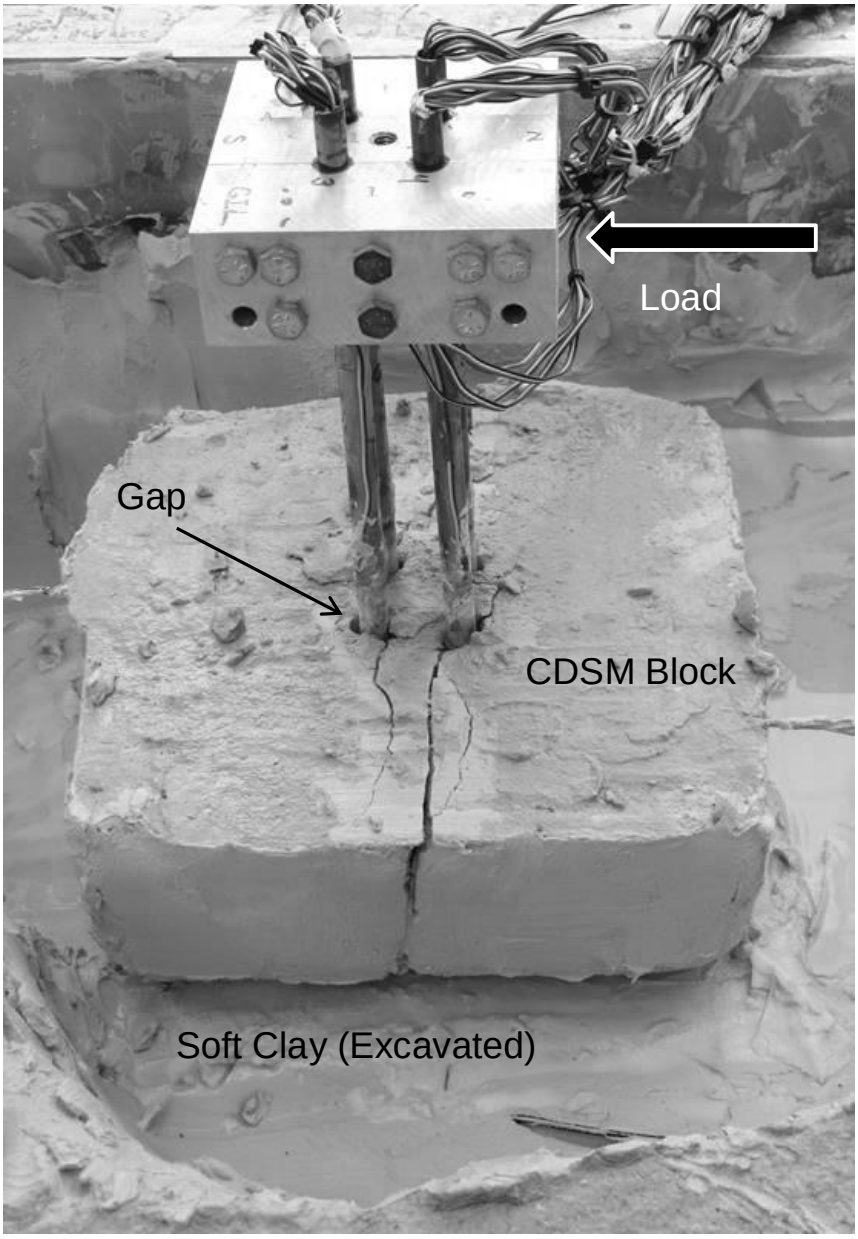

Figure 4-11. Tension Failure in the CDSM Block during Loading of the GIL-3D Pile Group

Chapter 5: Analysis of Laterally Loaded Pile Groups in Soft Clay Improved by Cement-Deep-Soil-Mixing

5.1 Overview

The use of p-multipliers in the analyses of lateral loading behavior of pile groups is based on the concept of modifying the single pile p-y curve to obtain that for a pile in a group (see Figure 2.6). The p-multipliers account for the reduced soil resistance mobilized at a given deflection due to overlapping of shear zones. Different factors can influence the p-multipliers; however, due to lack of experimental data, most researchers and design guidelines consider only the normalized pile spacing in the direction of loading in their recommendations. Reported in this chapter are the methods used to determine separate sets of p-multipliers for each row of the 2 × 2 pile groups as a function of pile spacing and clay stiffness. Computer analyses were performed to back-calculate the p-multipliers. Measured and computed lateral load-deflection, maximum bending moment-load, and bending moment-depth responses of the pile groups are presented. The computed results were obtained by the finite difference computer code GROUP (Reese et al. 2010) using the p-multipliers developed during this study. For the sake of comparison and also calibration of parameters needed for the analyses, the measured single pile results are also presented and compared with results computed by the finite difference computer code LPILE (Reese et al. 2004). The p-multipliers obtained in this study for stiff clay and soft clay for the 3D and 7D center-to-center pile spacings are compared with previously recommended values. Finally, a parametric study was performed on improved pile groups with 3D spacing. It was seen that for

CDSM block depths greater than 9D, increases in lateral resistance are practically negligible. At deflections less than 8 cm, lateral resistance of the improved pile groups is not sensitive to undrained shear strength of the improved clay representing typical cement contents. The centrifuge experiments and analyses described in this chapter represent, to the author's knowledge, the first study of pile-soil-pile interaction to explicitly include the effect of undrained shear strength of clay on p-multipliers. Some results in this chapter are also reported in Taghavi and Muraleetharan (2015c) and Taghavi and Muraleetharan (2014).

5.2 Factors affecting p-multipliers

The most important factor in determining p-multipliers is the pile spacing in the direction of loading (Brown et al. 1988; Brown et al. 1987; Chandrasekaran et al. 2010; Hannigan et al. 2006; Ilyas et al. 2004; Meimon et al. 1986; Reese and van Impe 2011; Rollins et al. 2006; Rollins et al. 1998; Rollins and Sparks 2002; Ruesta and Townsend 1997; Zhang et al. 1999). However, different researchers have mentioned or illustrated the effects of other parameters on p-multipliers. These parameters include pile spacing perpendicular to the direction of loading (Ashour and Ardalan 2011; Cox et al. 1984; Reese and van Impe 2011), type of soil and soil profile (Ashour and Ardalan 2011; Brown et al. 1988; Huang et al. 2001), pile arrangement in a group (Chandrasekaran et al. 2010; Ilyas et al. 2004), pile head fixity (Fayyazi et al. 2014), pile stiffness, width, and length (Brown et al. 1988; Rao et al. 1998), and the pile installation method (Brown et al. 2001; Huang et al. 2001; Reese and van Impe 2011). Moreover, p-multipliers vary along the length of a pile and also depend on the amount of lateral deflection (Brown et

al. 1987; Rollins et al. 2006). Most agencies and researchers (AASHTO 2012; FEMA 2012; Hannigan et al. 2006; Mokwa and Duncan 2005; Rollins et al. 2006; US Army 1993), however, have only considered the normalized pile spacing in the direction of loading in recommending p-multipliers for each row of piles. The p-multipliers suggested by different agencies and researchers for pile groups are presented in Table 5.1. Based on this table, there is a significant uncertainty in determining the p-multipliers for pile groups. For example, the suggested p-multiplier for the leading row of piles (Row 1) ranges from 0.33 to 0.87 for the normalized spacing of 3.

Table 5-1. Recommended p-multipliers for all soils

Pile group	S/D	*p*-multiplier (f_m)			Reference
		Row 1	Row 2	Row 3+	
2×2	3	0.87	0.68	---	Reese and van Impe (2011)
2×2	7	1.0	1.0	---	
Any group	3	0.79	0.57	0.41	FEMA (2012); Rollins et al. (2006)
	7	1.0	1.0	0.92	
Any group	3	0.8	0.4	0.3	AASHTO (2012); Hannigan (2006)
	5	1.0	0.85	0.7	
Any group	3	0.33	0.33	0.33	US Army (1993)[a]
	4	0.39	0.39	0.39	
	5	0.45	0.45	0.45	
	6	0.56	0.56	0.56	
	7	0.71	0.71	0.71	
	8	1.0	1.0	1.0	
Any group	3	0.8	0.6	0.45	Mokwa and Duncan (2005)

[a] US Army reported "group reduction factors" are same for all piles in a group

Due to lack of experimental data, analyzing pile groups in improved soils under lateral loading involves uncertainty and in most cases designs are conservative. This chapter utilizes the p-y curves and the p-multipliers to analyze the behavior of pile groups in improved and unimproved soft clay.

5.3 Analyses of Single Piles and Pile Groups in Improved and Unimproved Soft Clay

LPILE (Reese et al. 2004) and GROUP (Reese et al. 2010) were used to model the laterally loaded single piles and pile groups, respectively. The p-y curves of Matlock (1970), Reese et al. (1974) and Reese et al. (1975) were used to model the p-y behavior of piles in soft clay, sand, and stiff clay (CDSM block) with free water, respectively. These curves are provided within LPILE and GROUP as default curves and no changes were made to these curves.

The p-y curve of Matlock (1970) for soft clay varies with depth and mainly depends on effective unit weight (γ'), undrained shear strength (S_u), and the strain at one-half the maximum difference in principal stresses (ε_{50}). The effective unit weight was determined for each layer of centrifuge model and is provided in Table 5.2. The undrained shear strength values presented in Figure 3.8 and a typical ε_{50} value of 0.02 suggested by Reese and van Impe (2011) for soft clay were used to build the p-y curves for soft clay.

Table 5-2. Soil Properties at the Bottom of Each Layer Used for the Analysis of the Unimproved Pile Group

Layer	Undrained Cohesion (kPa)	Strain at 50% Stress, ε_{50}	Friction Angle (degree)	p-y Modulus, k (MN/m^3)	Submerged Unit Weight, γ' (kN/m^3)
Soft Clay- (top)	8.17	0.02	-	-	8.17
Soft Clay	9.96	0.02	-	-	8.68
Soft Clay	15.34	0.02	-	-	9.04
Soft Clay-(bot)	20.76	0.02	-	-	9.27
Sand	-	-	38	34.0	10.43

The Reese et al. (1974) p-y curve for sand mainly depends on the initial stiffness and the ultimate soil resistance. The ultimate soil resistance depends on the internal friction angle of sand and pile diameter. The friction angle of dense Nevada sand was assumed to be 38 degrees, which is consistent with the values reported in the VELACS (VErification of Liquefaction Analysis by Centrifuge Studies) project (Arulmoli et al. 1992). The initial stiffness (k) was determined by back analysis of measured single pile response. The analyses were performed to obtain the best possible match between the measured and calculated response for the unimproved single pile. Figure 5.1 shows the measured and LPILE computed lateral load versus deflection responses for the unimproved single pile. Figure 5.2 presents the measured and computed bending moment profiles of the unimproved single pile for two different deflection values. In both lateral load-deflection and bending moment-depth curves there is a good agreement between measured and computed responses. The back-calculated value of the initial stiffness for the dense Nevada sand was 34.0 MN/m^3. The final calibrated unimproved soil input data for the GROUP analyses are shown in Table 5.2.

The Reese et al. (1975) p-y curve provided within the program GROUP for stiff clay in the presence of free water was used to model the p-y behavior of piles in CDSM block. In order to build this curve in each desired depth, effective unit weight (γ'), undrained shear strength (S_u), strain at one-half the maximum difference in principal stresses (ε_{50}), and initial stiffness (k) are required. The effective unit weight of the improved soil was assumed to be 8.17 kN/m^3 and a typical value of ε_{50} suggest by Reese and van Impe (2011) for stiff clays (0.004) was used for the improved clay. As mentioned earlier, the unconfined compression tests revealed the undrained shear

strength of the improved clay is 380 kPa. The initial stiffness (k) was determined by back analysis of measured GIL-7D pile group response. The analyses were performed to obtain the best possible match between the measured and predicted response for the GIL-7D improved pile group at very small deflections to lower the axial response effects. Single piles were not used in this step, because none of the CDSM layers in the tested improved single piles could be assumed to be semi-infinite, an LPILE assumption. The results of numerical modeling of the GIL-7D improved pile group are presented later. Using this procedure, the initial stiffness (k) was back-calculated as 460.0 MN/m^3 for the CDSM block. This matches well with the k values available in literature (Reese and van Impe 2011; Reese et al. 2010). The input data for the CDSM improved soil is shown in Table 5.3.

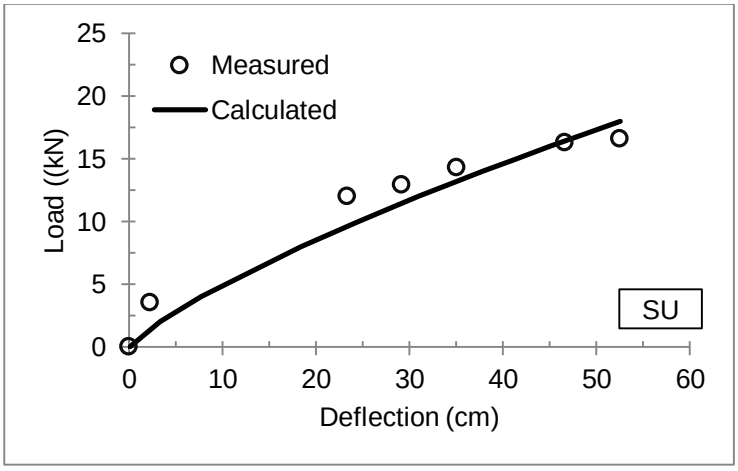

Figure 5-1. Comparison of Measured and LPILE Computed Load - Deflection Curves for the Single Pile in Unimproved Soft Clay.

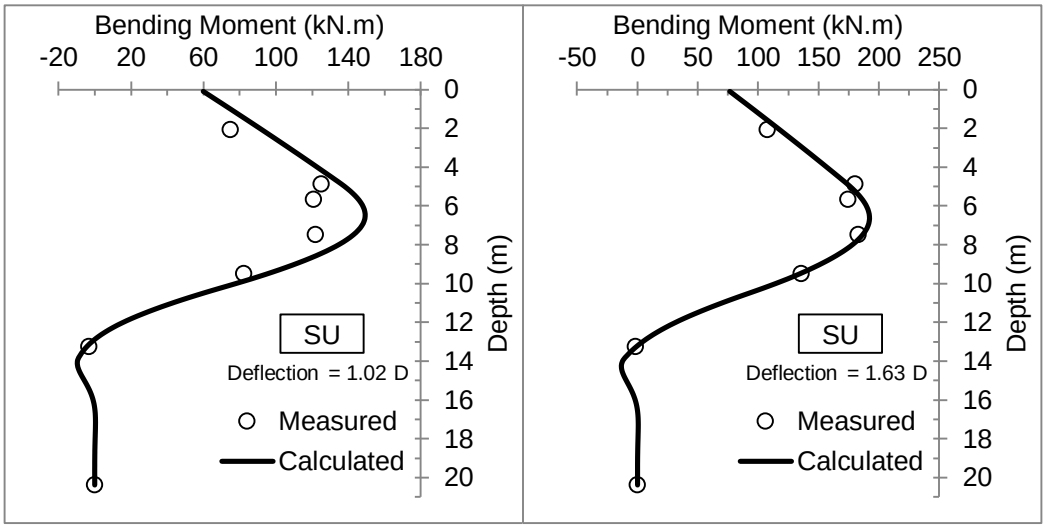

Figure 5-2. Comparison of Measured and LPILE Computed Bending Moment - Depth Curves for the Single Pile in Unimproved Soft Clay for Lateral Deflections 0f 1.02 D and 1.63 D.

Table 5-3. CDSM Properties used for the Analyses of the Improved Pile Groups.

Layer	Undrained Shear Strength (kPa)	Strain at 50% Stress, ε_{50}	Soil Modulus, k (MN/m^3)	Submerged Unit Weight, γ' (kN/m^3)
Improved Soil	380	0.004	460.0	8.17

In all the analyses, a total of 61 nodes were used to discretize pile foundations into equal increments (60 increments). Each node was connected to the adjacent soil using the specified p-y spring. Sensitivity analyses performed using 61 and 101 nodes revealed that the responses are identical.

5.4 Determination of p-multipliers

After calibrating the soil properties as described above, the GU-3D and GIL-3D pile group results were used to back-calculate p-multipliers using GROUP. The p-multipliers were initially obtained by matching the measured and computed total lateral load – deflection responses. These p-multipliers were then adjusted for each row of pile groups in improved and unimproved pile groups by matching the measured and computed responses for each row.

The p-multipliers suggested by different researchers for pile groups in clay, including the present study, are presented in Table 5.4. Since different p-multipliers were obtained for pile groups with same arrangement and spacing, this table illustrates that these two parameters are not the only governing factors in determining p-multipliers. The p-multipliers obtained for the leading and the trailing rows of a 2x2 improved pile group with 3D spacing in this study are 0.89 and 0.60, respectively. For the unimproved group, these values are 0.84 and 0.43, respectively. The set of (0.84, 0.43) obtained in this study for the 2 × 2 pile group with 3D spacing in soft clay is comparable with the suggested sets of FEMA (2012), Rollins et al. (2006), and Mokwa and Duncan (2005) for all soils (see Table 5.1, Row 1 and Row 3+). Moreover, the set of (0.89, 0.60) obtained for the 2 × 2 pile group with 3D spacing in stiff clay is close to the suggested set by Huang et al. (2001) pile groups driven in silt and silty clay (Table 5.4). This observation implies that using the recommendations of most agencies, as indicated in Table 5.1, will result in an overly conservative design of piles in improved soft clay sites.

Table 5-4. Comparison of p-multipliers obtained from Lateral Load Tests on Pile Groups in Cohesive Soils.

		p multiplier (f_m) in row							
Pile group	S/D	1	2	3	4	5	Type and Strength (kPa)	Test type	Reference
2×2	3	0.89	0.60	---	---	---	Stiff clay, S_u=380 kPa	Centrifuge	Present study
2×2	7	1.0	1.0	---	---	---			
2×2	3	0.84	0.43	---	---	---	Soft clay, S_u=4-10 kPa		
2×2	7	1.0	1.0	---	---	---			
3×4	3[a]	0.89	0.61	0.61	0.66	---	Silt and silty clay, S_u=110-190kPa	Full scale	Huang et al. (2001)
2×3	3[b]	0.93	0.70	0.74	---	---			
3×3	3[c]	0.7	0.6	0.5	---	---	Stiff clay, S_u=70-180 kPa	Full scale	Brown et al. (1987)
3×3	3[d]	0.7	0.5	0.4	---	---			
3×3	5.65	0.95	0.88	0.77	---	---	Stiff clay, S_u=70-105 kPa	Full scale	Rollins et al. (2006)
3×4	4.4	0.90	0.80	0.69	0.73	---			
3×5	3.3[e]	0.82	0.61	0.45	0.45	0.46			
3×5	3.3[f]	0.82	0.61	0.45	0.45	0.51			
3×3	3	0.60	0.38	0.43	---	---	Silt and clay, S_u=25-60 kPa	Full scale	Rollins and Sparks (2002)
3×3	3	0.60	0.38	0.43	---	---	Clay and silt, S_u=25-50 kPa	Full scale	Rollins et al. (1998)
2×2	3	0.9	0.5	---	---	---	Silty clay, S_u=25 kPa	Full scale	Meimon et al. (1986)
3×3	3	0.65	0.5	0.48	---	---	Soft clay, S_u=0-20 kPa	Centrifuge	Ilyas et al. (2004)
2×2	3	0.96	0.78	---	---	---			
1×2	3	0.8	0.63	---	---	---			
1×4	3	0.76	0.56	0.46	0.54	---	Soft clay, S_u = 9 kPa	Small	Chandrasekaran et al. (2010)
3×3	3	0.66	0.41	0.44	---	---		scale at1g	
2×2	3	0.74	0.48	---	---	---			
2×2	5	0.85	0.58	---	---	---			
1×2	3	0.81	0.70	---	---	---			

[a] Driven group piles
[b] Bored group piles
[c] Lateral deflection = 3 cm
[d] Lateral deflection = 5 cm
[e] Lateral deflection < 5 cm
[f] Lateral deflection > 5 cm

As mentioned earlier, p-multipliers should generally vary with lateral deflection and also by depth. However, this consideration is beyond the scope of this research. As it is shown below, the p-multipliers obtained in this study predict lateral load behavior of both improved and unimproved pile groups well and, therefore, are valid for all deflection ranges less than 35 cm.

Comparing the full scale tests results of Rollins et al. (1998) and Rollins et al. (2006) show that they have obtained greater p-multipliers for the pile group in stiff clay than the group in soft to medium-stiff clay and silt (see Table 5.4). These two pile groups both had a free-head condition and were tested under lateral loading in two sites located in Utah. The first pile group tested by Rollins et al. (1998) in soft to medium-stiff clay and silt had a 3 × 3 arrangement, 3D spacing in both longitudinal and transverse directions, a 0.315 m OD pile made from steel pipe filled with pea-gravel concrete, and were driven to a depth of approximately 9.1 m. The second pile group in stiff clay tested by Rollins et al. (2006) had a 3×5 arrangement, 3.3D spacing in both longitudinal and transverse directions, a 0.324 m OD pile made from steel pipe, and were driven to a depth of approximately 11.9 m. The key differences in these two pile groups that can contribute to the magnitude of p-multipliers are the clay stiffness and pile group arrangement. Based on their test results and other results available in literature, Rollins et al. (2006) proposed equations for p-multipliers. Considering the fact that these equations are same for 3 × 3 and 3 × 5 pile groups, the difference in p-multipliers obtained from aforementioned tests can be reasonably related to the difference in clay stiffness.

Furthermore, suggesting a larger values of p-multipliers for pile groups in stiff clay than soft clay is consistent with the findings of Ashour and Ardalan (2011). They used the strain wedge (SW) model technique (Ashour et al. 1998) to perform lateral load analyses on a 3×3 pile group with 3D spacings in both longitudinal and transverse directions. They used two different clay profiles in their analyses and kept all other factors the same and obtained greater p-multipliers for the medium to stiff clay profile (S_u = 72–144 kPa) than the soft to medium stiff clay profile (S_u = 24–72 kPa).

5.5 Comparing the Measured and Computed Responses

The total lateral load versus deflection curves of the unimproved and improved pile groups with 3D and 7D spacings are compared with the GROUP computed curves in Figures 5.3 and 5.4, respectively. Generally, the agreement between the measured and the GROUP computed total load-deflection responses is good; however, in GU-7D greater deviations are observed. Some of this error may be a result of uncertainties in interpretation of load and deflection measurements as well as the inadequacy of the numerical model. The measured and computed bending moment-depth and load-maximum bending moment curves of GU-7D (shown later), however, are in good agreement. Next, the responses for the leading and trailing row of piles are presented. Measured and computed load-deflection, maximum bending moment-load, and bending moment-depth responses are discussed below. These comparisons between measured and computed responses indicate that the lateral dimension of the CDSM layer in the GIL pile groups (23D) is long enough to be assumed as semi-infinite layers, an inherent assumption in GROUP.

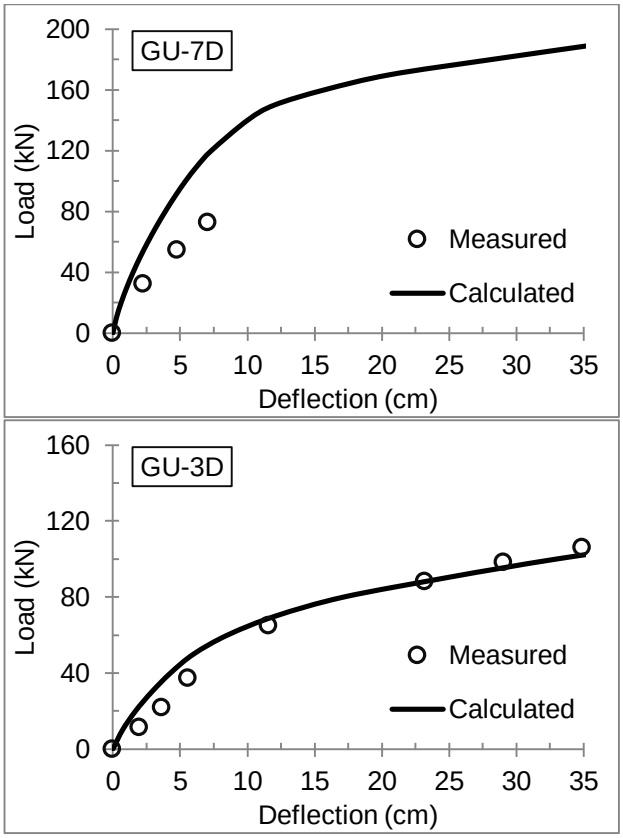

Figure 5-3. Comparison of Measured and GROUP Computed Total Load - Deflection Curves for the Unimproved Pile Groups at 7D and 3D Spacings.

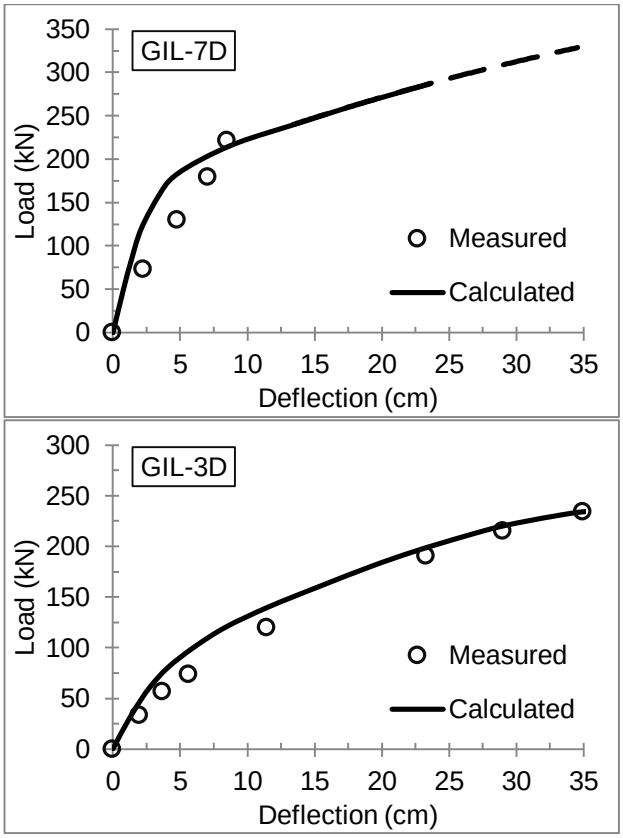

Figure 5-4. Comparison of Measured and GROUP Computed Total Load–Deflection Curves for the Improved Pile Groups at 7D and 3D Spacings.

5.5.1 Load – Deflection Curves

By integrating soil reaction profiles, lateral loads carried by each pile can be deduced. Soil reaction (p) can be obtained by double differentiating the bending moment using the weighted residual method. Readers are referred to Wilson (1998) and Brandenberg et al. (2010) for details on applying this method to double differentiate discrete bending moment profiles. Figures 5.5 and 5.6 show the lateral loads carried by the leading and trailing row of piles of the GU pile groups at 3D and 7D spacings, respectively. Load–deflection curves for each row computed using GROUP with the p-

multipliers developed in this study are also plotted in these figures for comparison. The agreement is generally good.

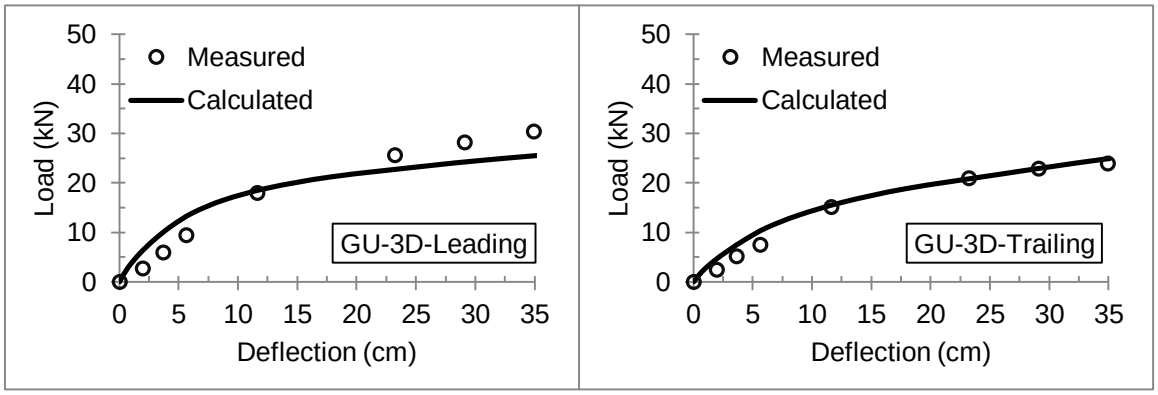

Figure 5-5. Comparison of Measured and GROUP Computed Load - Deflection Curves for Each Row of the Unimproved Pile Group at 3D Spacing.

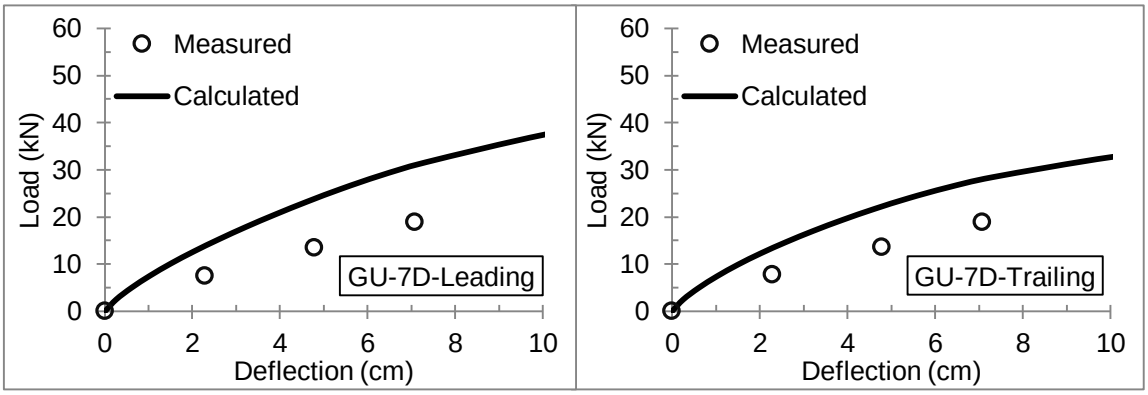

Figure 5-6. Comparison of Measured and GROUP Computed Load - Deflection Curves for Each Row of the Unimproved Pile Group at 7D Spacing.

Figures 5.7 and 5.8 depict similar plots, but for the improved GIL pile groups with 3D and 7D spacing, respectively. The agreement is again good, particularly considering the simplicity of the adjustment factor and different soils involved.

In the GIL-7D and GU-7D groups, both leading and trailing piles carried approximately the same amount of loads at a given deflection. This indicates there are no group interaction effects in the GU-7D and GIL-7D pile groups. However, at 3D

spacing, leading row of piles in GIL-3D and GU-3D carried larger loads than the trailing row of piles. Difference between lateral loads carried by trailing and leading piles is small in small deflections and gets larger as the deflections get larger. This indicates pile-soil-pile interactions increases as the deflection increases. The fact that leading row of piles carry larger portion of load than the trailing row of piles in closely spaced groups is in agreement with the findings of Rollins et al. (1998), Rollins et al. (2006), Brown et al. (1987), and Meimon et al. (1986).

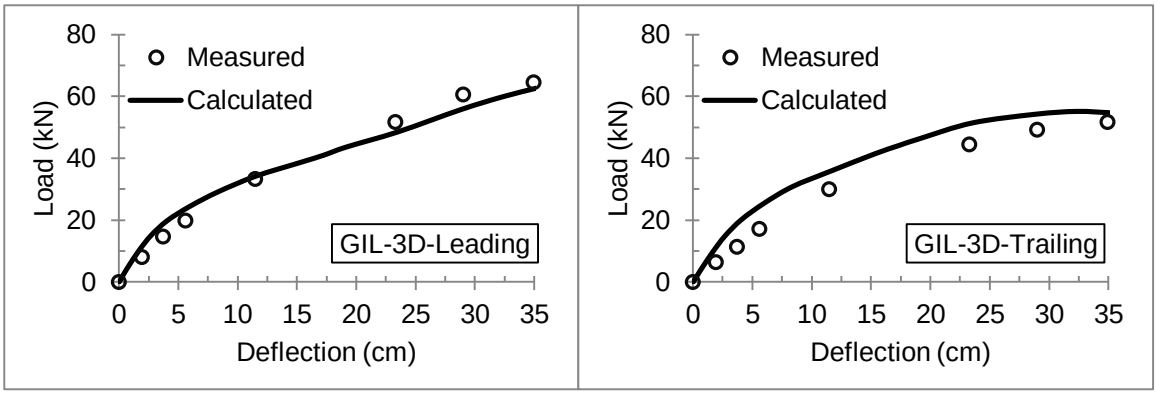

Figure 5-7. Comparison of measured and GROUP computed load - deflection curves for each row of the improved pile group at 3D spacing.

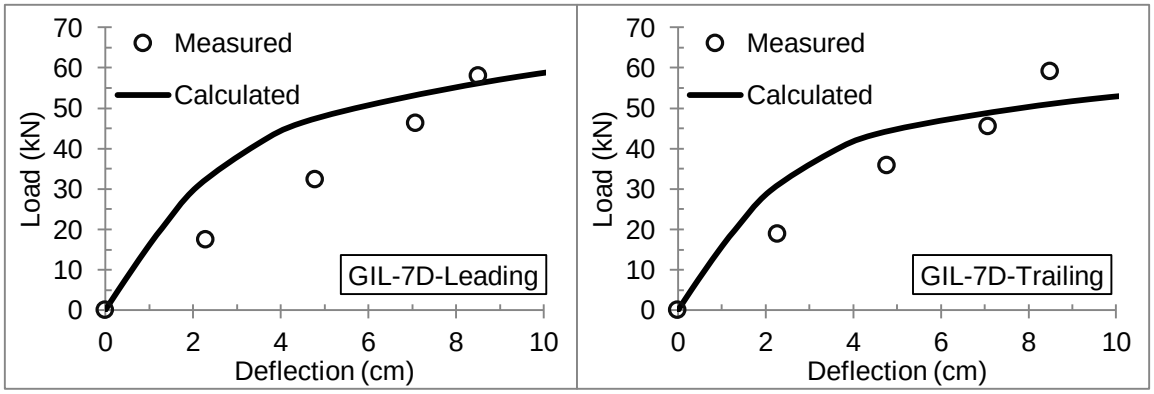

Figure 5-8. Comparison of measured and GROUP computed load - deflection curves for each row of the improved pile group at 7D spacing

5.5.2 Maximum Bending Moment–Load Curves

Measured and computed (using the p-multipliers from this study) maximum bending moment-load curves for improved (GIL) and unimproved (GU) piles are shown in Figures 5.9-5.12. The maximum bending moment is the largest moment along the length of each leading or trailing row of piles in each group and the load is the total load carried by that pile group. Calculating maximum bending moments and the resulting stresses are important as they often control design of piles (e.g. number of piles). The agreement between measured and computed maximum bending moment versus load curves is very good for all four pile groups.

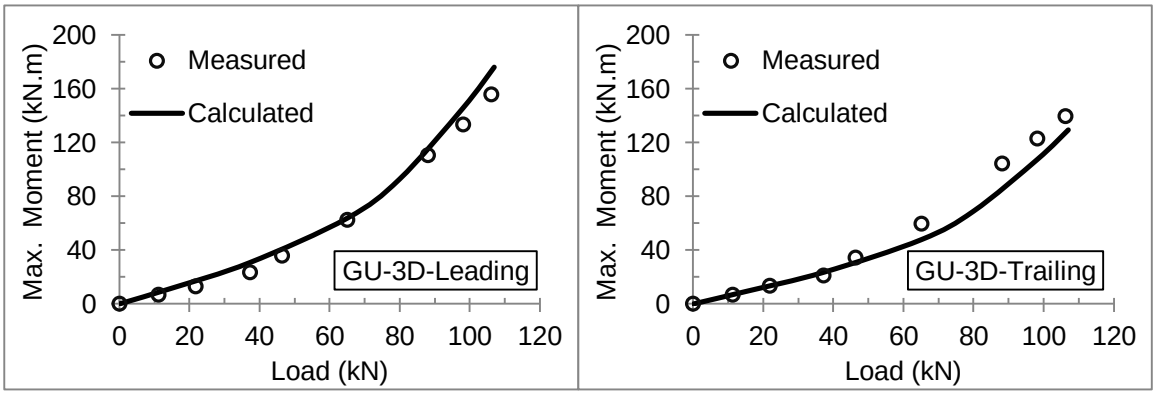

Figure 5-9. Comparison of Measured and GROUP Computed Maximum Bending Moment - Load Curves for Each Row of the Unimproved Pile Group at 3D Spacing.

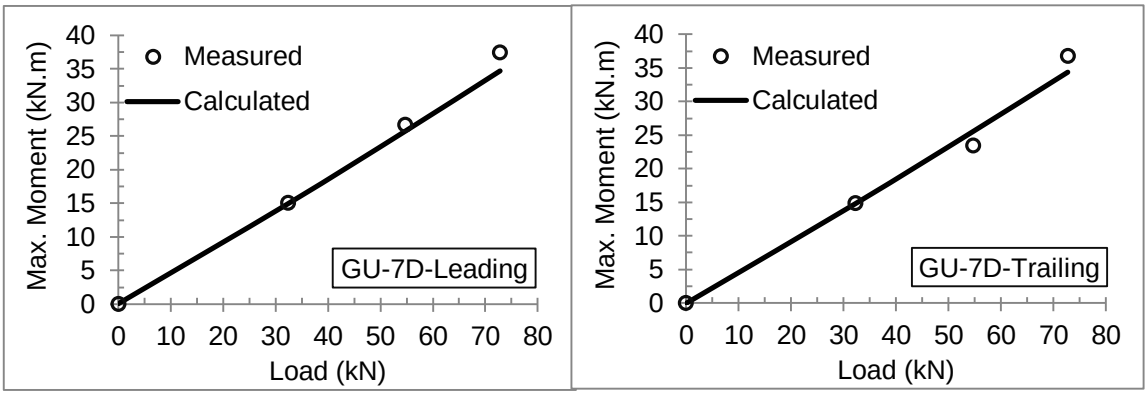

Figure 5-10. Comparison of Measured and GROUP Computed Maximum Bending Moment - Load Curves for Each Row of the Unimproved Pile Group at 7D Spacing.

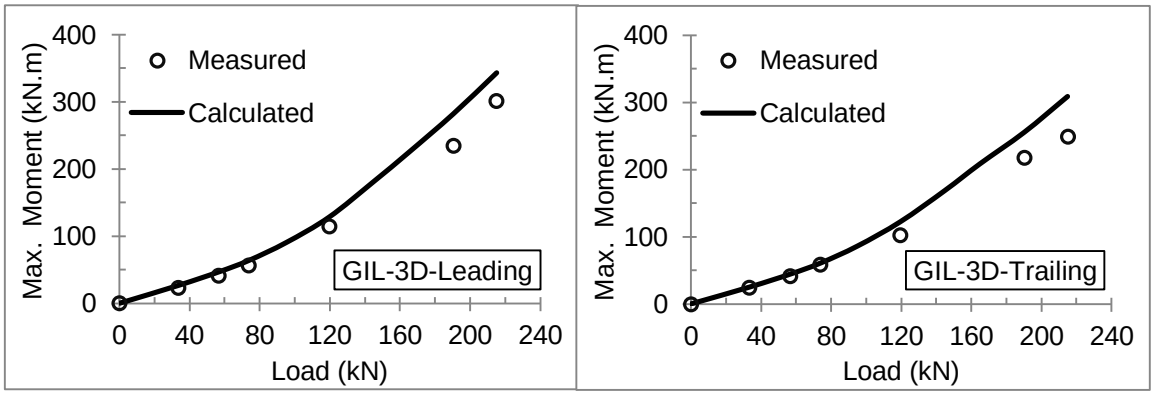

Figure 5-11. Comparison of Measured and GROUP Computed Maximum Bending Moment - Load Curves for Each Row of the Improved Pile Group at 3D Spacing.

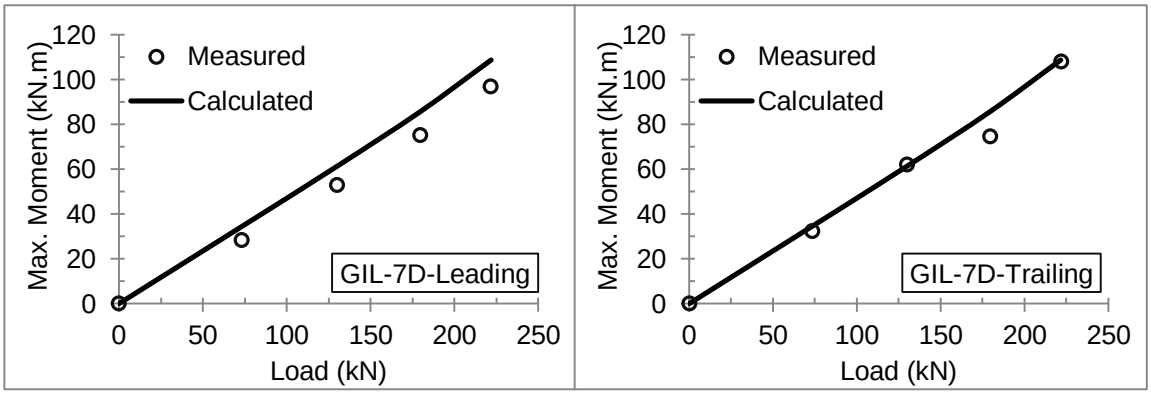

Figure 5-12. Comparison of Measured and GROUP Computed Maximum Bending Moment - Load Curves for Each Row of the Improved Pile Group at 7D Spacing.

5.5.3 Bending Moment–Depth Curves

Bending moment versus depth curves are plotted for each row of the 3D and 7D pile groups in unimproved and improved soft clay in Figures 5.13–5.16. For the GIL and GU pile groups with the largest spacing (7D), the maximum moments for both leading and trailing piles are close to one another for a given deflection. Depths to the maximum bending moment for GU (3D and 7D) and GIL (3D and 7D) piles are about 9 – 10D and 1– 2D below the ground surface, respectively. The bending moment increases with the applied deflection for all pile groups. For a given deflection, the piles in improved clay experience higher bending moments than those in the unimproved clay. This is as expected as the piles in the unimproved clay would resist considerably less load as compared to the piles in the improved clay at the same deflection, as illustrated in Figures 5.3 and 5.4. Figures 5.13-5.16 illustrate that a reduction in the pile spacing from 7D to 3D leads to larger bending moments being mobilized in the leading row of piles than the trailing row at the same amount of deflection. Although this effect is more pronounced at larger deflections, it can be seen even at smaller deflections for 3D spacing. This points to pile-soil-pile interactions resulting in trailing row of piles carrying lower loads than the leading row of piles for 3D spacing.

Bending moment versus depth curves computed using the program GROUP with the p-multipliers developed in this study are also plotted in these figures for comparison purposes. These comparisons show that the implemented p-multipliers in GROUP are capable of successfully predicting the shape of the curve and the depth to the maximum bending moment for all pile groups in improved or unimproved soft clay.

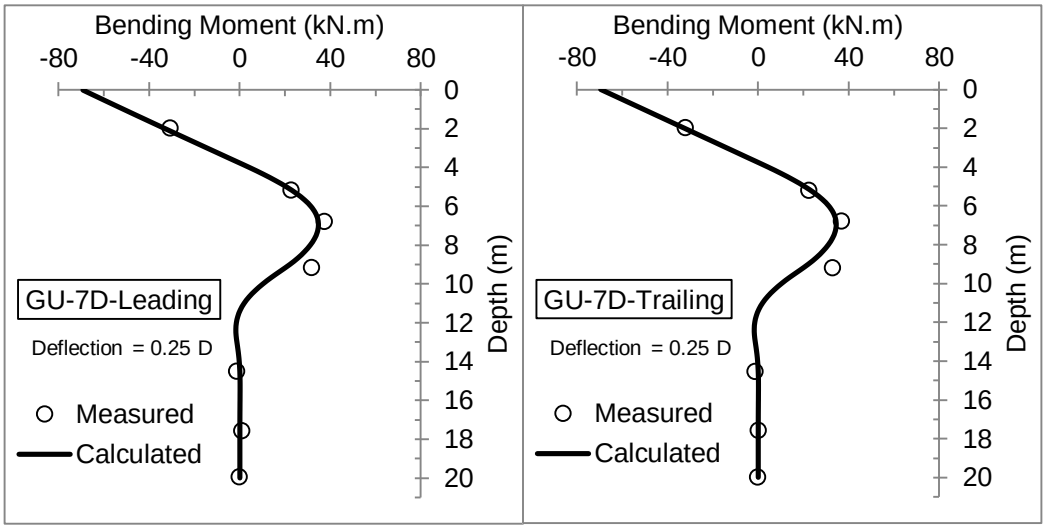

Figure 5-13. Comparison of Measured and GROUP Computed Bending Moment - Depth Curves for Each Row of the Unimproved Pile Group at 7D Spacing.

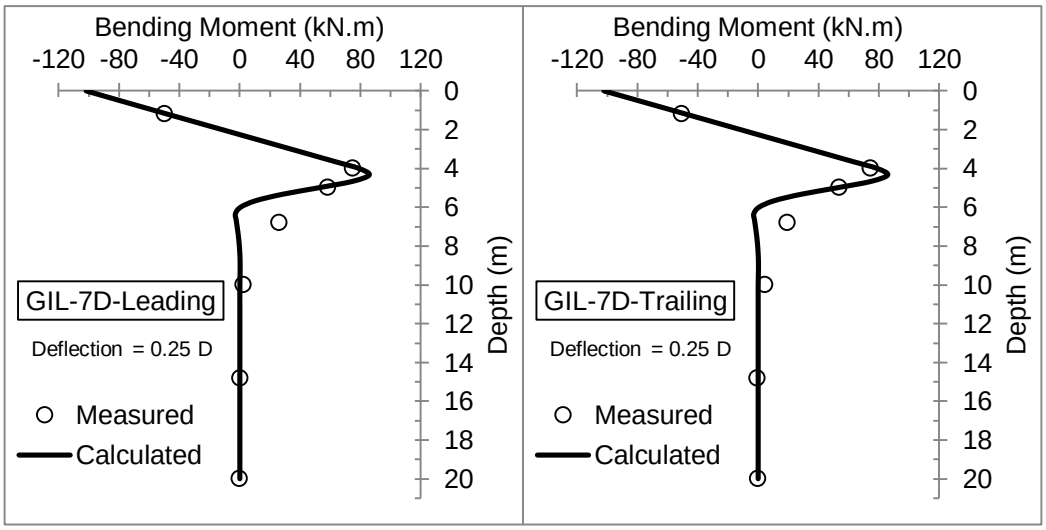

Figure 5-14. Comparison of Measured and GROUP Computed Bending Moment - Depth Curves for Each Row of the Improved Pile Group at 7D Spacing.

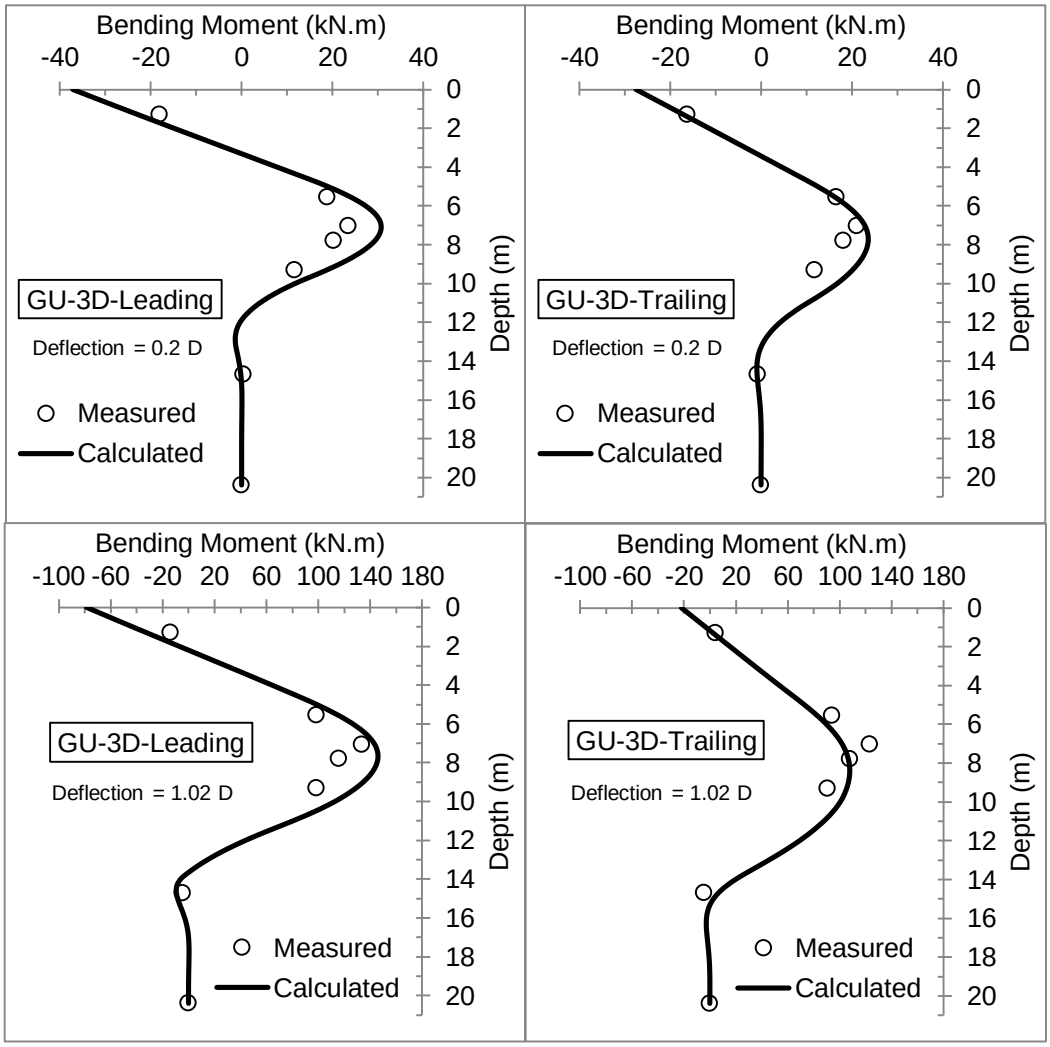

Figure 5-15. Comparison of Measured and GROUP Computed Bending Moment - Depth Curves for Each Row of the Unimproved Pile Group at 3D Spacing.

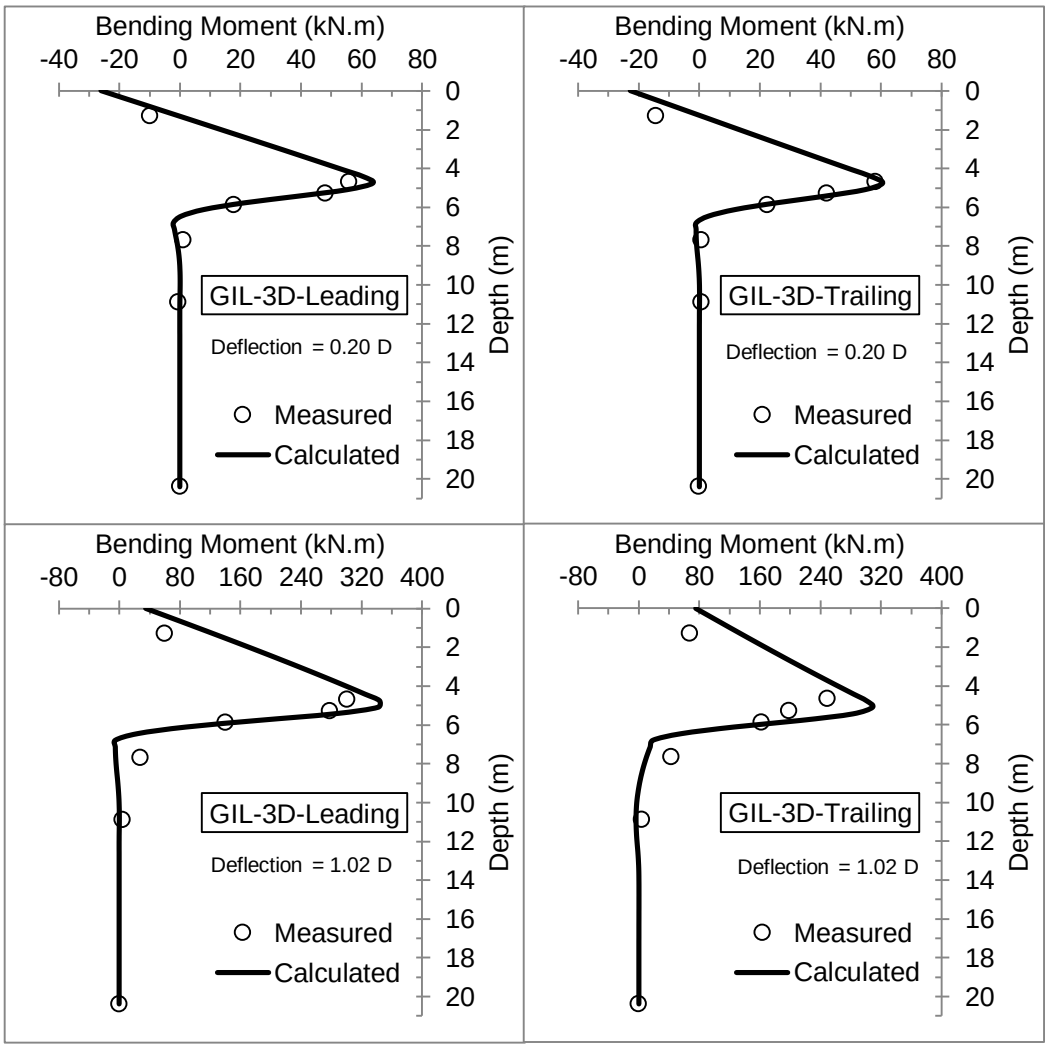

Figure 5-16. Comparison of Measured and GROUP Computed Bending Moment - Depth Curves for Each Row of the Improved Pile Group at 3D Spacing.

5.6 CDSM Block Depth Effect

The calibrated numerical model is used to study the depth effect of the CDSM blocks on the lateral capacity of pile groups. As mentioned above, the lateral dimensions equal to or greater than 23D (6.57 m) can be considered as infinitely long.

The depth effect of the CDSM blocks with infinitely long lateral dimensions is investigated in this section. Figure 5.17 shows that in small deflection (e.g. less than 3 cm), the depth effect on lateral resistance of pile groups is negligible. However, in large deflections, increasing the CDSM block depth increases the lateral resistance. When the CDSM block bottom reaches a certain depth, say 9D, increasing depth of CDSM block further has negligible effect on the lateral resistance. Therefore the dimensions of the CDSM blocks used in this study for GIL pile groups (23D × 23D × 9D) can be considered the optimum dimensions to provide the maximum increase in lateral resistance for the tested soil and pile conditions. For improvement depths of 2D to 4D, a plateau in the load-deflection curves can be seen. This is an indication that the soil in the CDSM blocks for these cases has reached its failure stress (the plateau in the p-y curves).

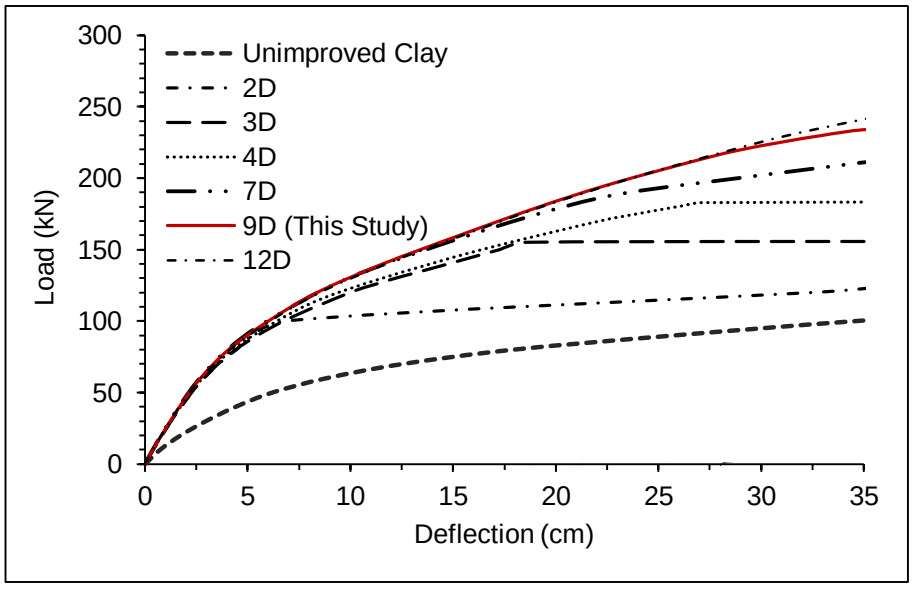

Figure 5-17. Depth Effect of the CDSM Block on Load-Deflection Behavior of a Pile Group at 3D Spacing

5.7 CDSM Block Strength Effect

Unconfined Compression Tests (UCT) were performed using multiple cement contents at a water/cement ratio of 1.0. The cement-improved soft clay samples were cured for 28 days. Cement contents of 10% (used for the CDSM blocks in this study) and 20% produced 760 kPa and 1270 kPa unconfined compression strengths, respectively. No significant increase in strength was noticed from 10% to 15% cement content. 20% cement content did provide a substantial increase in strength; however, the workability suffered with additional cement (Thompson 2011). GROUP was used to study the strength effect of the CDSM blocks on the lateral resistance of pile groups. Figure 5.18 shows the effect of the undrained shear strength on the lateral resistance of pile groups. The undrained shear strength (S_u) is obtained by dividing UCT compressive strength by 2.0. CDSM blocks were assumed infinitely long and had a fixed depth of 9D. Figure 5.18 shows that the strength effect is negligible in deflections less than 8 cm. In larger deflections, increasing the strength increases the resistance. When the undrained shear strength reaches a certain value (approximately 1000 kPa), however, increasing the strength has very limited effect on the lateral resistance. As the undrained shear strength increases, the initial stiffness (k) increases and the strain at one-half the maximum difference in principal stresses (ε_{50}) decreases. The results shown in Figure 5.18 were, however, obtained by keeping k and ε_{50} as same as those given in Table 5.3. However, additional analyses not shown here illustrated that compared to the S_u effect, variation of k and ε_{50} within the typical ranges suggested for a given Su value has negligible effects on the lateral resistance of a pile group for large deflections. This is because in large deflections, the value of the ultimate soil resistance, which depends on

Su, controls the results. Variations in k and ε50, however, affect the response in small deflections (less than 5 cm).

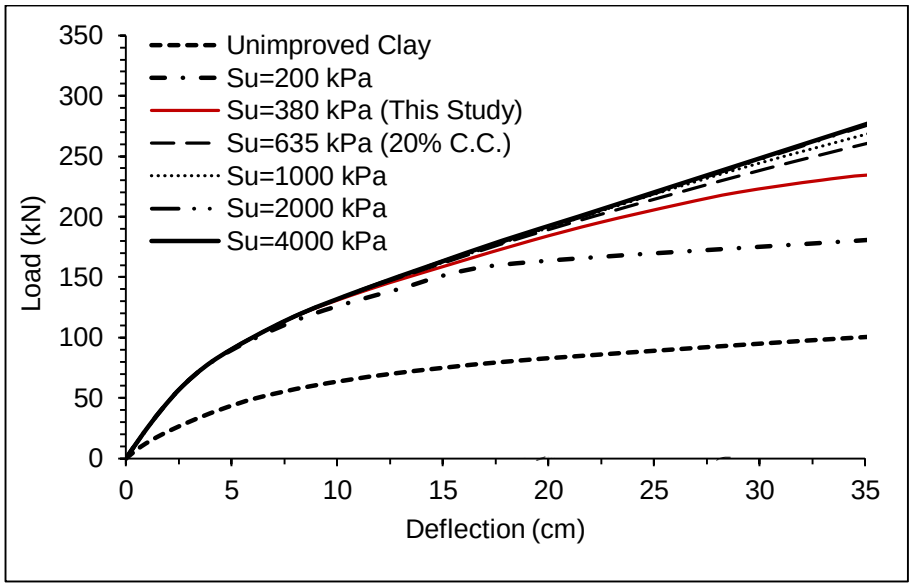

Figure 5-18. The effect of undrained shear strength of the CDSM block on the load-deflection behavior of a pile group at 3D spacing

Chapter 6: Nonlinear Seismic Behavior of Pile Groups in Improved Soft Clay

6.1 Overview

Centrifuge tests were performed to investigate the effects of ground improvement on the seismic behavior of pile groups in soft clay. The centrifuge model was subjected to seven different earthquake events with peak accelerations (PBA) ranging from 0.03 to 0.66g. The transient acceleration and displacement responses of the structural models, their settlement, and their effect on the dissipation of excess pore water pressure (EPWP) are presented and discussed in detail. The series of centrifuge tests performed in this study, to the author's knowledge, represent the first attempt to characterize nonlinear SPSI effects of pile groups in improved and unimproved soft clay. The centrifuge test results revealed that, compared to the surface free-field motion, a reduction in the amplitude of the foundation level motions of the improved pile groups occurred. This reduction is mostly contributed to the kinematic interaction in the pile group system. The foundation level motion in the unimproved pile group was, however, identical to that in the free-field. Higher peak acceleration was observed in the pile cap for smaller CDSM block (GIS) compared to the unimproved pile cap (GU) and the pile cap with larger CDSM block (GIL). Higher pile cap to soil surface spectral ratio was also observed in the GIS pile cap in short and long periods. The period where the maximum spectral amplification occurred became smaller as the size of the ground improvement increased. Cement-Deep-Soil-Mixing was an effective method in reducing the peak displacements of the GIL pile cap. The peak displacements for the GIS pile cap were about the same as the GU pile cap. The cohesion between soft clay

and CDSM blocks helped to reduce the soft clay settlement in the vicinity of CDSM blocks compared to the free-field and in the vicinity of unimproved pile group. More residual excess pore water pressures were, however, generated in the vicinity of CDSM blocks compared to free-field and the corresponding location near the unimproved pile group. Some results in this chapter are also reported in Taghavi et al. (2015d) and Taghavi et al. (2015a).

6.2 Free-Field Site Response

In order to study seismic soil-structure interaction, it is important to obtain the free-field site response and compare it to structural response in time and/or frequency domain. This simultaneous comparison can reveal some important information about the nature and significance of the interaction. The free-field motion is defined as the motion far from the structure or any other natural or manmade irregularities (e.g. topography and ground improvement). Trifunac (1972) has suggested to record the free-field motion at distances of at least one order of magnitude greater than the characteristic length of the foundation. Considering the 3D center to center distance between piles of a group and assuming pile groups as single piles with a 4D diameter, this distance for the GU pile group would be 11.6 m. Furthermore, considering the dimensions of the CDSM blocks, free-field motions should be recorded at distances greater than 31.9 m and 66.7 m for the GIS and GIL pile groups, respectively. Due to the space limitations in the centrifuge container, however, it was not practical to record motions at these distances. The free-field motions recorded during these tests hence are

not ideal free-field motions; they were recorded as far as possible from the effects of the foundations and the container walls.

Figures 6.1 and 6.2 depict the recorded free-field motions for a low intensity Kobe earthquake (Event B) and a high intensity Santa Cruz earthquake (Event G), respectively. These free-field motions were recorded at two different locations (see Figure 3.7a) with respect to the structural models and are presented in the forms of acceleration-time history and Fourier spectrum. In all shakings, the recorded free-field motions at these two locations are in a good agreement with each other implying these motions can adequately represent the free-field motions.

As described in Chapter 3, the acceleration-time histories were filtered using a Butterworth bandpass filter (Taghavi et al. 2015a). The selection of corner frequency was based on applying smallest possible amount of filtering while obtaining realistic displacement and velocity time histories. A typical set of centrifuge results from a vertical dense accelerometer array are presented in Figures 6.3 and 6.4 during two scaled Kobe earthquake motions (Events A and D) with PBA of 0.026 g and 0.273 g. The top motions represent the free-field motions and the bottom motions are the base input earthquake motions. The peak acceleration is amplified 2.3 times at the ground surface during Event A, while it is attenuated by a factor 0.8 during Event D. A PBA of about 0.2 g can be considered as the point where attenuation starts to occur. At higher acceleration levels, the low stiffness and nonlinearity of soft clay prevent it from developing peak accelerations as large as those during lower acceleration levels. Dependence of peak ground acceleration (PGA) amplification on PBA indicates soil nonlinearity.

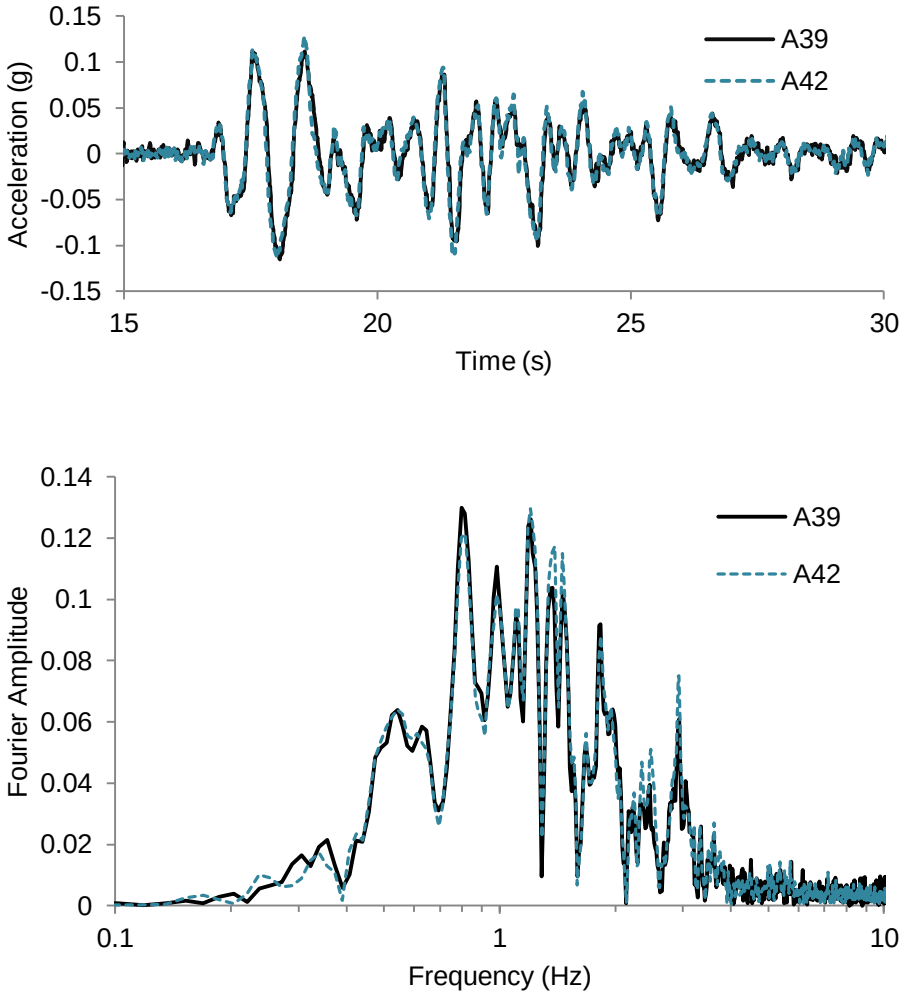

Figure 6-1. Acceleration-Time Histories and Fourier Amplitudes for Event B Recorded at Two Different Free-Field Locations

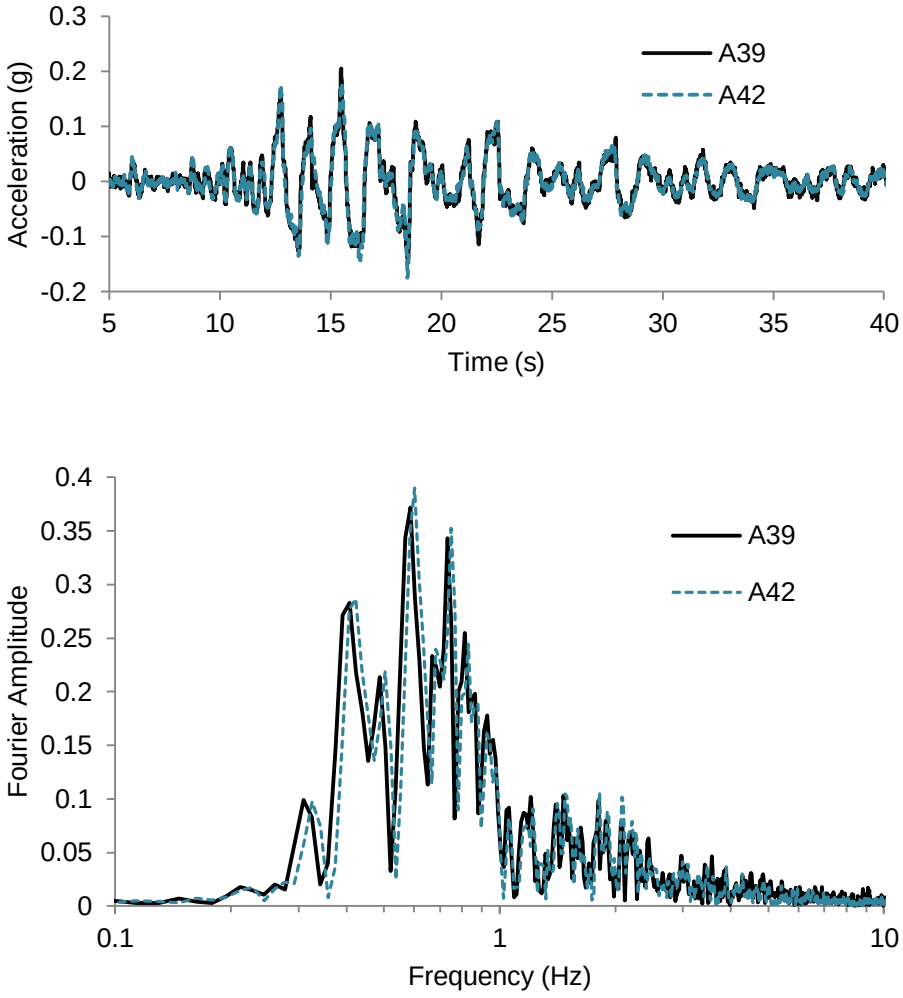

Figure 6-2. Acceleration-Time Histories and Fourier Amplitudes for Event G Recorded at Two Different Free-Field Locations

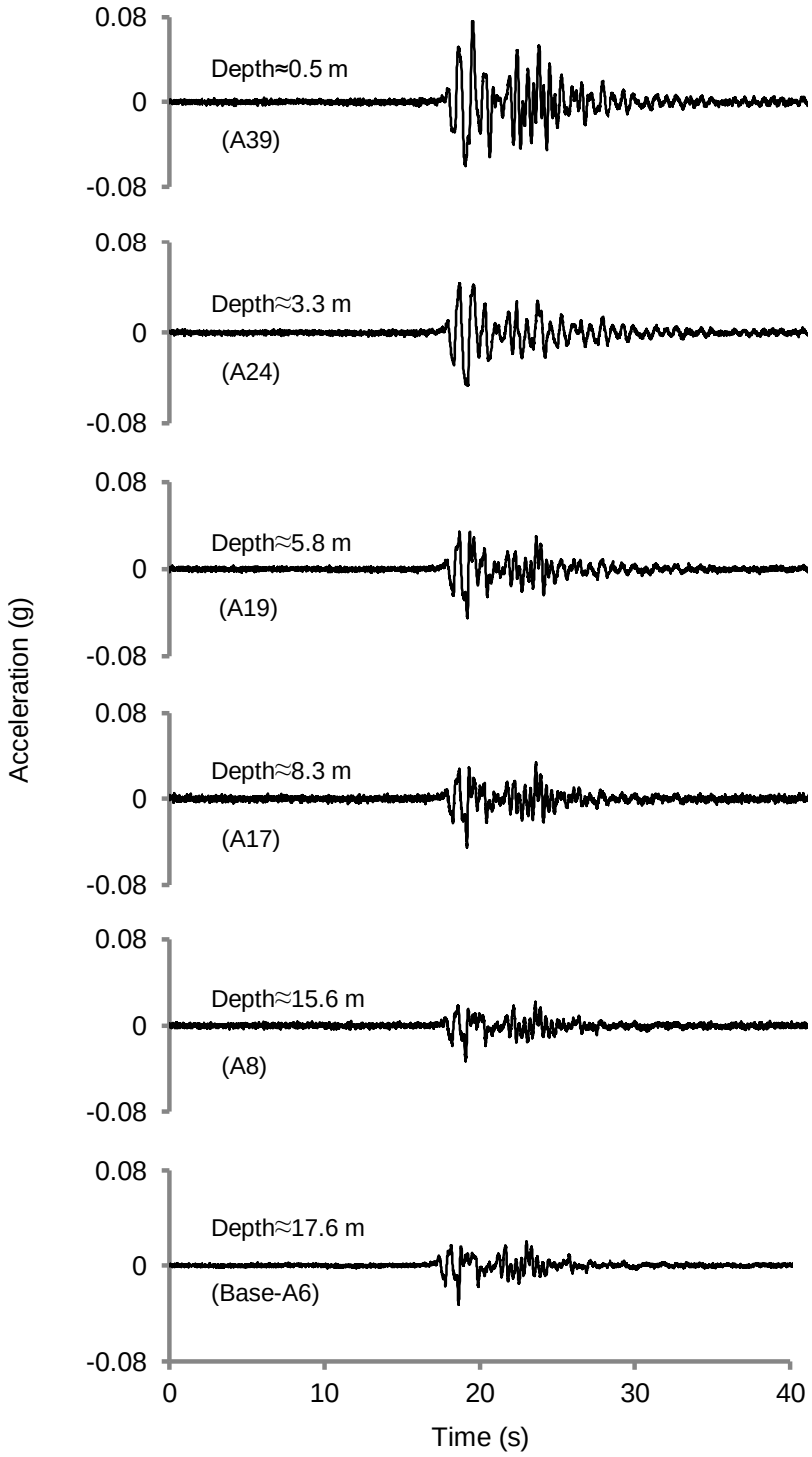

Figure 6-3. Acceleration-Time Histories in Soil Profile during Event A (PBA=0.026 g)

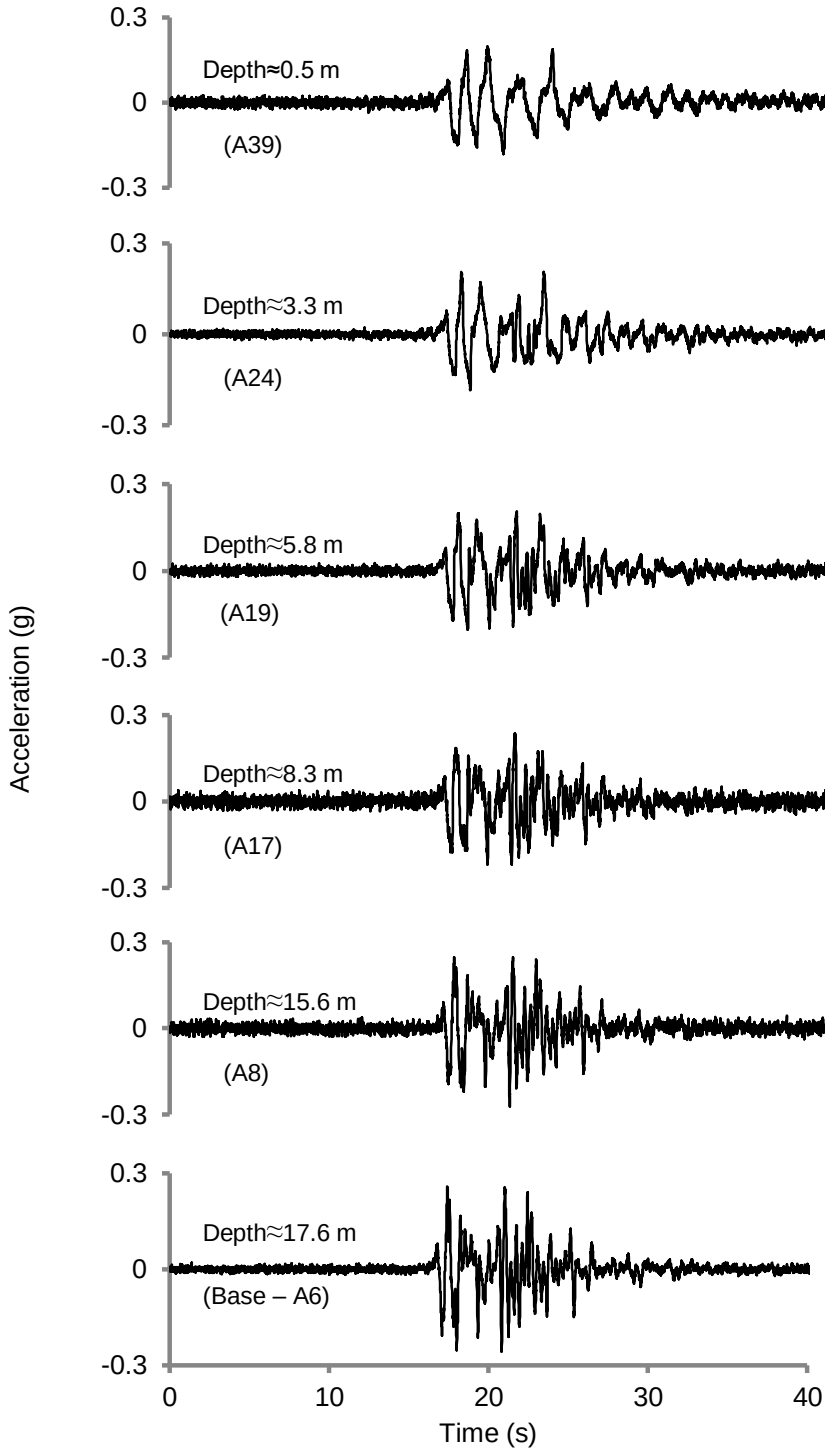

Figure 6-4. Acceleration-Time Histories in Soil Profile during Event D (PBA=0.273 g)

Figure 6.5 presents the acceleration response spectra in free-field (top) and container base for the scaled Kobe earthquake during Events A, B, C, and D. Figure 6.6 shows spectral amplification factors (F) of the site as a function of period. The spectral amplification factors are defined as the ratio of the acceleration response spectrum (ARS) of the site in free field to its base in 5% damping. It can be seen that increasing the PBA from 0.026 g in Event A to 0.273 g in Event D has increased the fundamental period of the site from 0.8 s to 1.3 s. While the site has experienced attenuation in some periods during Events B, C, and D, amplification has occurred for nearly all periods for Event A. The spectral amplification factors are relatively flat in periods less than 0.3 s and strongly depend on the peak base acceleration level; increasing the PBA has decreased the spectral amplification. A relatively narrow band of amplification can be observed near the elastic site specific period (0.8 s) for the Event A with a maximum amplification of 4.0, whereas the strongest motion has decreased the amplification, widen the band, and lengthen this period to about 4.0 s. In periods larger than 2.0 s, amplification has occurred for all events and the amplification trend is opposite of what was seen in smaller periods. This appears to be a result of transferring the input motion energy to longer site periods as the site softens during intense events.

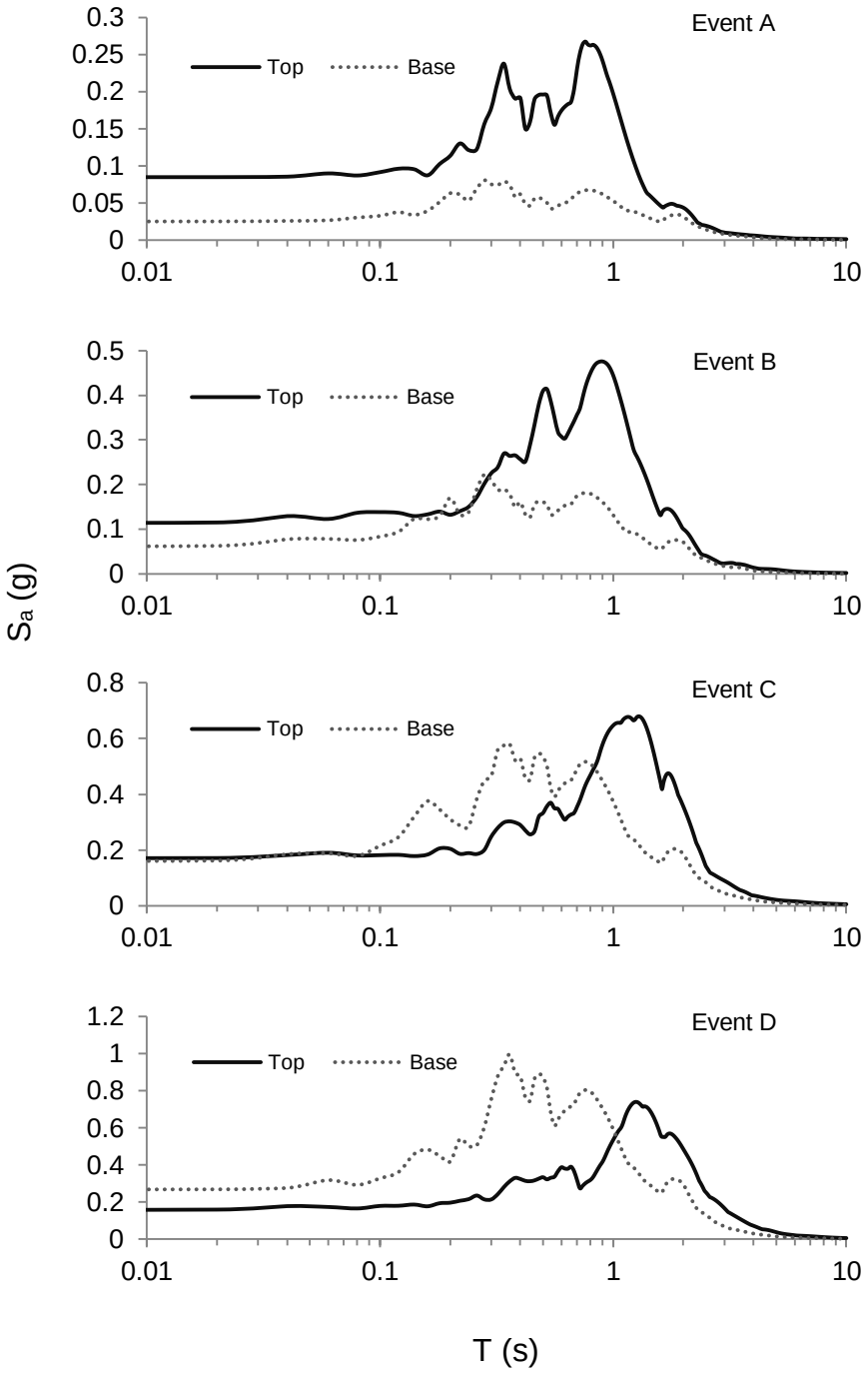

Figure 6-5. Acceleration Response Spectra (5% Damping) in Free-Field and Base of the Soil Profile during Scaled Kobe Earthquake Motions.

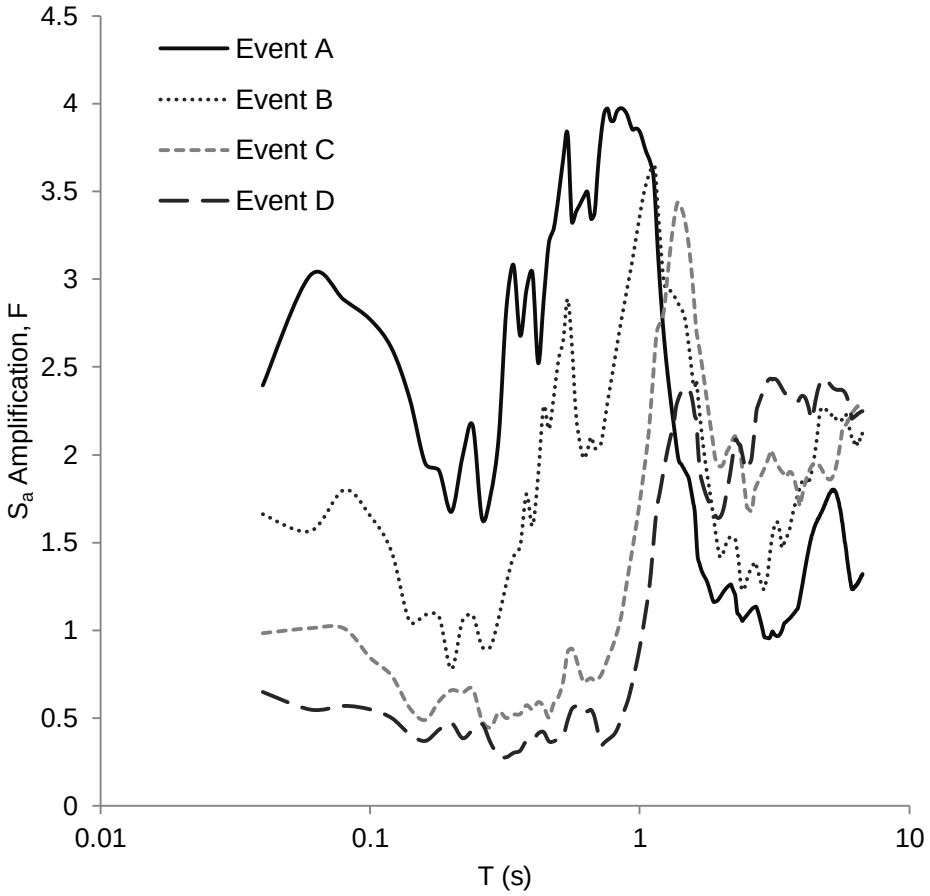

Figure 6-6. Site Amplification Factors

6.3 Foundation-Level Input Motions

Dynamic interactions that occur between the superstructure, pile foundations, and geologic media surrounding pile foundations can affect the behavior of superstructure during an earthquake event. Vibrations of superstructure give rise to deformations in piles, which is called the inertial interaction. On the other hand, soil deformation due to the passage of seismic waves causes pile motions to deviate from that of a free-field, which is called the kinematic interaction.

The importance of kinematic interaction has been recently recognized by few seismic codes such as the Eurocode 8 and the Italian national provisions (European Committee for Standardization (CEN) 2003; Ministero delle Infrastrutture 2008). Moreover, there is extensive research illustrating the significance of kinematic interaction, including field measurements and post-earthquake observations (Kim and Stewart 2003; Nikolaou et al. 2001; Pender 1993), and centrifuge tests (Mason et al. 2013; Tazoh et al. 2009). In practice, however, earthquake engineers commonly just take the inertial interaction into account and neglect the effects caused by kinematic interaction.

Kinematic interaction may significantly modify the base excitation of a supported structure. Therefore, the Foundation Input Motion (FIM) needed for inertial interaction analyses would be different from that of a free-field (Di Laora and de Sanctis 2013; Gazetas 1984; Kim and Stewart 2003; Pender 1993). Different factors affecting FIM include base-slab averaging and embedment in deep foundations. Base-slab averaging occurs in the incidence of inclined and/or incoherent waves and "averages" the free-field motions within and below the foundation footprint.

Embedment also causes reduction of the peak ground acceleration and high frequency spectral ordinates with depth for the embedded foundation (FEMA-440 2005; Kim and Stewart 2003; Stewart et al. 1999).

Because the objective of this study was to investigate the fundamental characteristics of the seismic behavior of pile groups in improved ground, none of the pile groups had a superstructure. The weight of the pile cap (footing), however, contributes to the inertial interaction. Hence, in interpreting the experimental observations of kinematic interaction, it should be noted that it is impossible to eliminate inertial effects and produce perfect kinematic interaction. Therefore, Foundation Level Motion (FLM) terminology is used to differentiate this motion from the theoretical Foundation Input Motion (FIM). Figure 6.7 shows the zoomed-in acceleration-time histories obtained from the accelerometers located in the vicinity of pile groups and also in free-field. In the both GIL and GIS improved pile groups, the accelerometers were securely embedded inside the CDSM blocks prior to curing. All accelerometers were buried at the same depths from the ground surface; moreover, the accelerometers in the vicinity of pile groups had same distances from the pile groups. Lower peak accelerations in FLM have been observed in both improved pile groups compared to the free-field motion. However, this reduction is negligible in the unimproved pile group. The reduction in the peak accelerations in FLM is related to the increased stiffness of the improved ground and kinematic interaction. This observations is consistent with FEMA-440 (2005) recommendation, where it says “Kinematic interaction effects should be neglected for soft clay sites such as Site Class E.” Different codes (European Committee for Standardization (CEN) 2003) and research

(Di Laora et al. 2013; Di Laora and Rovithis 2015; Kavvadas and Gazetas 1993; Nikolaou et al. 2001) also indicate kinematic loading maybe particularly large in the

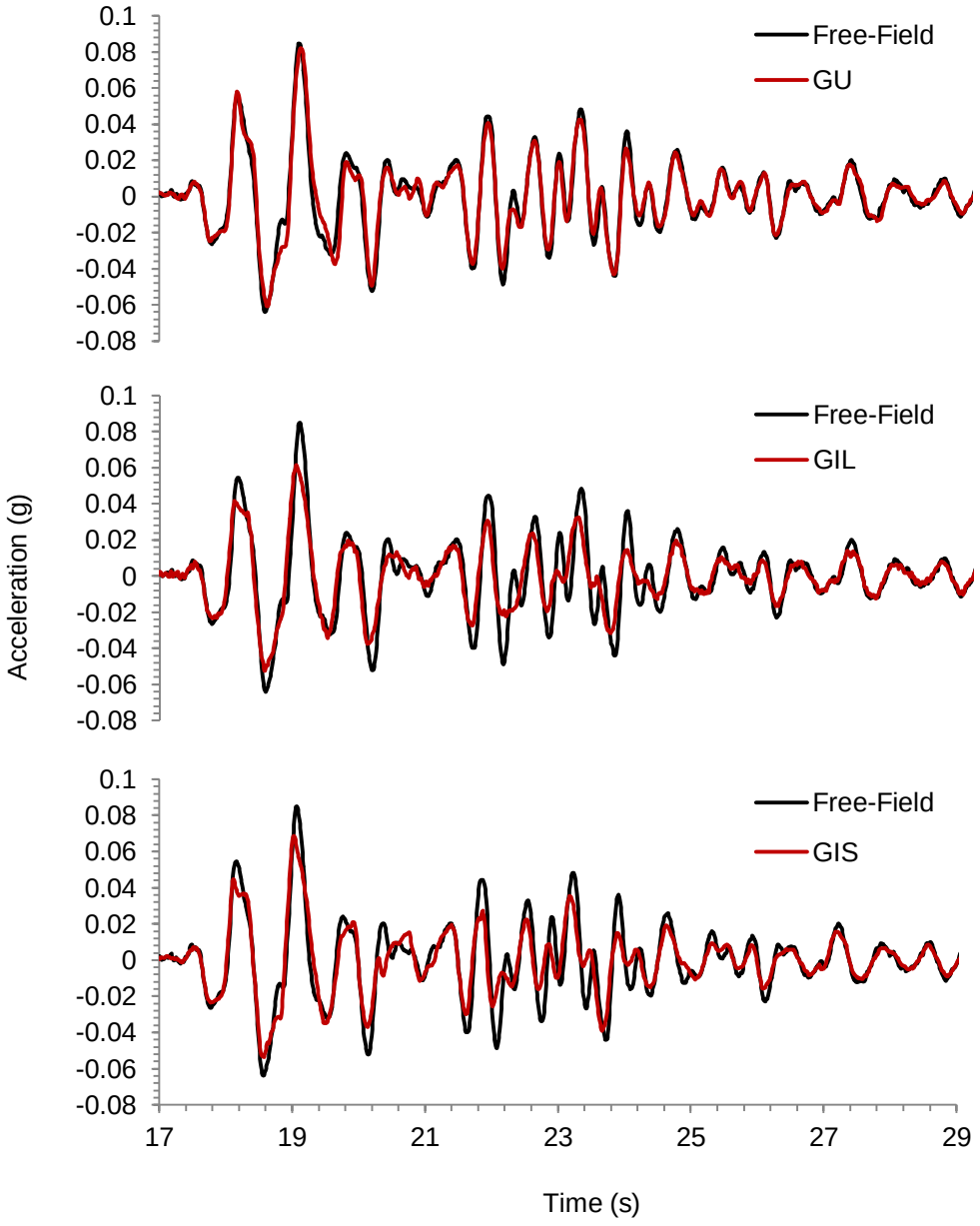

Figure 6-7. Foundation Level Motions and Their Comparison with the Free-Field Motion during Event A

vicinity of interfaces of alternating soft and stiff soil layers and also at the pile head when pile heads are restrained by a stiff cap. This is consistent with the kinematic interaction observed in the GIL and GIS pile groups. It is worth mentioning that the observed kinematic interaction in centrifuge tests is mostly contributed to the embedment effects as the incident waves are mostly coherent and propagate vertically.

6.4 Pile Group System Response

The acceleration, lateral displacement, settlement, and EPWP responses of the three pile group systems during Events A-G are presented in this section. Events A and B, respectively, correspond to weak and moderate shaking; whereas, Events C-G are strong shakings.

6.4.1 Acceleration and Lateral Displacement

Figure 6.8 compares the recorded peak horizontal acceleration (PHA) for the pile caps of the groups versus peak base acceleration. For reliability and repeatability purposes, two accelerometers were installed at similar locations on the pile caps and also in the soil (CDSM blocks and soft clay) near the structural models. Recordings from both accelerometers are presented in Figure 6.8. Compared to the GU and GIL pile caps, the GIS pile cap had higher peak accelerations during all events. The peak accelerations were almost same for the GIL and GU pile caps during scaled Kobe earthquakes and were somewhat higher for the GIL pile cap during very strong Santa Cruz earthquakes (Events F and G). For a given pile group, PHAs were higher for Kobe motions than Santa Cruz Motions. Increasing the peak base acceleration decreased time-

domain amplification ratios (ratio of the peak pile cap acceleration to peak base acceleration). This nonlinear behavior is consistent with the range of structural model periods, soil profile periods, and frequency content of the base motion. The nature of this nonlinear behavior will be discussed further in the following paragraphs.

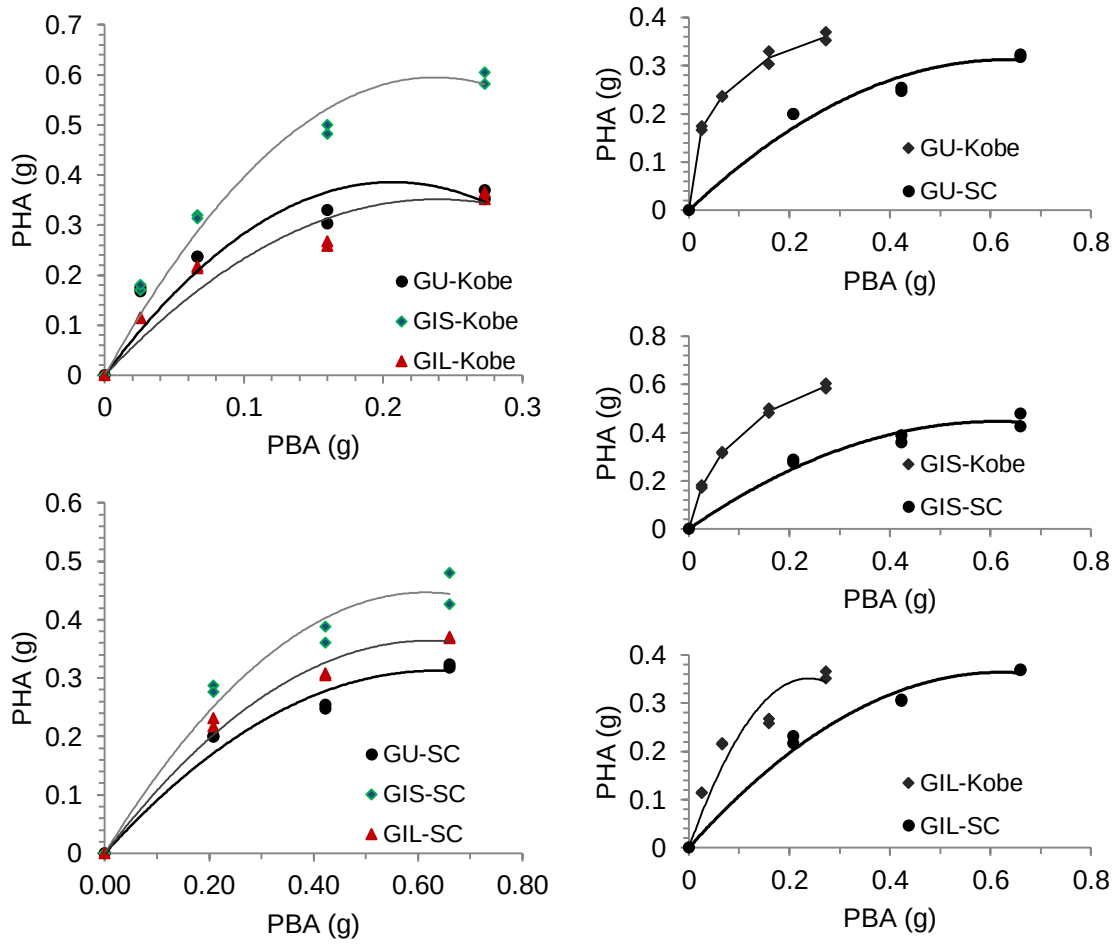

Figure 6-8 Variation of Peak Horizontal Acceleration (PHA) of Pile Cap with Peak Base Acceleration (PBA) during Different Scaled Kobe and Santa Cruz (SC) Earthquakes

Figure 6.9 depicts the recorded peak horizontal displacement (PHD) of the pile caps versus peak base acceleration. Displacement values were obtained by double

integration of accelerations. As discussed in Chapter 3, there is a good agreement between the transient displacement-time histories measured by LPs and calculated by double integration of acceleration values. Similar to the acceleration responses observed in Figure 6.8, higher peak displacements were obtained for all pile caps during scaled Kobe earthquake than scaled Santa Cruz earthquakes. Cement-deep-soil-mixing was an effective method in reducing the peak displacements of the GIL pile cap. The peak displacements of the GIS pile cap remained about the same as the GU pile cap.

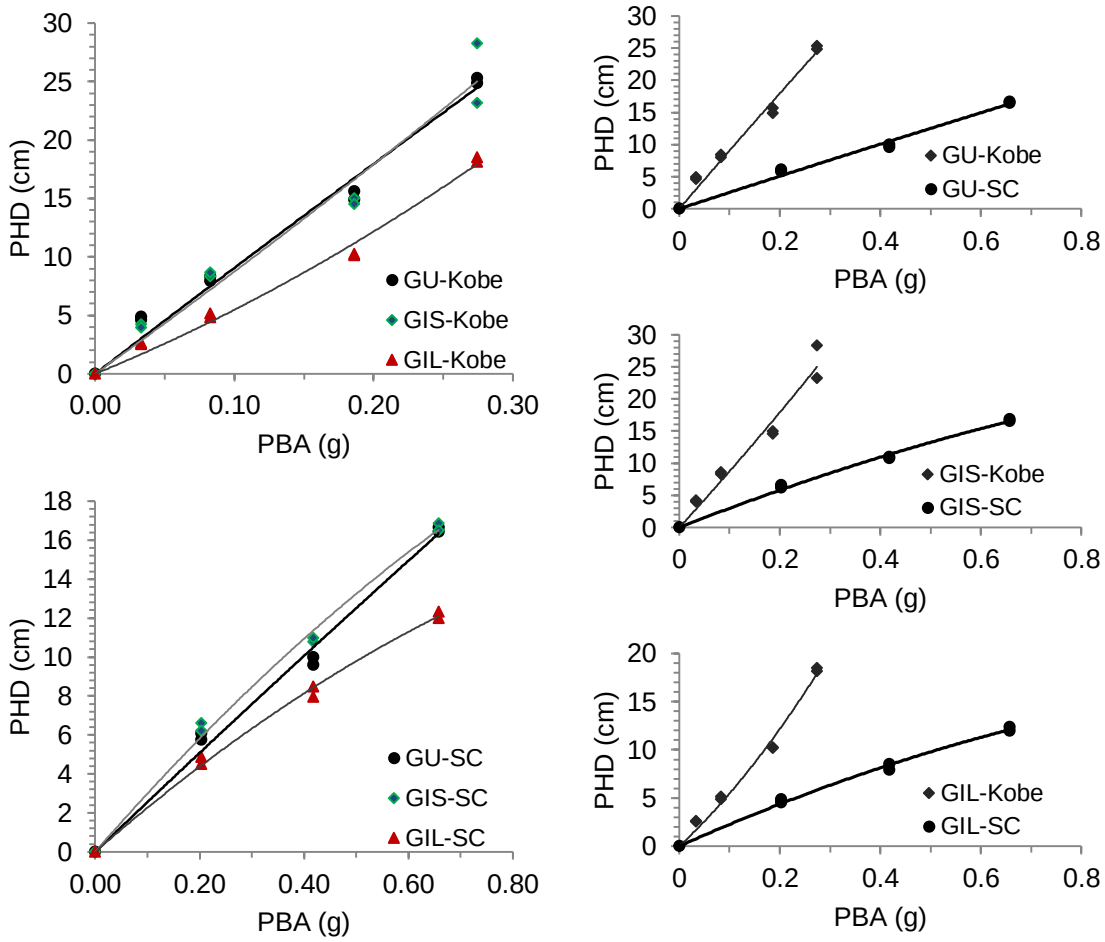

Figure 6-9. Variation of Peak Horizontal Displacement (PHD) of Pile Caps with Peak Base Input Acceleration (PBA) during Different Scaled Kobe and Santa Cruz Earthquakes

Figure 6.10 shows acceleration response spectra of the three pile caps during Events A-D. Increasing the shaking level from Event A to event D has increased the fundamental period in all three pile caps. This increase was larger for the GU pile cap and was much smaller for the GIL pile cap (except Event D). Two significant spectral acceleration peaks were developed in the GIL pile cap during Events C and D. In Event D, the fundamental period has shifted from the first peak to the second peak indicating dominance of a second mode of vibration. Higher spectral acceleration responses were obtained for the GIS pile cap during all events. Figure 6.11 shows the normalized acceleration response spectra of Kobe with PBA of 0.27g (Event D) and Santa Cruz with PBA of 0.21g (Event E) earthquakes. Higher spectral acceleration can be seen in the period range of 0.3s-3.0s in Kobe motion than Santa Cruz motion. This period range corresponds to the fundamental period range of structural models and explains why the pile caps have experienced higher peak acceleration during scaled Kobe earthquakes. These observations indicate the response of pile caps is strongly affected by the frequency content of base motion and the level of shaking.

Figure 6.12 illustrates acceleration spectral ratios obtained by dividing soil acceleration response spectra in the immediate vicinity of pile groups to that of base motion. The spectral ratios are obtained for the Events D and G. This figure shows that spectral ratios and variation patterns of all three pile group systems are almost similar. An attenuation in periods less than 1 s followed by amplification in longer periods were observed. Relatively lower spectral ratios were obtained for the GIL pile group system during both Kobe and Santa Cruz earthquakes. The comparisons shown in Figure 6.12

indicate that while motions near all pile groups are similar, the CDSM block of the GIL group reduces the motion somewhat.

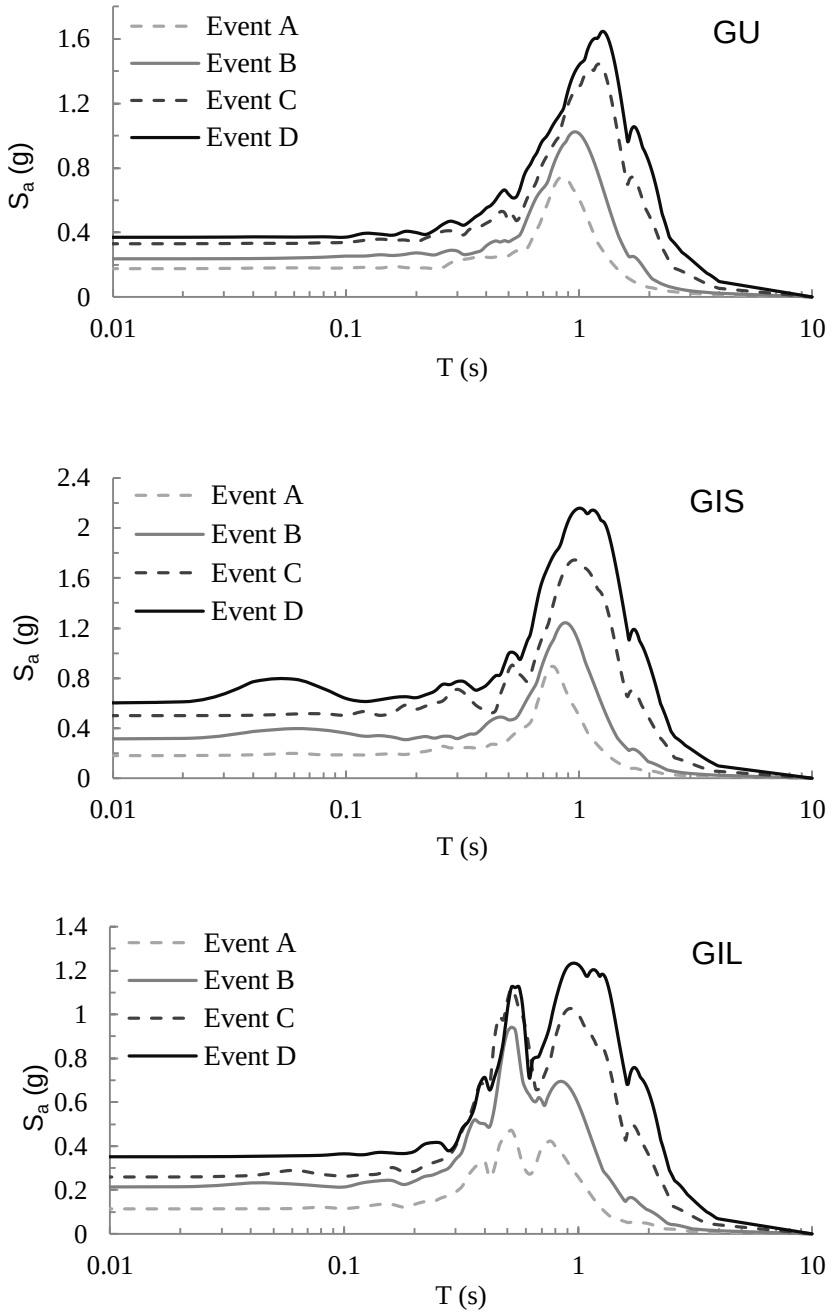

Figure 6-10. Pile Cap Acceleration Response Spectra during Scaled Kobe Earthquakes

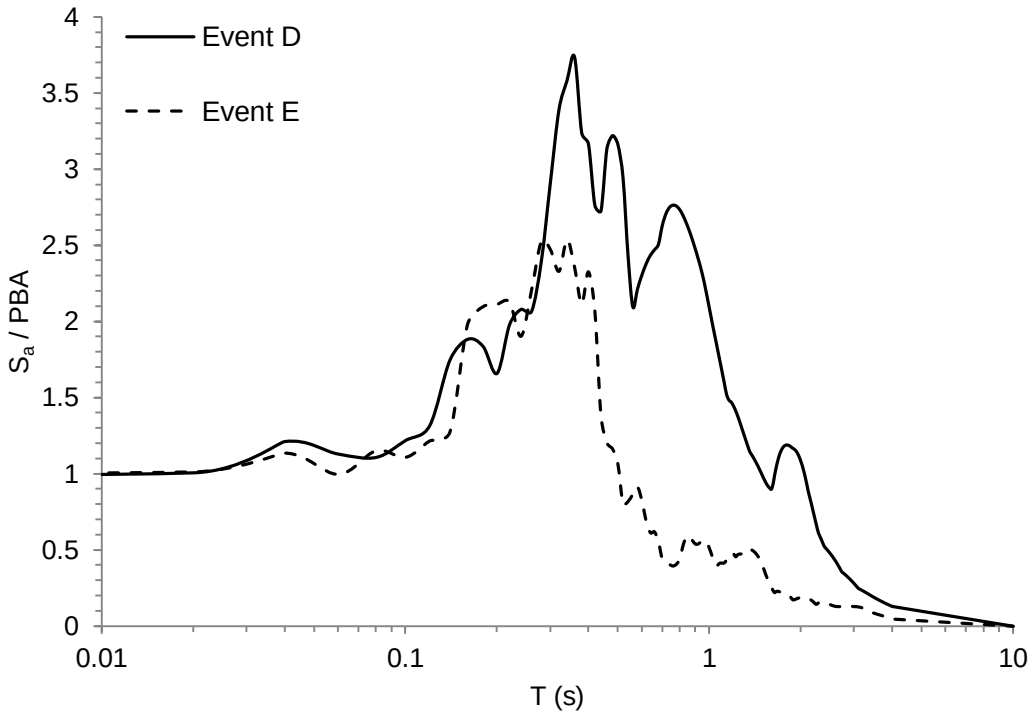

Figure 6-11. Normalized Base Input Acceleration Response Spectra for Event D (Kobe) and Event E (Santa Cruz)

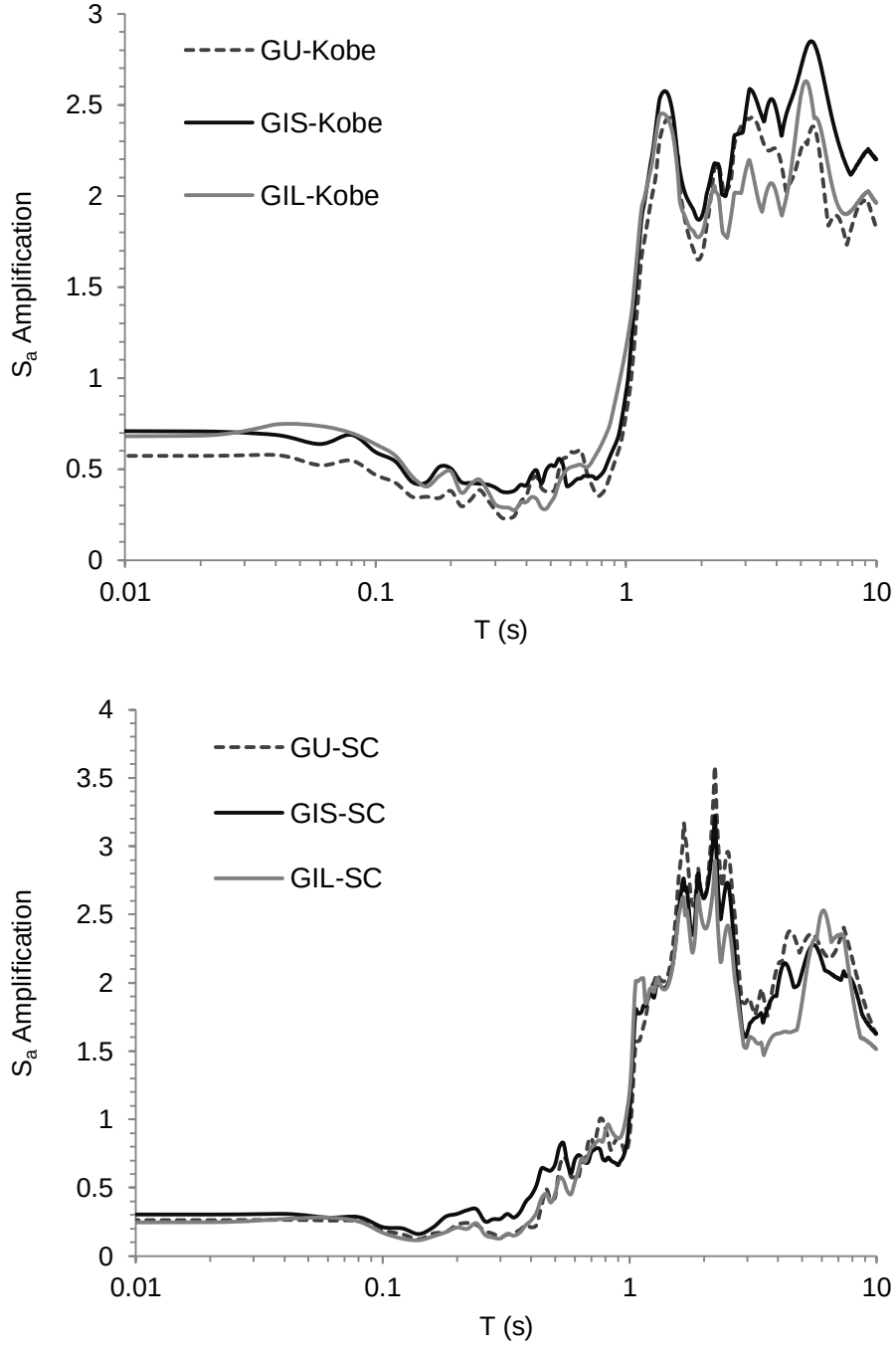

Figure 6-12. Spectral Acceleration (Damping =5%) Ratios of the Soil in the Immediate Vicinity of Pile Groups to the Base Input Motion during Event D (Kobe) and Event G (Santa Cruz)

Spectral acceleration ratios are also presented in Figure 6.13 for the pile caps with respect to the surface soil in the vicinity of pile groups. Several trends are evident from the spectral ratio plots. First, in short periods, the GIS group has experienced higher amplification than the GIL and GU groups, especially for Event D. The GIL amplification in short periods was lowest during Event D but was between the GIS and GU during Event G. Second, the maximum amplification was higher in the GIS pile group than the GIL and GU pile groups. The period where maximum amplification occurs becomes smaller as the dimensions of the CDSM block increases; that is, the GIL has the lowest period and the GU has the longest period. Third, much wider amplification bands can be observed for the GIS pile group near the fundamental period of the site. Forth, the GIS amplification was slightly higher than GIL and also GU in longer periods. In both events, the GIL amplification was lowest in periods longer than 0.8 s. These observations confirm the measured larger GIS pile cap responses during both Kobe and Santa Cruz earthquakes.

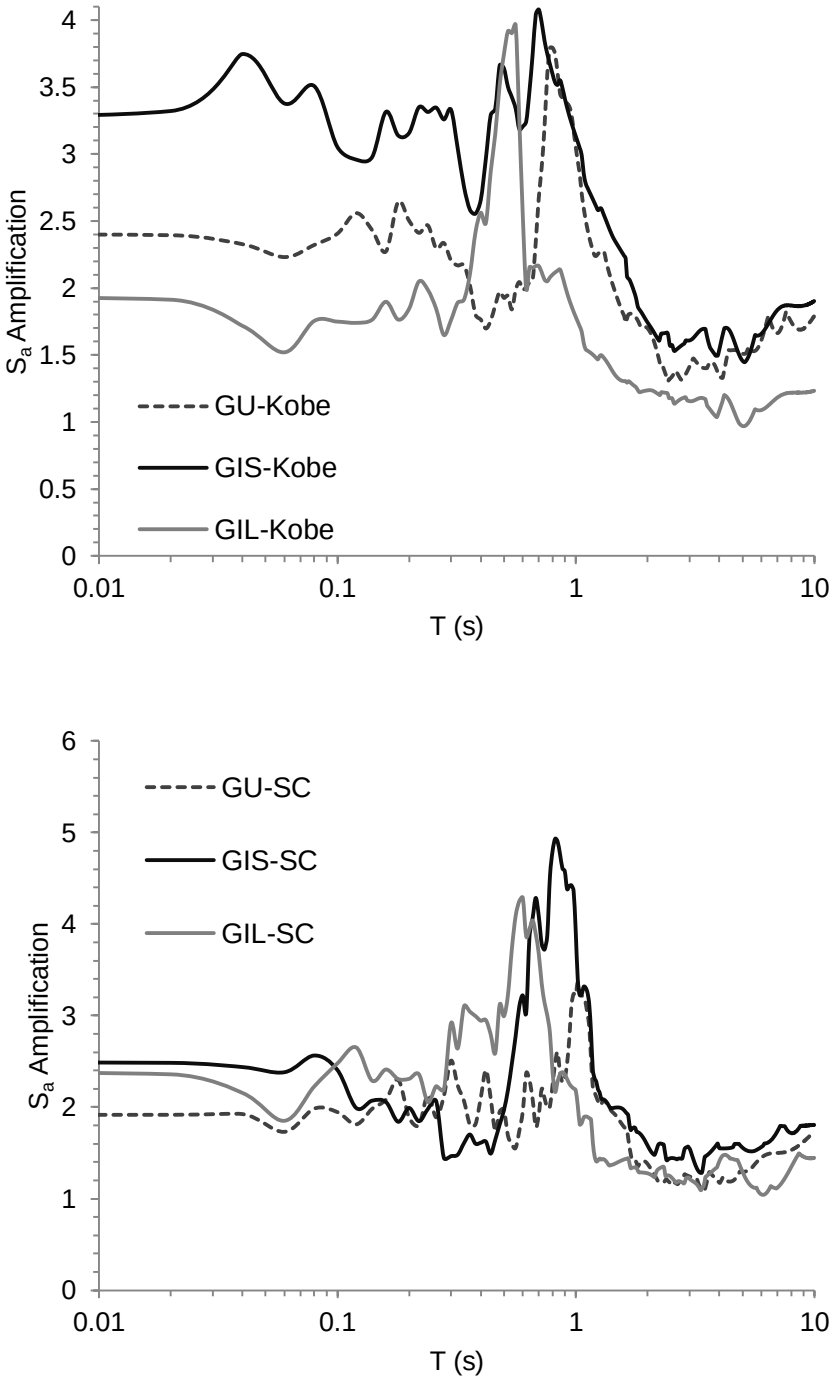

Figure 6-13. Spectral Acceleration (Damping =5%) Ratios of the Pile Caps to the Soil in the Immediate Vicinity of Pile Groups during Event D (Kobe) and Event G (Santa Cruz)

6.4.2 Settlement

Figure 3.7(a) shows the vertical LPs installed on the CDSM block of the GIL pile group, in soft clay in the vicinity of CDSM blocks, and in the free-field. Figure 6.14 compares the measured settlement during Events D and G. The GIL CDSM block has experienced the minimum amount of settlement during both events. It also appears that the cohesion between CDSM blocks and soft clay has reduced the settlement in the vicinity of the GIL and the GIS CDSM blocks compared to similar locations near the GU pile group. Increasing dimensions of CDSM blocks increases the cohesion and therefore less settlement has occurred in soft clay in the vicinity of the GIL than the GIS pile group. The free-field settlement is less than soft clay settlement in the vicinity of both GIS and GU pile groups during Event D and is comparable with that in the GU pile group during Event G.

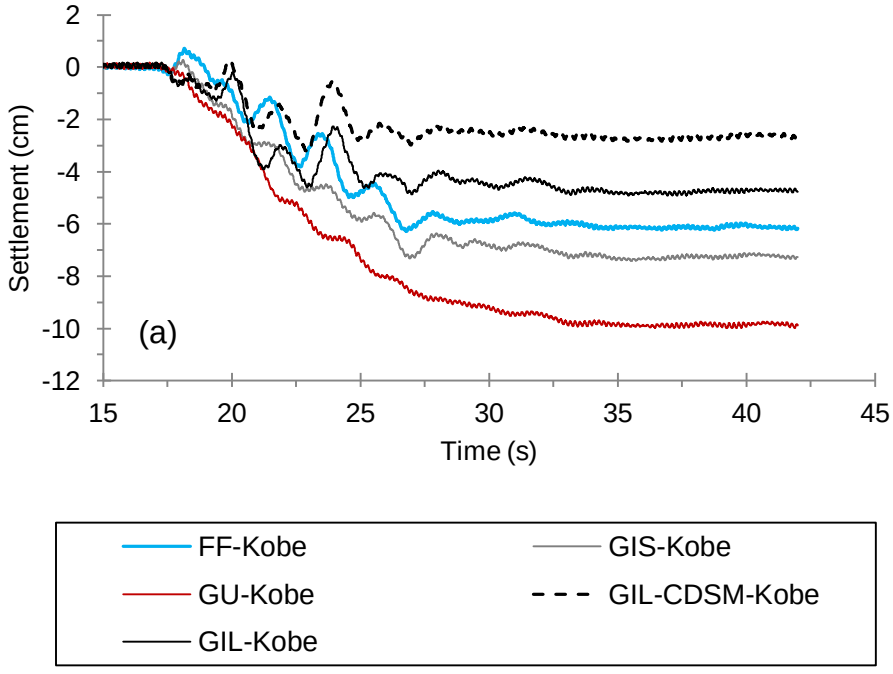

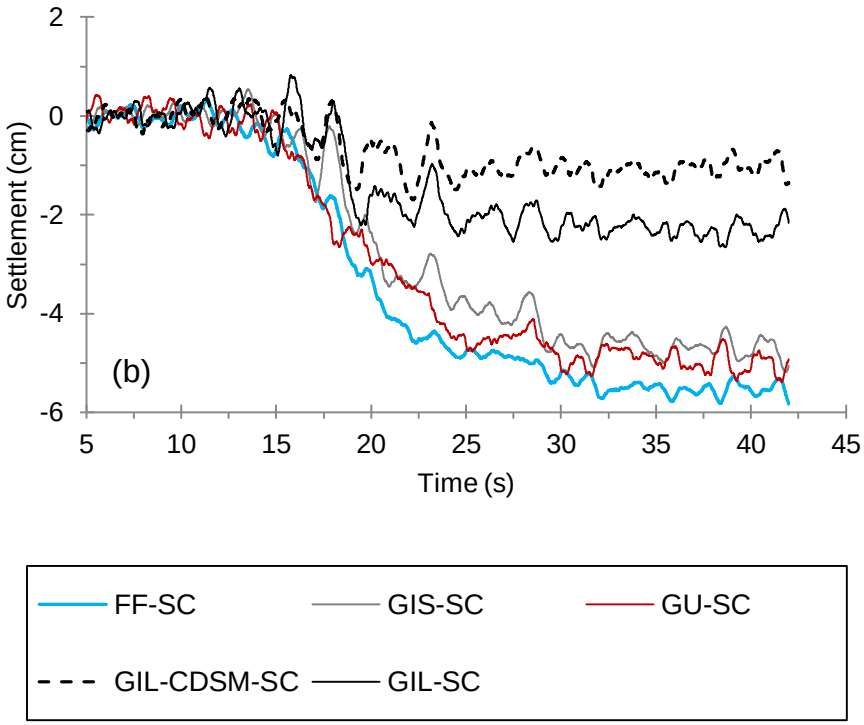

Figure 6-14. Measured Settlements in Free-Field, Near the Pile Groups, and on the CDSM Block of the GIL Pile Group during (a) Event D (Kobe); and (b) Event G (Santa Cruz)

6.4.3 Excess Pore Water Pressure (EPWP)

The locations of PPTs used for measuring EPWP are shown in Figure 3.7(a). All PPTs were located at 1.6m depths (almost mid-height of the top clay layer). The GIL and GIS PPTs were located at the similar lateral distances (0.9 m) from the CDSM blocks. The same distance (0.9 m) but from the outer edge of pile group was used for the PPT of the GU pile group. Figure 6.15 compares the measured EPWP at the aforementioned locations and in free field during Events D and G. For comparison purposes, initial vertical effective stress is also calculated and shown at the location of PPTs. More residual EPWP has been generated in soft clay in the vicinity of CDSM

blocks than the corresponding location in the GU pile group or in the free-field. It appears vibrations of CDSM blocks and elongation of seepage path in the vicinity of CDSM blocks have caused an increase in the EPWP. The residual EPWP is also somewhat higher near the GU pile group than the free-field. Residual EPWP ratio (r_u) is defined as the ratio of average residual EPWP to the initial vertical effective stress. The residual r_u values during event G for the GIL, GIS, GU, and free-field were 0.19, 0.18, 0.10, and 0.06, respectively. These values during event D were 0.26, 0.23, 0.14, and 0.16, respectively.

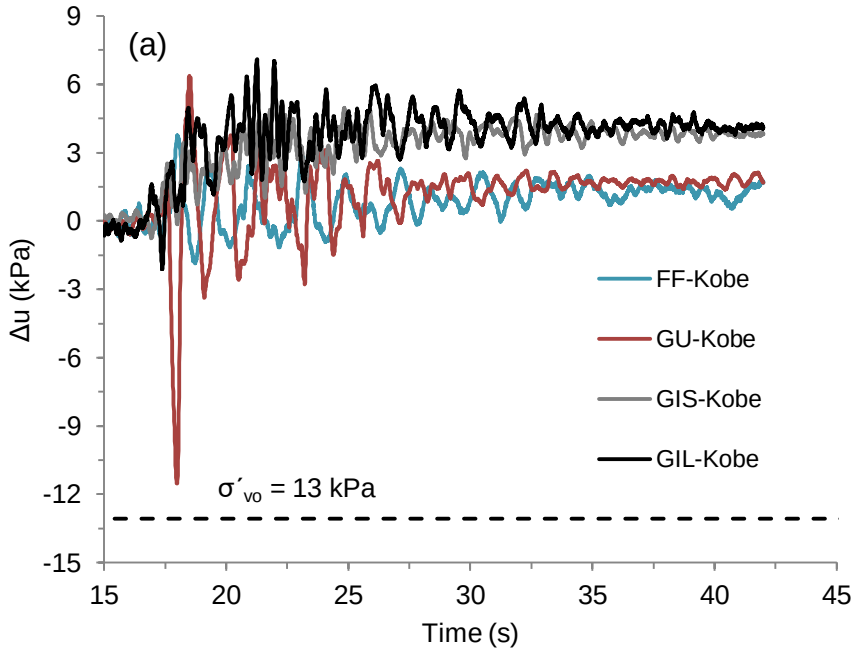

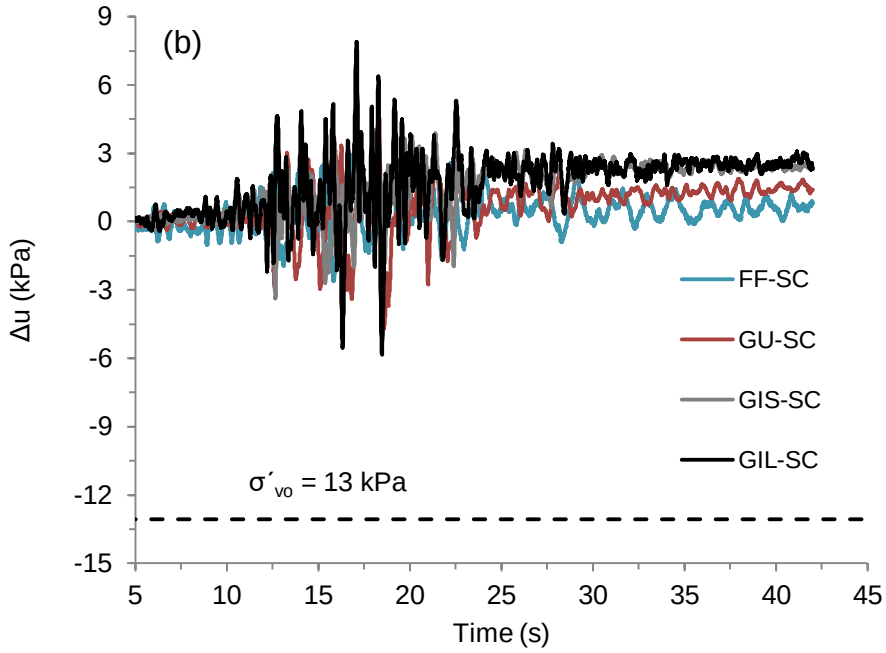

Figure 6-15. EPWP-Time Histories in Free-Field and Near the Pile Groups during (a) Event D (Kobe); and (b) Event G (Santa Cruz)

Chapter 7: FEM Analyses of Dynamic Soil-Pile-Structure Interaction in Improved Soft Clay

7.1 Overview

TeraDysac (Muraleetharan et al. 2003), a three-dimensional parallel computer code, is used for two-dimensional numerical modeling of pile groups in unimproved and improved soft clay under base shaking in centrifuge tests. TeraDysac is developed using the TeraScale framework (ANATECH Corp. 2001) and solves the fully coupled dynamic governing equations for saturated (Muraleetharan et al. 1994) and unsaturated (Ravichandran 2005) porous media. The main objectives of this preliminary numerical analyses are to compute the seismic response of pile groups in unimproved and improved soft clay in centrifuge tests in a fully coupled manner; and compare the computed results with centrifuge test results and thereby validate TeraDysac.

7.2 Soil Element

The soils modeled in this study are assumed to be saturated, but capabilities exist to model unsaturated soils in TeraDysac (Ravichandran 2005). The formulation of the governing equations can be found in Muraleetharan et al. (1994). Pore water pressure is assumed positive in compression. Tensile normal stresses and strains are assumed positive. Four-noded, isoparametric, uniform gradient elements are used in this study. Nodal variables per node are two soil skeleton and two fluid displacements.

7.3 Constitutive Models

7.3.1 Bounding Surface Model for Clays

In TeraDysac, stress–strain behavior of the soil skeleton can be described by the isotropic linear elastic model and bounding surface elastoplastic models. Dafalias and Herrmann (1986) bounding surface plasticity model was used for soft clay and CDSM improved clay (see Figure 7.1). The bounding surface is comprised of two ellipses and a hyperbola. During loading, inelastic deformations occur for stress points within and on the bounding surface. Unloading is treated as a purely elastic phenomenon. A radial mapping rule is used to relate the actual stress point (I, J) to an "image" stress point on the bounding surface ($\bar{I}$, $\bar{J}$). The value of the plastic modulus depends on the distance between the actual stress point and the "image" stress point.

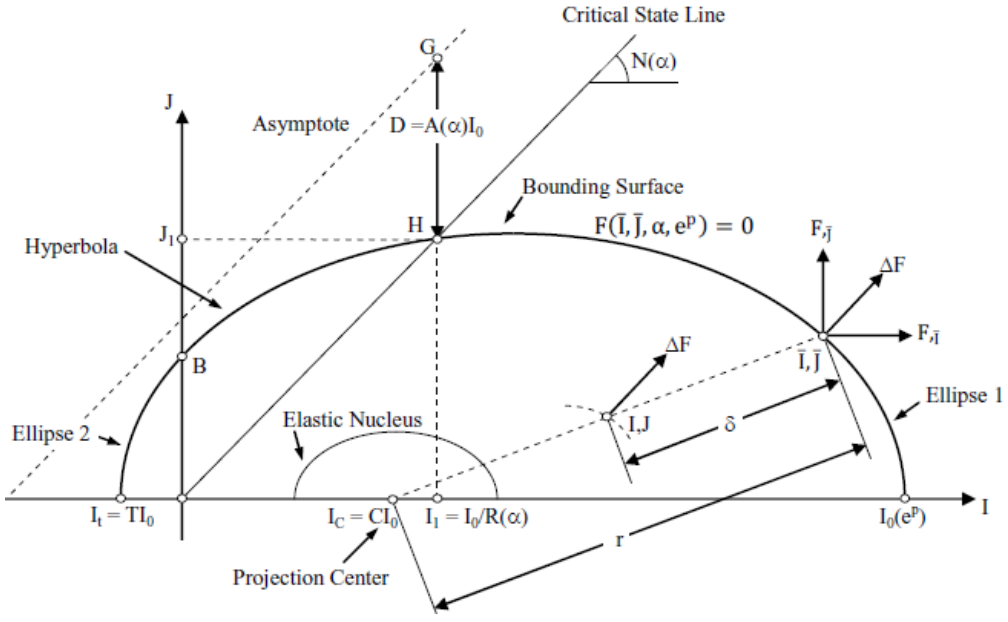

Figure 7-1. Schematic Illustration of Bounding Surface and Radial Mapping Rule in Stress Invariants Space (Dafalias and Herrmann 1986)

The bounding surface model was calibrated based on the results of different laboratory tests including oedometer tests and CIUC and CIUE triaxial test results (Thompson 2011). The calibrated parameters are given in Tables 7.1 and 7.2. Laboratory test results revealed that using an overconsolidation ratio (OCR) of 24 can reasonably capture the important characteristics of the stress-strain relationship of the CDSM improved clay used in this study.

Table 7-1. Calibrated Model Parameters for Soft Clay

Property	Symbol	Value
Traditional Model Parameters		
Slope of the isotropic consolidation line on $e - \ln p'$ space	λ	0.14
Slope of the elastic rebound line on $e - \ln p'$ space	κ	0.029
Slope of the critical state line in $q - p'$ space (compression)	M_c	1.0
Ratio of extension to compression value of M	M_e/M_c	0.83
Poisson's ratio	v	0.3
Bounding Surface Configuration Parameters		
Parameter defining ellipse 1 in compression	R_c	2.5
Parameter defining the hyperbola in compression	A_c	0.1
Parameter defining ellipse 2 (the tension zone)	T	0.05
Projection center parameter	C	0.2
Elastic nucleus parameter	S	1.2
Ratio of triaxial extension to triaxial compression value of R	R_e/R_c	1.0
Ratio of triaxial extension to triaxial compression value of A	A_e/A_c	1.0
Hardening Parameters		
Shape hardening parameter in triaxial compression	h_c	1.0
Ratio of triaxial extension to triaxial compression value of h	h_e / h_c	1.0
Hardening parameter for states in the vicinity of I-axis	h_0	1.0

Table 7-2. Calibrated Model Parameters for Improved Clay

Property	Symbol	Value
Traditional Model Parameters		
Slope of the isotropic consolidation line on $e - \ln \acute{p}$ space	λ	0.045
Slope of the elastic rebound line on $e - \ln \acute{p}$ space	κ	0.0027
Slope of the critical state line in $q - \acute{p}$ space (compression)	M_c	3.0
Ratio of extension to compression value of M	M_e/M_c	0.4667
Poisson's ratio	v	0.3
Bounding Surface Configuration Parameters		
Parameter defining ellipse 1 in compression	R_c	2.0
Parameter defining the hyperbola in compression	A_c	0.1
Parameter defining ellipse 2 (the tension zone)	T	0.05
Projection center parameter	C	0.0
Elastic nucleus parameter	S	1.0
Ratio of triaxial extension to triaxial compression value of R	R_e/R_c	1.0
Ratio of triaxial extension to triaxial compression value of A	A_e/A_c	1.0
Hardening Parameters		
Shape hardening parameter in triaxial compression	h_c	200.0
Ratio of triaxial extension to triaxial compression value of h	h_e / h_c	1.0
Hardening parameter for states in the vicinity of I-axis	h_0	200.0

Permeability of unimproved clay was obtained using the following equation:

$$k = C_v \times \frac{\lambda \gamma_w}{\sigma_v^{/} (1 + e_0)} \qquad \textbf{Equation 7-1}$$

where C_v is the coefficient of consolidation and was obtained by oedometer tests for different initial vertical stresses. A C_v value of 4.5×10^{-8} m^2/s corresponding to the average effective stress in the unimproved clay layer was utilized. Permeability of clay layer was found to be 7.0×10^{-10} m/s. Same procedure was used for improved clay and the permeability was found to be 2.89×10^{-10} m/s.

7.3.2 Linear Elastic Model for Sand

In order to simplify calculations and reduce computational time, dense sand layer was modeled as an isotropic linear elastic material. Considering high relative density of this layer, linear elastic assumption seems reasonable for the problem studied. For the linear elastic problems, only Young's modulus and Poisson's ratio are required. Poisson's ratio for the dense Nevada sand was set to 0.3 (Muraleetharan et al. 2004). Young's modulus was calculated using the average of the following equations:

$$E = \frac{\sigma_v^{/}(1+e_0)}{\lambda} \times \frac{(1+\nu)(1-2\nu)}{(1-\nu)} \qquad \textbf{Equation 7-2}$$

$$E = \frac{\sigma_v^{/}(1+e_0)}{\kappa} \times \frac{(1+\nu)(1-2\nu)}{(1-\nu)} \qquad \textbf{Equation 7-3}$$

The values used for λ and κ were 0.009 and 0.002, respectively (Muraleetharan et al. 2004). The average young's modulus was found to be 45575 kPa. The value used for combined bulk modulus of water and soil grains was 2.2×10^6 kPa. A permeability value of $k = 2.30 \times 10^{-5}$ m/s was used for the dense sand layer (Arulmoli et al. 1992).

7.3.3 Initial Stress States

In analyzing a problem with an elasto-plastic model, the first and foremost task is to simulate the loading history as accurately as possible, so that the values of stresses and plastic internal variables could be established at different stages of loading. The initial vertical stresses were obtained by multiplying the unit weight of soil to mid-depth of the element. By multiplying initial vertical stresses by K_0, the coefficient of earth pressure at rest, horizontal stresses were obtained for each element.

K_0 for normally consolidated clay was calculated using the following equation (Massarsch 1979).

$$K_0 = 0.44 + 0.42\,PI/100 \qquad \textbf{Equation 7-4}$$

K_0 values for normally consolidated clay layers of this study were found to be about 0.52. Equation 7-5 can be used to obtain K_0 for overconsolidated improved and unimproved clay (Das 2010; Michalowski 2005).

$$K_{0(OC)} = K_{0(NC)} \times \sqrt{OCR} \qquad \textbf{Equation 7-5}$$

Jaky (1948) equation was used to obtain K_0 for sand (Das 2010; Michalowski 2005).

$$K_0 = 1 - \sin\varphi \qquad \textbf{Equation 7-6}$$

7.4 Beam Element

In TeraDysac, piles and pile caps are modeled using low order Timoshenko beam elements (Krier 2009). The low order element is compatible with the four node quadrilaterals and eight node hexagonal soil elements, which have a linear variation of displacement between nodes. The nodal unknowns for a pile element are solid displacements and rotations. In the simulations presented in this paper, the pile elements are tied to the soil elements, i.e., no interface elements were used. Figure 7.2 illustrates two beam elements and adjoining soil elements. Relatively rigid horizontal beam elements were used to connect the piles and provide fixed-end conditions (see Figures 7.3 and 7.4). In order to model the pile cap and reasonably capture the inertial forces, vertical beam elements with a total height and mass equal to those of the pile cap in the centrifuge tests were rigidly connected to the mid-section (node) of the horizontal beam

elements. The flexural stiffness of the beam elements modeling the pile cap was same as that for the pile cap in the centrifuge tests.

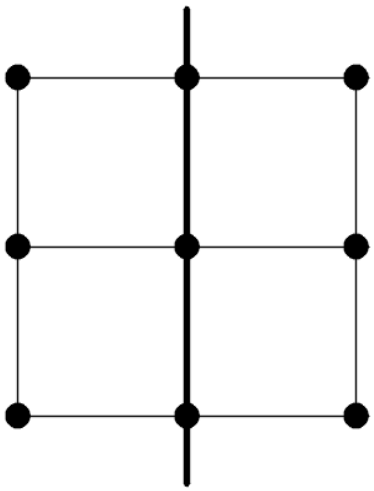

Figure 7-2. Soil and Beam Elements

In order to approximate the 3D behavior using a 2D FEM model in the current study, the two-by-two group of piles was represented by two piles, each having twice the axial and bending stiffness of a single pile (Chang et al. 2013; Krier 2009; Zhang et al. 2008).

7.5 Numerical Integration

A three-parameter time integration scheme called the Hilber-Huges-Taylor α-method (Hilber et al. 1977) is used, together with a predictor multi-corrector algorithm, to integrate the spatially discrete finite element equations (Muraleetharan et al. 1994). This time integration scheme provides quadratic accuracy and desirable numerical damping characteristics to damp the high-frequency spurious modes.

In the α-method, the relationships between acceleration, velocity, and displacement are controlled by the time-integration parameters α, β, and γ. If the three parameters are chosen such that $-1/3 \leq \alpha \leq 0$; $\gamma = ½ (1-2\alpha)$; and $\beta = ¼ (1-\alpha)^2$, then this method produces a quadratic accuracy and desirable numerical damping characteristics to damp the high-frequency spurious modes (Muraleetharan et al. 1994).

7.6 Finite Element Mesh

The finite element meshes for the GU and GIL pile groups are shown in Figures 7.3 and 7.4. Kuhlemeyer and Lysmer (1973) showed that for accurate modeling of wave propagation through a model, the spatial element size, Δl, must be smaller than approximately one-tenth to one-eighth of the wavelength associated with the highest frequency component of the input wave. Considering a maximum frequency of the filtered base motion equal to 15 Hz, this recommendation was met in determining element sizes in this study. Based on the sensitivity analyses, it was found that using 3324 and 3126 elements to model the GU and GIL pile groups, respectively, gives satisfactory results. The dimensions of FE model were same as the centrifuge model. With respect to the x-y-z coordinate system shown in Figures 7.3 and 7.4, the soil is taken to be a meter thick in the z-direction. The pile foundations were located at the same locations as the centrifuge model. Except the nodes at the surface, all surrounding nodes of the soil medium were impervious. The ground water level was set at the surface during the analyses, similar to the centrifuge experiments. In order to simulate 1D wave propagation in 2D space, nodes on the two vertical boundaries at the same elevation were assumed to have the same motion using the master/slave node technique.

The bottom nodes were fixed in both the horizontal and vertical directions (Taghavi and Muraleetharan 2012). The acceleration time history of Event B (Kobe earthquake with peak base acceleration of 0.066g) recorded in the centrifuge test at the base of the container was applied as the base motion to the meshes shown in Figures 7.3 and 7.4.

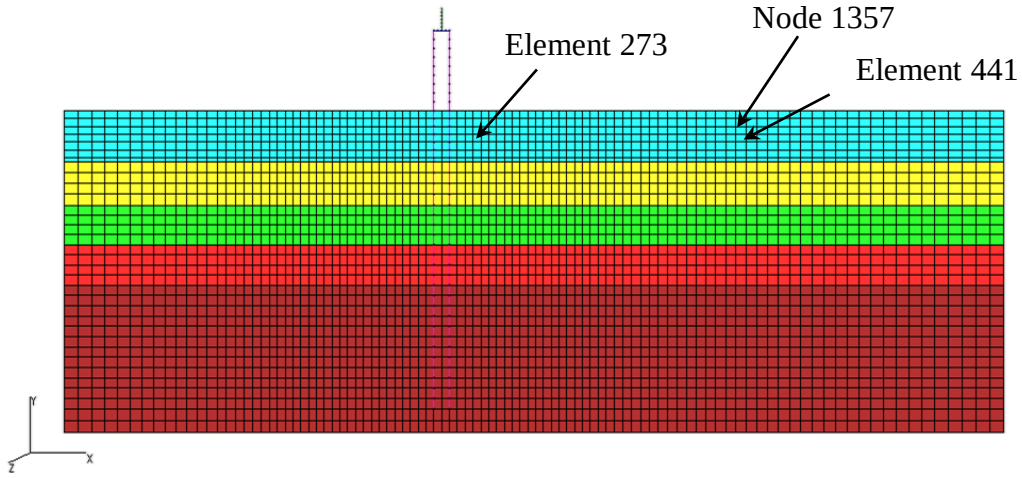

Figure 7-3. Finite Element Mesh for the GU Pile Group

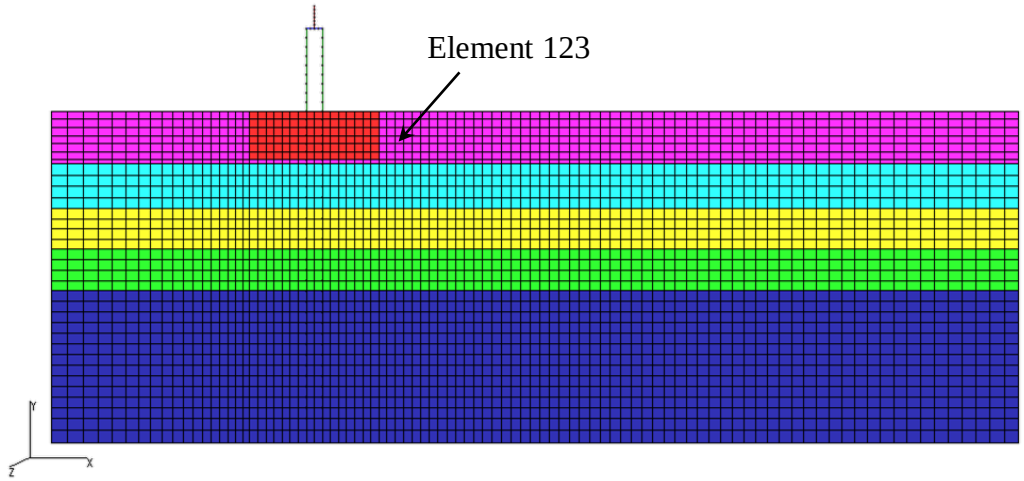

Figure 7-4. Finite Element Mesh for the GIL Pile Group

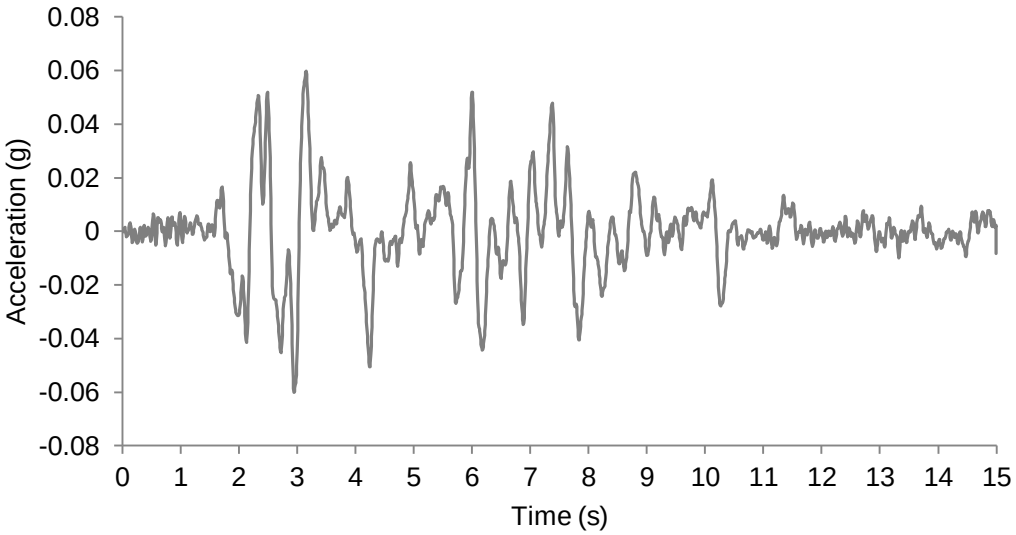

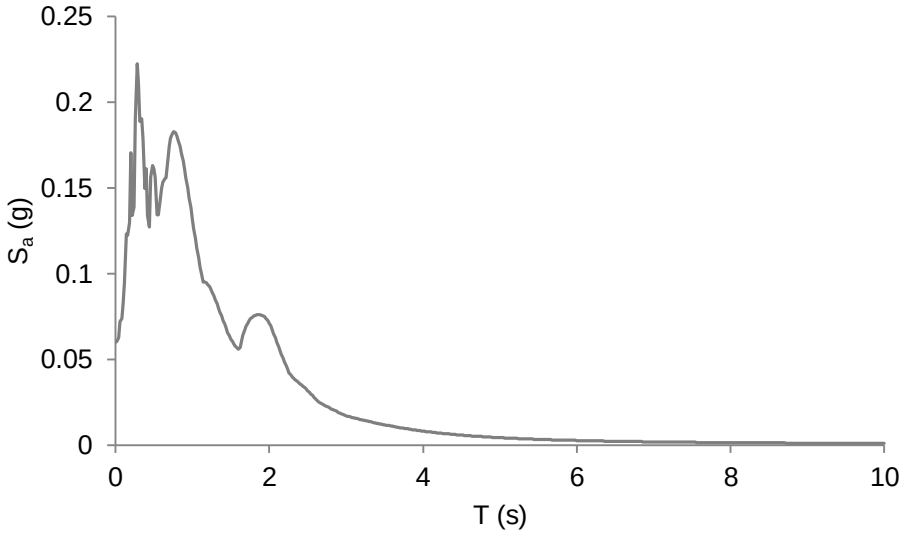

Figure 7-5. Base Acceleration - Time History and its Response Spectrum (Event B)

7.7 Comparison of FEM and Centrifuge Tests Results

The two-dimensional, plane strain, finite element models of the improved and unimproved pile groups shown in Figures 7.3 and 7.4 were analyzed. The meshes shown in these figures are intended to be a sectional plane of the centrifuge model container through the center of pile group and parallel to the direction of shaking. In order to reduce the computational time, only the strong motion part of the acceleration (15-second long) is used in the analyses (see Figure 7.5). From the end of this strong motion, a free vibration analysis is carried out for another 30 seconds.

The results obtained from centrifuge tests are compared with the TeraDysac results. Figures 7.6-7.16 compare acceleration-time histories, acceleration response spectra, displacement-time histories, and EPWP-time histories in the free-field and also on or near the GU and GIL pile groups. It can be observed that the TeraDysac results agree reasonably well with the centrifuge test results in most cases. For example, the peak value of the accelerations at the GU and GIL pile caps were experimentally found to be 0.24 g and 0.21 g, respectively, in centrifuge tests, and it is computed to be 0.22 g and 0.23 g by the TeraDysac analysis. The peak acceleration value in free field is overestimated in the TeraDysac analyses. The acceleration peaks after shaking (beyond 15 s) is also overpredicted. This is because all energy dissipation mechanisms such as gapping are not considered or modeled properly in the TeraDysac analyses. Furthermore, material damping provided by the bounding surface model may not be sufficient.

It may be observed that the experimental response spectra of accelerations at the pile caps and free-field compare reasonably well with the corresponding theoretical

response spectra. The peak spectral acceleration value in free-field is overestimated; however, it is underestimated in the GU pile cap. The peak spectral acceleration value of the GIL pile cap matches well with the measured value.

There is a good agreement between the measured and computed peak displacement values. For example, the peak value of the displacements at the GU and GIL pile caps were experimentally found to be 8.3 cm and 4.8 cm, respectively, in centrifuge tests and it is computed to be 8.7 cm and 6.9 cm by the finite element analysis. Both centrifuge test results and TeraDysac analyses show a reduction in the peak displacement value of the improved (GIL) pile cap. The residual displacements of the GU and GIL pile caps predicted by the finite element method are 3.2 cm and 2.8 cm, respectively. Because accelerometers are not capable of measuring permanent displacements, no residual displacements were measured by the accelerometers. In contrast to the centrifuge test results, larger amplitude displacements and accelerations are observed in the TeraDysac predictions during free vibrations (after 15 s of the excitation by the input motion). These large amplitude displacements are again related to gapping and not enough material damping modeled in TeraDysac.

It may be observed that the experimental EPWP-time histories in the free-field and in the vicinity of the GU and GIL pile groups compare reasonably well with the corresponding TeraDysac predictions. The locations of PPTs used in the centrifuge tests are depicted in Figure 3.7(a) and are explained in Section 6.5.3. The peak value of the EPWP in the free-field and the vicinity of GU pile group was experimentally found to be 4.7 kPa and 5.0 kPa, respectively, in centrifuge tests and it is computed to be 3.1 kPa and 6.2 kPa by the finite element analysis. The residual EPWPs in the free-field and the

vicinity of GU pile group were experimentally found to be 2.0 kPa and 1.4 kPa, respectively, in centrifuge tests and computed to be 2.0 kPa and 1.1 kPa by the finite element analysis. The computed EPWP-time history in the vicinity of the GIL pile group is depicted in Figure 7.16. Due to malfunctioning of the PPT in this location during Events A and B, the measured data were not available. The peak and residual computed EPWP were 5.23 kPa and 0.9 kPa, respectively.

Considering the implemented approximate procedure in 2D FEM modeling of the studied 3D dynamic soil-structure interaction problem, it can be concluded that the experimental responses compare reasonably well with the corresponding theoretical responses.

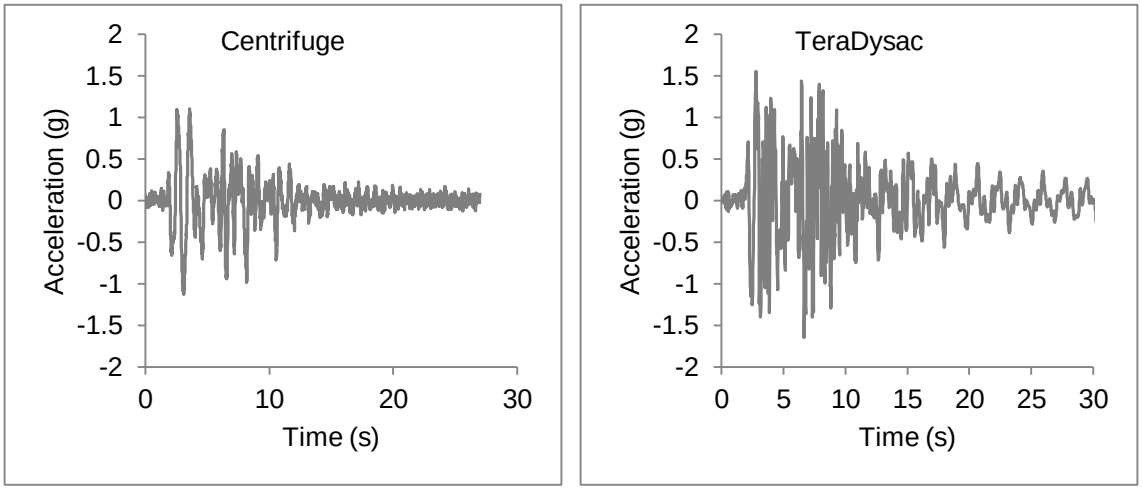

Figure 7-6. Measured (A39) and Computed (Node 1357) Acceleration-Time Histories in the Free-Field during Event B. (The Computed Response is obtained from the GU Analysis.)

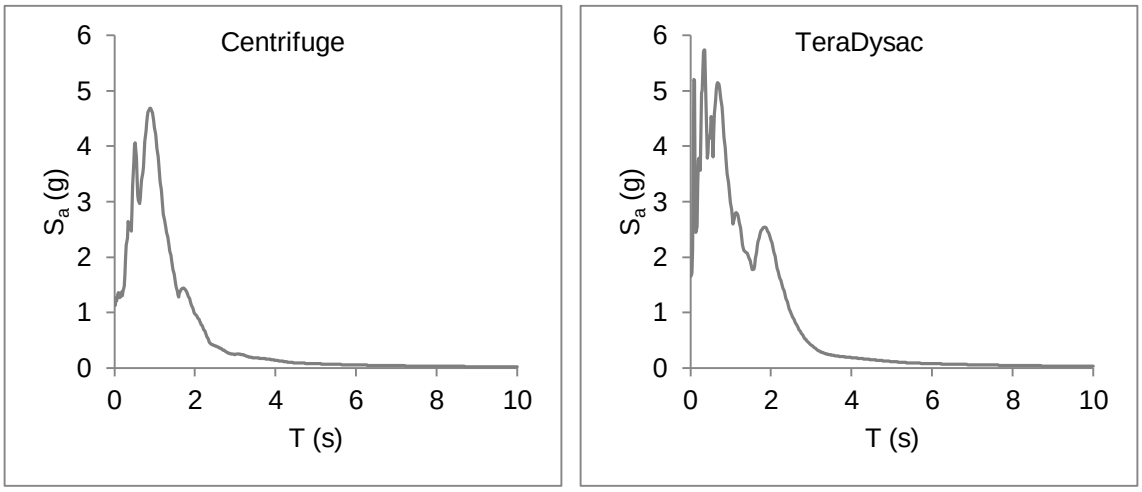

Figure 7-7. Measured (A39) and Computed (Node 1357) Acceleration Response Spectra in the Free-Field during Event B. (The Computed Response is obtained from the GU Analysis.)

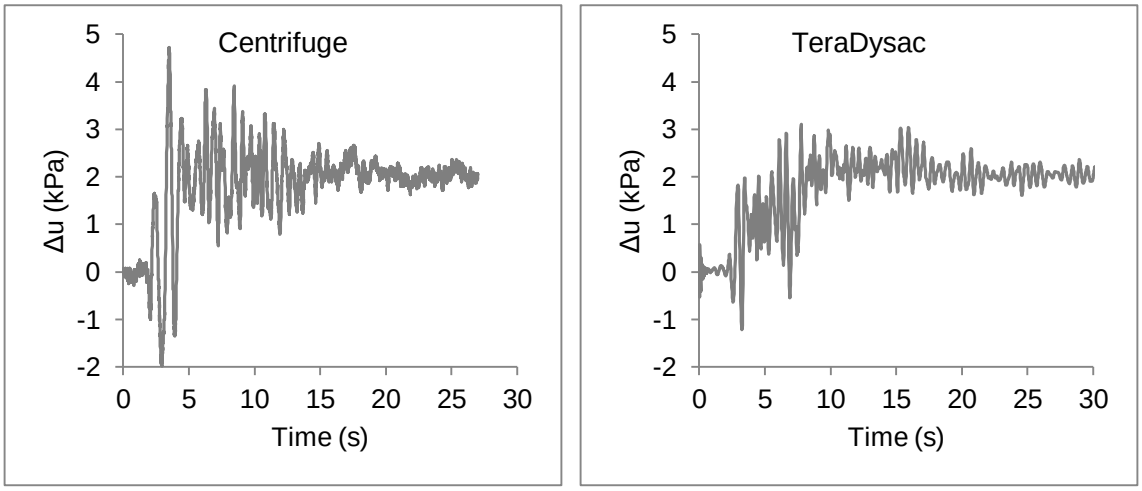

Figure 7-8. Measured (P12) and Computed (Element 441) EPWP-Time Histories in the Free-Field during Event B. (The Computed Response is obtained from the GU Analysis.)

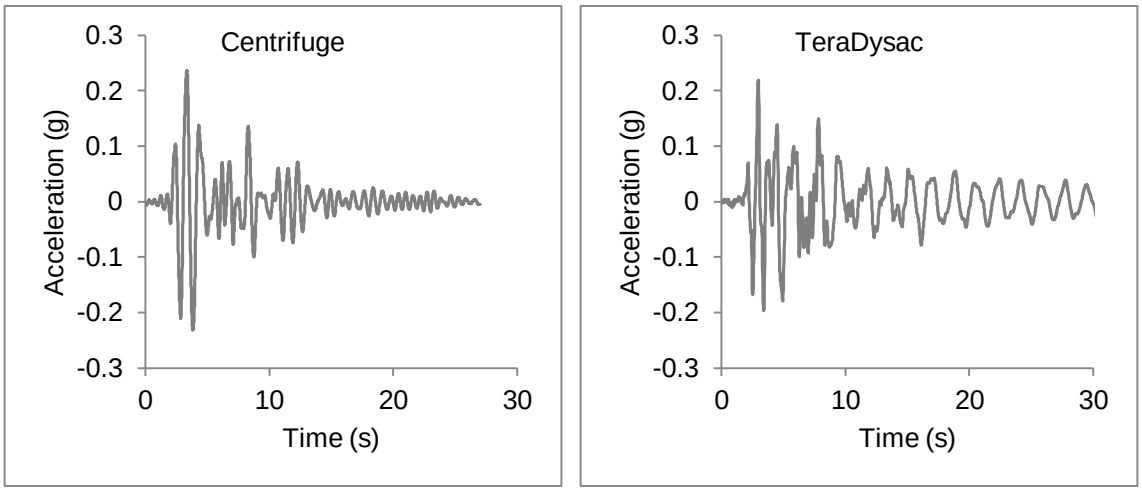

Figure 7-9. Measured and Computed Acceleration-Time Histories of the GU Pile Cap during Event B

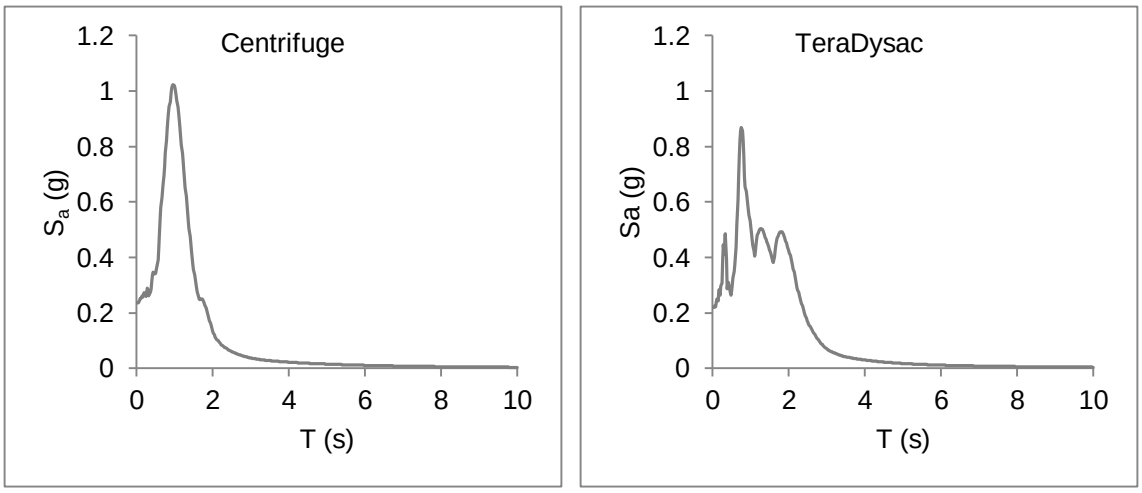

Figure 7-10. Measured and Computed Acceleration Response Spectra of the GU Pile Cap during Event B

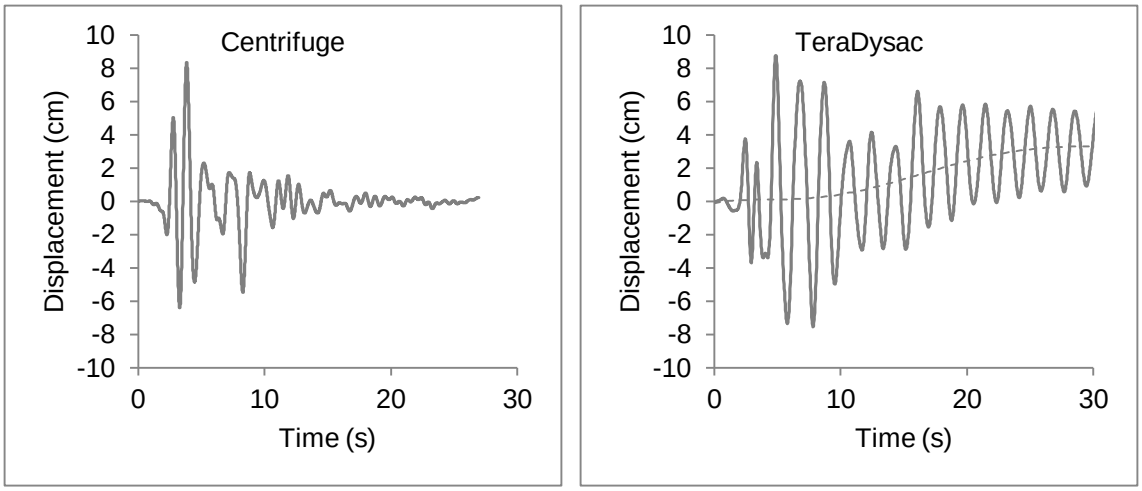

Figure 7-11. Measured and Computed Displacement-Time Histories of the GU Pile Cap during Event B

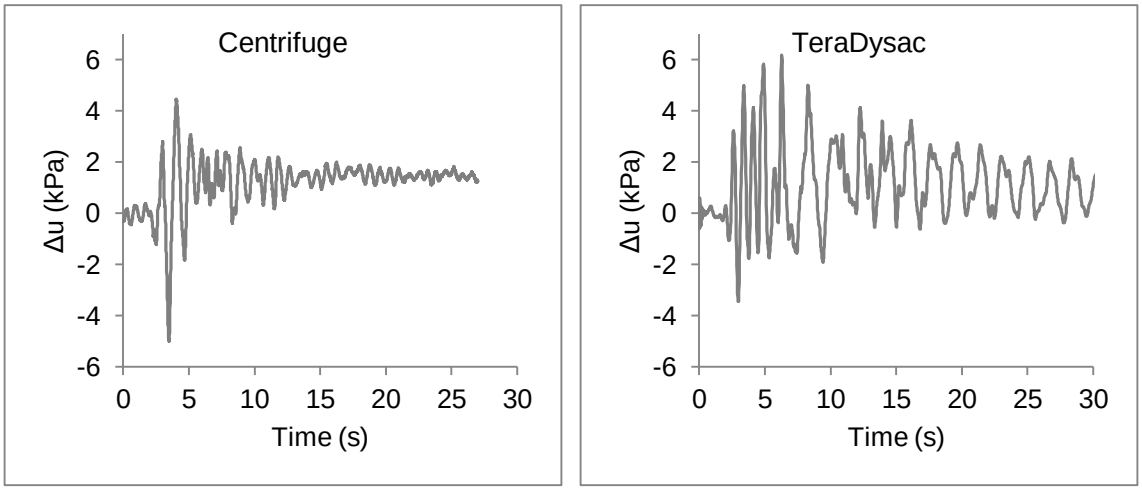

Figure 7-12. Measured (P10) and Computed (Element 273) EPWP-Time Histories in the vicinity of the GU Pile Group during Event B

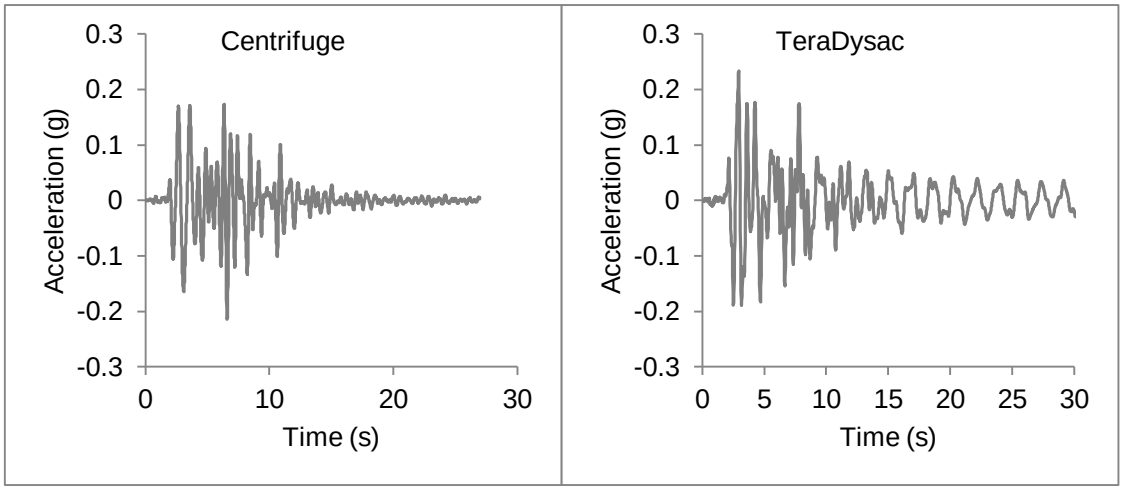

Figure 7-13. Measured and Computed Acceleration-Time Histories of the GIL Pile Cap during Event B

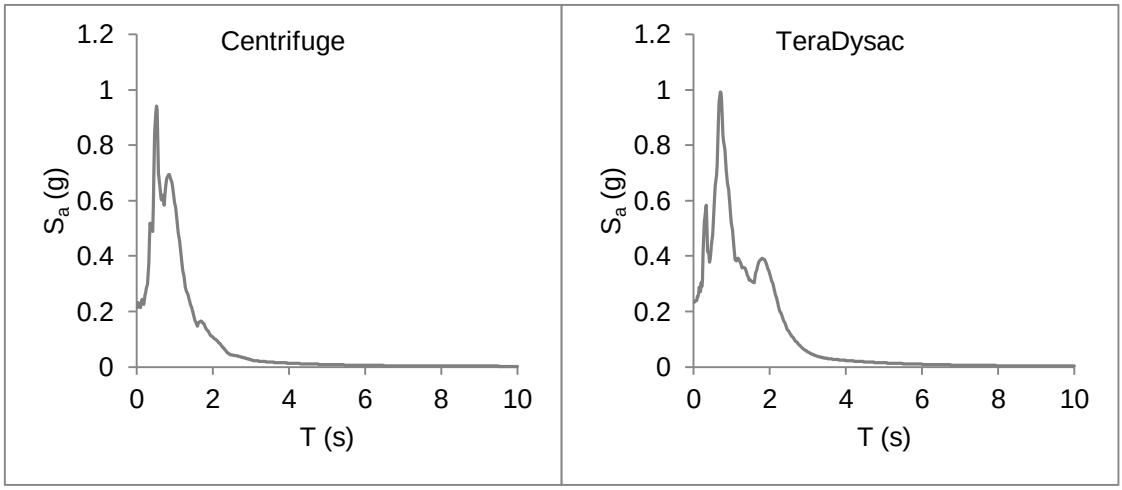

Figure 7-14. Measured and Computed Acceleration Response Spectra of the GIL Pile Cap during Event B

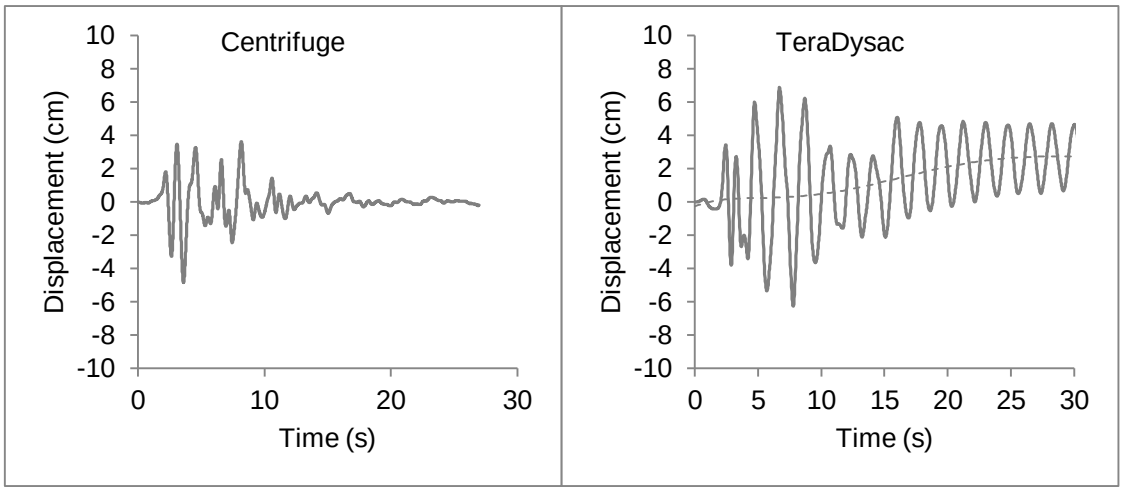

Figure 7-15. Measured and Computed Displacement-Time Histories of the GIL Pile Cap during Event B

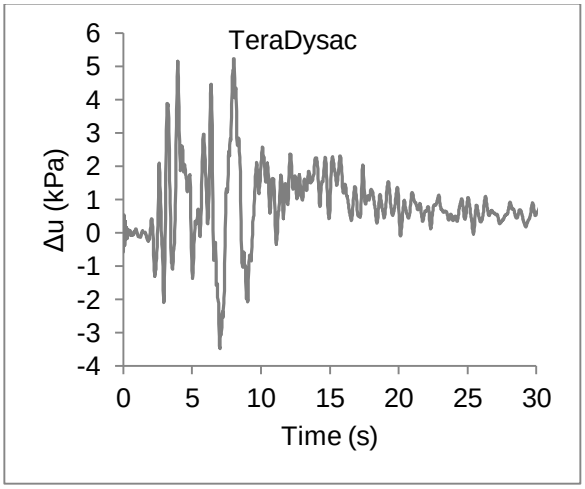

Figure 7-16. Computed (Element 123) EPWP-Time History in the vicinity of the GIL pile group during Event B

7.8 Global Responses of the Pile Groups in Unimproved and CDSM Improved Soft Clay

Deformed meshes during the GU and GIL analyses are presented in this section. Selected contours of shear stresses and EPWP are also presented.

7.8.1 Model Deformation

The deformed shapes of the GU and GIL pile groups are shown at t=6.00s and t=6.75s in Figures 7.17 and 7.18, respectively. At t=6.75s, the maximum acceleration occurs in the free-field at the ground surface. The scale exaggeration factor for the deformed meshes is 50. Comparison of the deformed meshes of the GU and GIL pile groups reveals that ground improvement reduces deformations of the soil profile (especially at the top clay layer near the piles) and also the GIL pile foundation. During both movements to the left and right, the CDSM block moves as a relatively rigid body. The deformations of the CDSM block are negligible compared to those of the soft clay.

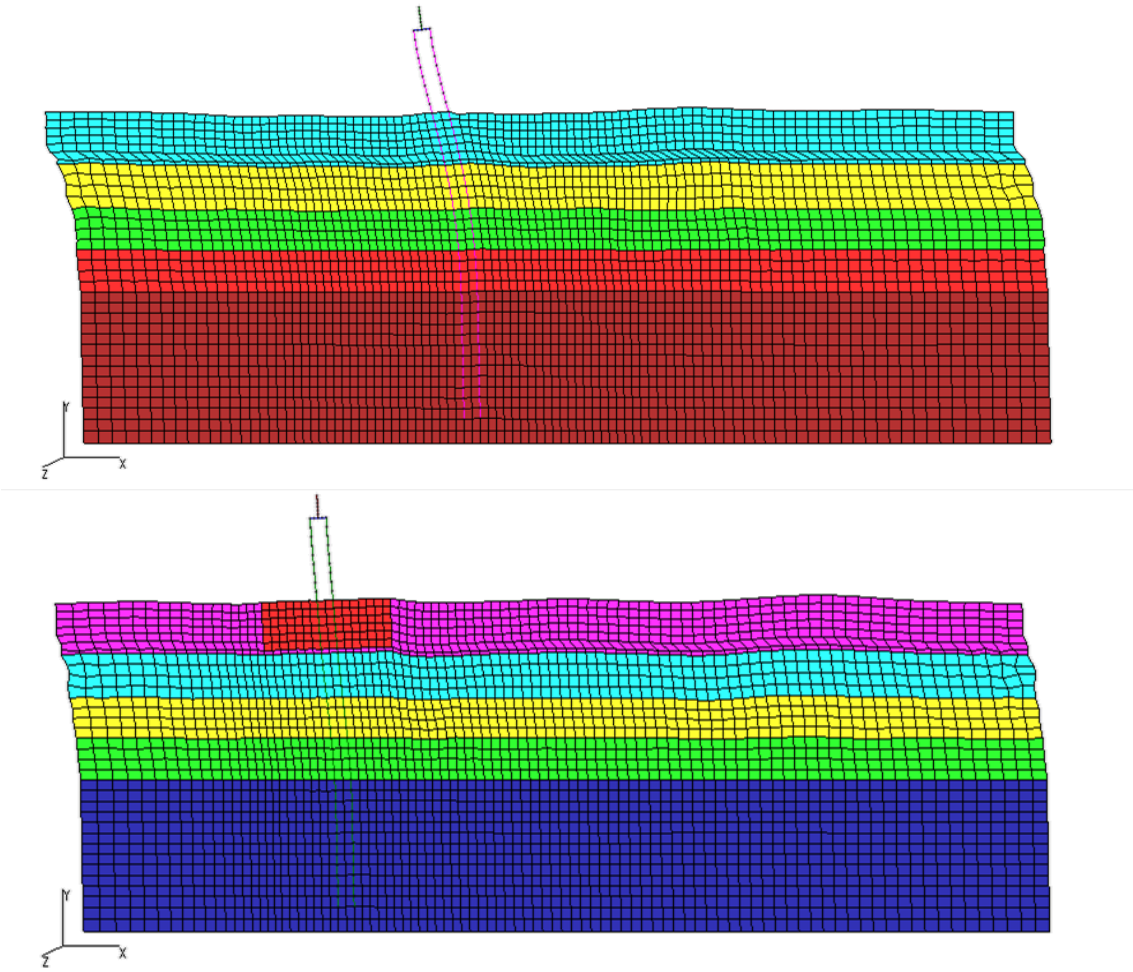

Figure 7-17. Deformed Meshes of the GU (Top) and the GIL (Bottom) Pile Groups at t=6.00 s

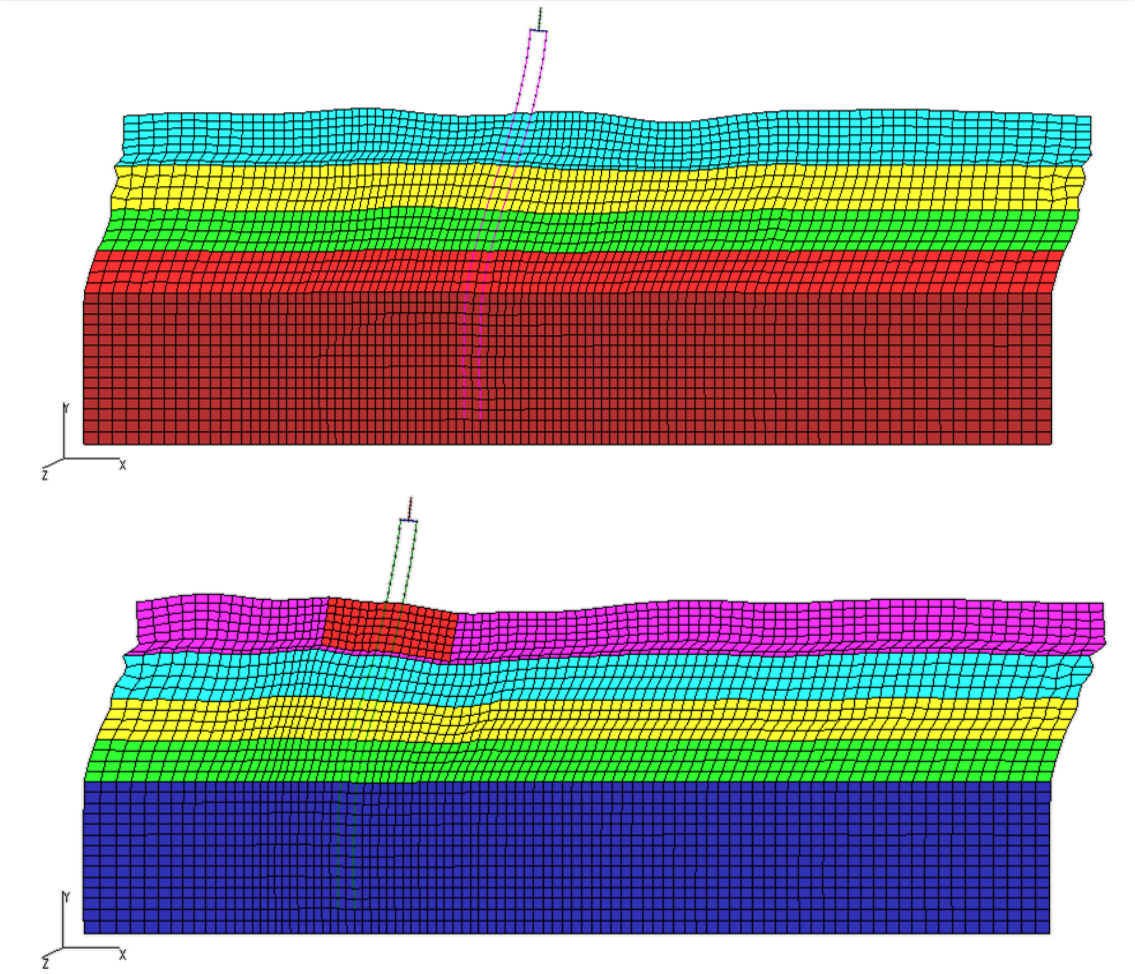

Figure 7-18. Deformed Meshes of the GU (Top) and the GIL (Bottom) Pile Groups at t=6.75 s

7.8.2 Shear Stresses

Based on Figure 7.19, shear stresses are concentrated between the group piles, in their lower sections. Maximum shear stress in the improved pile group occurs within the CDSM block.

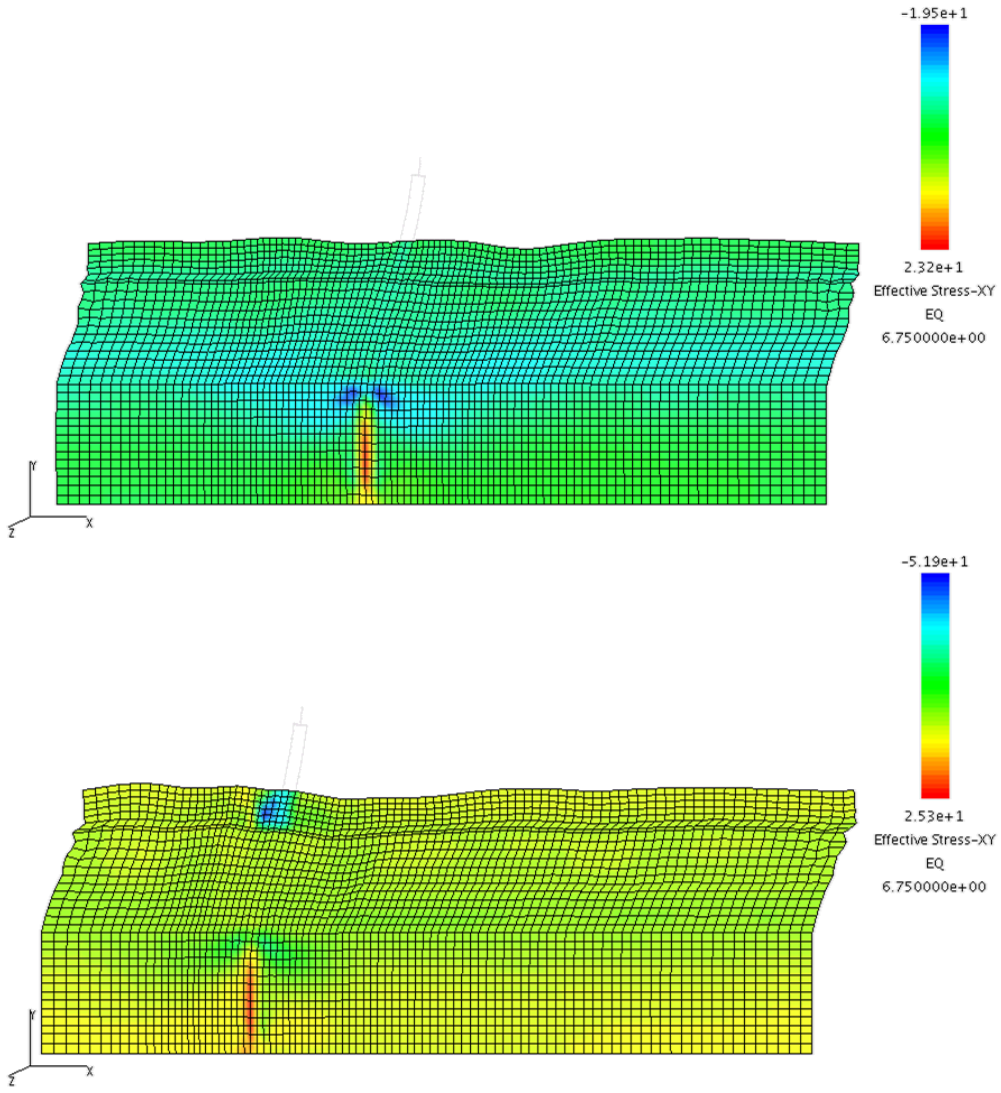

Figure 7-19. Contours of Shear Stress for the GU (Top) and GIL (Bottom) Pile Groups at t=6.75 s

7.8.3 Excess Pore Water Pressure (EPWP)

Similar EPWP contours are obtained for both pile groups (see Figure 7.20). Deeper soft clay layers have experienced greater EPWP than the shallower layers. The maximum positive EPWP occurs in the interface of dense sand and bottom soft clay layer. Negative EPWP is observed in the CDSM block illustrating dilative behavior in the CDSM.

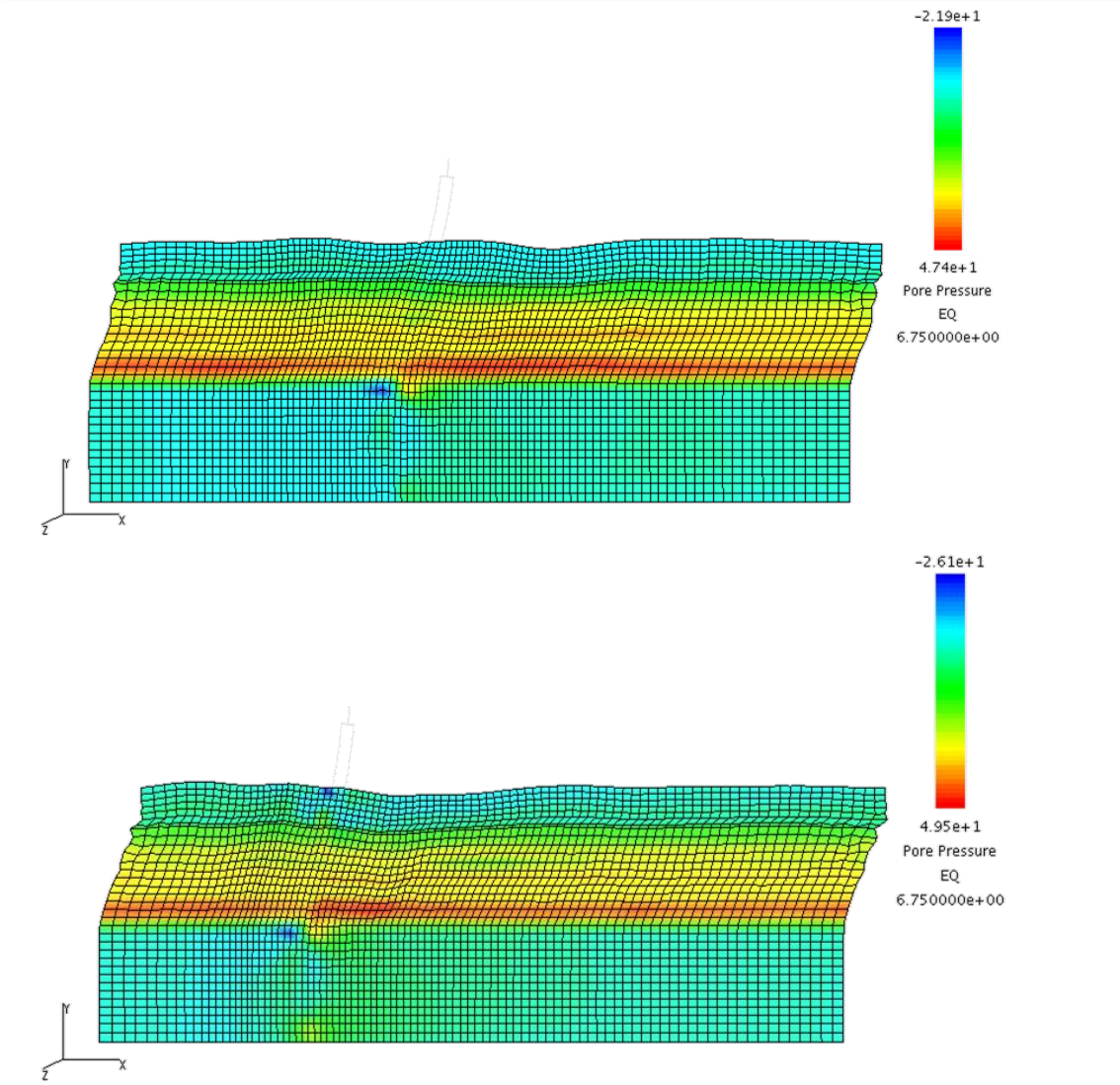

Figure 7-20. Contours of Excess Pore Water Pressure for the GU (Top) and GIL (Bottom) Pile Groups at t=6.75 s

Chapter 8: Conclusions and Recommendations

8.1 Overview

Centrifuge model tests were performed to increase our understanding of the quasi-static and seismic lateral load behavior of pile groups in CDSM improved and unimproved soft clay. The pile groups had a symmetrical plan layout consisting of 2×2 piles spaced at 3 and 7 pile diameters (D). The quasi-static lateral load behavior was simulated using the concept of Beam on Nonlinear Winkler Foundation implemented in the finite difference codes GROUP and LPILE. The seismic behavior of pile groups in unimproved and improved pile groups were modeled using a 2D plain strain, fully coupled, nonlinear finite element method implemented in the computer code TeraDysac. The following conclusions can be made based on this research for the soil and pile conditions investigated.

8.2 Conclusions

Cement Deep Soil Mixing is an effective ground improvement method. CDSM increased the lateral resistance of pile groups at 7D spacing by about 157%. At the same deflection, the lateral resistance of the 3D pile groups increased by 112%. Increasing the lateral dimensions of CDSM blocks increased the lateral resistance of pile groups. The load–deflection responses of piles in improved soft clay were significantly stiffer than those in the unimproved soft clay. In both pile groups at 3D spacing in improved (GIL-3D) and unimproved soil (GU-3D), the leading row of piles carried larger loads than the trailing row of piles. Moreover, for a given deflection, the maximum bending moment in the leading row of piles was also larger than that of the trailing row of piles.

Increasing the deflection increased the difference between maximum bending moments in the leading and trailing row of piles. The maximum bending moments were about the same in the leading and trailing row of piles for the 7D groups. The pile-soil-pile interactions in 3D groups led to the above described differences. The bending moment profiles show that the depth to the maximum bending moment for unimproved pile foundations and improved pile foundations were at about 9 – 10D and 1– 2D below the ground surface, respectively. At the same deflection, the piles in improved soil experienced higher bending moment than the piles in unimproved soil. At a deflection of about 80 cm, the CDSM block of the GIL-3D pile group failed in tension. The cracks first formed near the surface, perpendicular to the direction of loading, at the interface between the piles and the CDSM block and then propagated to the outside and through the depth until the CDSM block fractured.

Using the centrifuge test results the p-multipliers for pile groups in CDSM improved and unimproved soft clay were back-calculated. The p-multipliers account for the reduced soil resistance due to overlapping of shear zones in piles of a group. The p-multipliers "squash" the p-y curve of an isolated single pile to obtain those for a pile in a group. Centrifuge test results and analyses revealed that the computer codes LPILE and GROUP, utilizing the p-multipliers developed in this study, were able to simulate the lateral load behavior of single and group piles satisfactorily. The p-multipliers for the leading row of piles are greater than those for the trailing row of piles indicating that more overlapping between shear zones occur for the trailing row of piles. Increasing the center-to-center pile spacing from 3D to 7D increased the p-multipliers. No pile-soil-pile interaction was observed in pile groups with 7D spacing in both improved and

unimproved soft clay. The p-multipliers for stiff clay were greater than those for soft clay. This finding is in agreement with the previous strain wedge model analyses and also with the p-multipliers obtained from different full scale test results of similar pile groups. Assuming same p-multipliers for all clays and neglecting clay stiffness will result in a relatively conservative design of pile groups in stiff clay. The p-multipliers obtained for the pile group in soft clay are in good agreement with those suggested by FEMA (2012), Rollins et al. (2006), and Mokwa and Duncan (2005) for all soils. The p-multipliers obtained in this study for the 2 × 2 pile groups in stiff clay are higher than those recommended by AASHTO (2012), FEMA (2012), US Army (1993) and most other recommendations for all soils. The p-multipliers recommended by these agencies appear to be relatively conservative. The stiff clay p-multipliers are, however, comparable with those obtained by Huang et al. (2001) in a stiff silt and silty clay site.

For the soil and pile conditions tested, lateral and vertical dimensions of the CDSM blocks (23D × 23D × 9D) in the GIL pile groups can be considered the optimum to provide the maximum lateral resistance under quasi-static loading conditions. Moreover, for depths greater than 9D, the depth effect on lateral resistance was negligible. At deflections smaller than 8 cm, the undrained shear strength of CDSM blocks does not influence the lateral resistance of pile groups. At larger deflections, increasing the undrained shear strength of CDSM blocks can increase the lateral resistance of pile groups; however, this effect becomes negligible for undrained shear strengths greater than about 1000 kPa.

Considering free-field site conditions during shakings, test results revealed that the peak base acceleration was amplified at the ground surface during low-amplitude

base motions, while it was attenuated during high amplitude base motions indicating the nonlinearity of the soil profile. Increasing the peak base acceleration increased the fundamental period of the site. Compared to the surface motion in the free-field, a reduction in the amplitude of the foundation level motions of the improved pile foundations was observed, which is attributed to ground improvement and kinematic interactions. This observation is consistent with the Eurocode 8 recommendations and also with previous research results where the significance of kinematic interaction in the vicinity of interfaces of alternating soft and stiff soil layers is reported. Contrary to the common practice in earthquake engineering design where engineers and designers neglect kinematic interaction, the results of this research strongly suggest taking these effects into account. The foundation level motion of the unimproved pile group was identical to the surface free-field motion. This observation is consistent with FEMA-440 recommendations in neglecting kinematic interaction in soft clay sites. Dimensions of the CDSM block is an important factor in seismic design of improved pile groups. Higher peak acceleration was observed in the GIS pile cap compared to the GIL and GU pile caps. The GU and GIL had almost same peak accelerations. Greater pile cap to soil surface spectral ratio was observed in the GIS pile cap in short and long periods compared to the GIL and GU pile caps. The maximum spectral amplification was higher in the GIS pile cap. The period where the maximum spectral amplification occurred became smaller as the size of the ground improvement increased. The pile cap response was dependent on the frequency content of input motion. Spectral response acceleration of Kobe earthquake was higher than Santa Cruz earthquakes in the period range of 0.3-3.0 s. This period range corresponded to the fundamental period of pile

caps and explained why higher accelerations were observed during Kobe earthquake than Santa Cruz earthquake with the same peak base acceleration. Increasing the shaking level increased the fundamental period of pile cap. This increase was more for the GU and was less for the GIL pile cap. CDSM was an effective method in reducing the peak displacements of the GIL pile cap during all weak and strong motions. The peak displacements of the GIS pile cap remained about the same as the GU pile cap. The GIL CDSM block also experienced less settlements compared to all other locations of the model where settlement was measured. The cohesion between soft clay and CDSM blocks helped to reduce the soft clay settlement in the vicinity of CDSM blocks compared to the free field and in the vicinity of the unimproved pile group. Increasing dimensions of CDSM block reduced the soft clay settlement in the vicinity of the blocks. More residual EPWP was, however, generated in the vicinity of CDSM blocks compared to free-field and corresponding location in the unimproved pile group. Vibrations of CDSM blocks and elongation of seepage path are thought to be the contributing factors.

Two dimensional, plain strain, fully coupled, nonlinear, dynamic finite element analyses were performed using the computer code TeraDysac to study the seismic behavior of the pile groups in more detail. Dynamic centrifuge tests during Event B were simulated. Dafalias and Herrmann (1986) bounding surface constitutive model was used to model the stress-strain behavior of soft clay and CDSM block. A linear elastic model was also used to model the stress-strain behavior of dense sand layer. Beam elements were used to model pile cap and piles. Spectral acceleration responses as well as acceleration-time, displacement-time, and EPWP-time histories in free-field

and in the GU and GIL pile caps were computed and compared with the measured values. There was a satisfactory agreement between the measured and TeraDysac computed responses. The TeraDysac model was able to predict the peak values and variation trends of acceleration, displacement, and EPWP responses. TeraDysac analyses revealed that stress concentration occurred in the CDSM block. The negative EPWP in the CDSM block was illustration of dilative behavior of stiff clay.

8.3 Recommendations for Future Research

The seismic and quasi-static lateral load behavior of pile groups in unimproved and improved soft clay is a complex problem. Research in the following areas can help provide further insight into this problem.

8.3.1 Centrifuge Modeling

Centrifuge tests can be performed to study the seismic and quasi-static lateral load behavior of pile groups under different complex conditions. The following potential research areas can be investigated using these tests:

- Comparing different ground improvement techniques on the seismic and quasi-static behavior of pile foundations. These techniques include jet grouting, Cement-Deep-Soil-Mixing, replacement of surface clay with a compacted granular material; and constructing walls to increase the passive forces on the embedded pile cap.
- Analyze the behavior of pile foundations under combined torsional, axial, and lateral loading;

- Analyze the dynamic interaction of different adjacent pile groups as foundations of a geo-structural system (e.g. a bridge);
- Quantify and characterize kinematic and inertial interaction effects;
- Obtain p-multipliers in large pile groups in improved and unimproved ground; and
- Analyze different factors affecting p-multipliers

In order to improve centrifuge tests, it is recommended to use a more dense instrumentation array of strain gages to provide more detailed information on the distribution of bending moments and back-calculate experimental p-y curves along the piles. Performing more centrifuge tests can quantify container or instrument interaction effects. Quantifying these limitations can help with better interpretation of test results. Performing more centrifuge tests can also show the repeatability of test results.

8.3.2 Advanced Computational Modeling

Most of the research conducted on the seismic behavior of pile foundations has been studied through Winkler type models, finite element methods (FEM), and boundary element methods (BEM). Each of these techniques has their own advantages and disadvantages. FEM has proven effective in solving problems with bounded domains, particularly when inhomogeneities and nonlinear effects should be treated. For domains of infinite extensions, however, standard finite elements discretization leads to wave reflections at the boundaries of the FE mesh, which can be partly eliminated for some cases, by using so-called transmitting, silent and nonreflecting viscous boundaries. BEM has shown to be a very powerful numerical technique for linear and

homogeneous materials for both bounded and unbounded domains, and does not require domain discretization, which can be an advantage in many practical applications. Since this method automatically satisfies the radiation conditions at infinity, there is no need to model the far field in problems with semi-infinite or infinite domains. To utilize the advantages of both FEM and BEM, a combination of these techniques seems ideal. There are different methods to combine these two techniques. Treating a boundary element region as a finite element and combining with finite element is an appropriate method which enables the applicability of nonlinear analysis. In the bounded region, the finite element formulation can discretize the pile and soil and enforce the boundary conditions at interfaces. Implementing appropriate interface elements capable of capturing gapping between pile and soil, and also using improved bounding surface models capable of capturing enough material damping would result in accurate predictions of the lateral load behavior of pile foundation systems. Through this direct method of seismic analyses, future research can investigate the 3D response of pile groups to vertically and obliquely propagating incident seismic waves in homogeneous and non-homogeneous media. This method will be able to capture translational, torsional, and rocking modes of vibration.

8.3.3 Simplified Computational Modeling

Studying the seismic behavior of pile foundations using the substructure procedure is another recommended future research area. In this method, pile foundation impedances are determined by performing soil-pile interaction analyses considering group interaction effects. The superstructure model is then analyzed using these

impedances and input motions obtained from free-field. The Beam on Nonlinear Winkler Foundation (BNWF) model is a powerful tool in this area which is capable of analyzing the soil–pile interaction and characterizing kinematic and inertial interactions. This method can produce results of remarkable accuracy in much less time compared to rigorous continuum models in the direct method.

References

AASHTO (2012). *AASHTO LRFD bridge design specifications*, American Association of State Highway and Transportation Officials (AASHTO), Washington, D.C.

Abdoun, T., Dobry, R., O'Rourke, T., and Goh, S. (2003). "Pile Response to Lateral Spreads: Centrifuge Modeling." *Journal of Geotechnical and Geoenvironmental Engineering*, 129(10), 869-878.

Abdoun, T., Gonzalez, M., Thevanayagam, S., Dobry, R., Elgamal, A., Zeghal, M., Mercado, V., and El Shamy, U. (2013). "Centrifuge and Large-Scale Modeling of Seismic Pore Pressures in Sands: Cyclic Strain Interpretation." *Journal of Geotechnical and Geoenvironmental Engineering*, 139(8), 1215-1234.

Afacan, K., Brandenberg, S., and Stewart, J. (2014). "Centrifuge Modeling Studies of Site Response in Soft Clay over Wide Strain Range." *Journal of Geotechnical and Geoenvironmental Engineering*, 140(2), 04013003.

Alizadeh, M., and Davisson, T. (1970). "Lateral Load Tests on Piles—Arkansas River Project." *Journal of the Soil Mechanics and Foundations Division*, 96(5), 1583-1604.

Anandarajah, A., Rashidi, H., and Arulanandan, K. (1995). "Elasto-plastic finite element analyses of a soil-structure system under earthquake excitations." *Computers and Geotechnics*, 17(3), 301-325.

ANATECH Corp. (2001). *The TeraScale framework*, Albuquerque, New Mexico.

API (2007). "Recommended practice for planning, designing, and constructing fixed offshore platforms. API Recommended Practice 2A-WSD." American Petroleum Institute, Washington, D.C., 288.

Arulmoli, K., Muraleetharan, K. K., Hossain, M. M., and Fruth, L. S. (1992). "VELACS: Verification of liquefaction analyses by centrifuge studies, laboratory testing program, soil data report." The Earth Technology Corporation, Irvine, CA.

Ashford, S., Rollins, K., and Baez, J. (2000). "Comparison of Deep Foundation Performance in Improved and Non-Improved Ground Using Blast-Induced Liquefaction." *Soil Dynamics and Liquefaction 2000*, 20-34.

Ashford, S., Rollins, K., and Lane, J. (2004). "Blast-Induced Liquefaction for Full-Scale Foundation Testing." *Journal of Geotechnical and Geoenvironmental Engineering*, 130(8), 798-806.

Ashour, M., and Ardalan, H. (2011). "Employment of the P-Multiplier in Pile-Group Analysis." *Journal of Bridge Engineering*, 16(5), 612-623.

Ashour, M., Norris, G., and Pilling, P. (1998). "Lateral Loading of a Pile in Layered Soil Using the Strain Wedge Model." *Journal of Geotechnical and Geoenvironmental Engineering*, 124(4), 303-315.

Banerjee, S., Goh, S. H., and Lee, F. H. (2008). "Response of Clay-Pile System under Earthquake Loading." *Geotechnical Earthquake Engineering and Soil Dynamics IV*, 1-10.

Bentley, K. J., and Naggar, M. H. E. (2000). "Numerical analysis of kinematic response of single piles." *Canadian Geotechnical Journal*, 37(6), 1368-1382.

Blaney, G., and O'Neill, M. (1986). "Measured Lateral Response of Mass on Single Pile in Clay." *Journal of Geotechnical Engineering*, 112(4), 443-457.

Blaney, G., and O'Neill, M. (1989). "Dynamic Lateral Response of a Pile Group in Clay." *Geotechnical Testing Journal*, 12(1), 22–29.

Boulanger, R., Curras, C., Kutter, B., Wilson, D., and Abghari, A. (1999). "Seismic Soil-Pile-Structure Interaction Experiments and Analyses." *Journal of Geotechnical and Geoenvironmental Engineering*, 125(9), 750-759.

Brandenberg, S., Boulanger, R., Kutter, B., and Chang, D. (2005). "Behavior of Pile Foundations in Laterally Spreading Ground during Centrifuge Tests." *Journal of Geotechnical and Geoenvironmental Engineering*, 131(11), 1378-1391.

Brandenberg, S., Boulanger, R., Kutter, B., and Chang, D. (2007). "Liquefaction-Induced Softening of Load Transfer between Pile Groups and Laterally Spreading Crusts." *Journal of Geotechnical and Geoenvironmental Engineering*, 133(1), 91-103.

Brandenberg, S., Boulanger, R., Kutter, B., and Chang, D. (2007). "Static Pushover Analyses of Pile Groups in Liquefied and Laterally Spreading Ground in Centrifuge Tests." *Journal of Geotechnical and Geoenvironmental Engineering*, 133(9), 1055-1066.

Brandenberg, S., Wilson, D., and Rashid, M. (2010). "Weighted Residual Numerical Differentiation Algorithm Applied to Experimental Bending Moment Data." *Journal of Geotechnical and Geoenvironmental Engineering*, 136(6), 854-863.

Brown, D., Morrison, C., and Reese, L. (1988). "Lateral Load Behavior of Pile Group in Sand." *Journal of Geotechnical Engineering*, 114(11), 1261-1276.

Brown, D., Reese, L., and O'Neill, M. (1987). "Cyclic Lateral Loading of a Large-Scale Pile Group." *Journal of Geotechnical Engineering*, 113(11), 1326-1343.

Brown, D. A., O'Neill, M. W., Hoit, M., McVay, M., EL Naggar, M. H., and Chakraborty, S. (2001). "Static and Dynamic Lateral Loading of Pile Groups." *Rep. No. NCHRP 461*.

Bruce, M. E. C., Berg, R. R., Collin, J. G., Filz, G. M., Terashi, M., and Yang, D. S. (2013). "Federal Highway Administration Design Manual: Deep Mixing for Embankment and Foundation Support." *Rep. No. FHWA-HRT-13-046,* Washington, D.C.

Burke, G. K. (2004). "Jet Grouting Systems: Advantages and Disadvantages." *GeoSupport 2004*, 875-886.

Burke, G. K. (2012). "The State of the Practice of Jet Grouting." *Grouting and Deep Mixing 2012*, 74-88.

Burr, J., Pender, M., and Larkin, T. (1997). "Dynamic Response of Laterally Excited Pile Groups." *Journal of Geotechnical and Geoenvironmental Engineering*, 123(1), 1-8.

Cai, Y. X., Gould, P. L., and Desai, C. S. (2000). "Nonlinear analysis of 3D seismic interaction of soil–pile–structure systems and application." *Engineering Structures*, 22(2), 191-199.

Canadian Geotechnical Society (1978). *Canadian foundation engineering manual, Part III, Deep Foundations*, Canadian Geotechnical Society, Montreal.

Chandrasekaran, S., Boominathan, A., and Dodagoudar, G. (2010). "Group Interaction Effects on Laterally Loaded Piles in Clay." *Journal of Geotechnical and Geoenvironmental Engineering*, 136(4), 573-582.

Chang, D., Boulanger, R., Brandenberg, S., and Kutter, B. (2013). "FEM Analysis of Dynamic Soil-Pile-Structure Interaction in Liquefied and Laterally Spreading Ground." *Earthq Spectra*, 29(3), 733-755.

Chau, K. T., Shen, C. Y., and Guo, X. (2009). "Nonlinear seismic soil–pile–structure interactions: Shaking table tests and FEM analyses." *Soil Dyn Earthq Eng*, 29(2), 300-310.

Clemente, J. L. M., Bell, K. R., Gularte, F. B., and Lopez, R. A. "SuperJet Grouting Reduces Foundation Settlement for La Rosita Power Plant in Mexicali, Mexico." *Grouting and Ground Treatment*, 354-364.

Cox, W. R., Dixon, D. A., and Murphy, B. S. (1984). "Lateral load tests of 25.4-mm (1-in.) diameter piles in very soft clay in side-by-side and in-line groups." *Laterally loaded deep foundations: analysis and performance*, ASTM, West Conshohocken, Pennsylvania.

Craig, W. H. (1985). "Modeling pile installation in centrifuge experiments." *11th International Conference on Soil Mechanics and Foundation Engineering*San Francisco, California, 1101-1104.

Dafalias, Y., and Herrmann, L. (1986). "Bounding Surface Plasticity. II: Application to Isotropic Cohesive Soils." *Journal of Engineering Mechanics*, 112(12), 1263-1291.

Das, B. M. (2010). *Principles of Foundation Engineering (7th Edition)*, CL Engineering.

Davisson, M. T. (1970). "Lateral load capacity of piles." *49th Annual Meeting of the Highway Research Board*, Highway Research Board, Washington D.C., United States, 104-112.

Dezi, F., Carbonari, S., and Leoni, G. (2010). "Kinematic bending moments in pile foundations." *Soil Dyn Earthq Eng*, 30(3), 119-132.

Dezi, F., Carbonari, S., and Leoni, G. (2010). "Static equivalent method for the kinematic interaction analysis of single piles." *Soil Dyn Earthq Eng*, 30(8), 679-690.

Di Laora, R., and de Sanctis, L. (2013). "Piles-induced filtering effect on the Foundation Input Motion." *Soil Dyn Earthq Eng*, 46, 52-63.

Di Laora, R., Mandolini, A., and Mylonakis, G. (2012). "Insight on kinematic bending of flexible piles in layered soil." *Soil Dyn Earthq Eng*, 43(0), 309-322.

Di Laora, R., Mylonakis, G., and Mandolini, A. (2013). "Pile-head kinematic bending in layered soil." *Earthquake Engineering & Structural Dynamics*, 42(3), 319-337.

Di Laora, R., and Rovithis, E. (2015). "Kinematic Bending of Fixed-Head Piles in Nonhomogeneous Soil." *Journal of Geotechnical and Geoenvironmental Engineering*, 0(0), 04014126.

Dobry, R., Thevanayagam, S., Medina, C., Bethapudi, R., Elgamal, A., Bennett, V., Abdoun, T., Zeghal, M., El Shamy, U., and Mercado, V. (2011). "Mechanics of Lateral Spreading Observed in a Full-Scale Shake Test." *Journal of Geotechnical and Geoenvironmental Engineering*, 137(2), 115-129.

El-Marsafawi, H., Han, Y., and Novak, M. (1992). "Dynamic Experiments on Two Pile Groups." *Journal of Geotechnical Engineering*, 118(4), 576-592.

Elgamal, A., and Lu, J. (2009). "A Framework for 3D Finite Element Analysis of Lateral Pile System Response." *Contemporary Topics in In Situ Testing, Analysis, and Reliability of Foundations*, 616-623.

Emani, P. K., and Maheshwari, B. K. (2009). "Dynamic impedances of pile groups with embedded caps in homogeneous elastic soils using CIFECM." *Soil Dyn Earthq Eng*, 29(6), 963-973.

Essler, R. "The Design Of Jet Grouting From Concept To Execution." *Grouting and Deep Mixing 2012*, 2071-2081.

European Committee for Standardization (CEN) (2003). "Eurocode 8: Design of structures for earthquake resistance. Part 5: Foundations, retaining structures and geotechnical aspects." *EN 1998–5*.

Fayyazi, M. S., Taiebat, M., and Finn, W. D. L. (2014). "Group reduction factors for analysis of laterally loaded pile groups." *Canadian Geotechnical Journal*, 758-769.

FEMA-440 (2005). "Improvement of nonlinear static seismic analysis procedures." Federal Emergency Management Agency, Washington, DC.

FEMA (2012). "Foundation analysis and design. FEMA P-751." *NEHRP recommended provisions: design examples*, Federal Emergency Management Agency. National Institute of Building Sciences, Building Seismic Safety Council, Washington, D.C.

Fiegel, G. L., Hudson, M., Idriss, I. M., Kutter, B. L., and Zeng, X. (1994). "Effect of model containers on dynamic soil response." *Centrifuge 94*Singapore, 145-150.

Filz, G. M., Hodges, D. K., Weatherby, D. E., and Marr, W. A. (2005). "Standardized Definitions and Laboratory Procedures for Soil-Cement Specimens Applicable to the Wet Method of Deep Mixing." *Innovations in Grouting and Soil Improvement*, 1-13.

Finn, W. D. L. (2005). "A Study of Piles during Earthquakes: Issues of Design and Analysis." *B Earthq Eng*, 3(2), 141-234.

Fleming, B. J., Sritharan, S., Miller, G., and Muraleetharan, K. (2015). "Full-Scale Seismic Testing of Piles in Improved and Unimproved Soft Clay." *Earthq Spectra*, in press.

Focht, J., J.A., and Koch, K. J. (1973). "Rational Analysis of the Lateral Performance of Offshore Pile Groups." *5th Offshore Technology Conference*Houston, Texas, 701–708.

Garnier, J., Gaudin, C., Springman, S. M., Culligan, P. J., Goodings, D. J., Konig, D., Kutter, B. L., Phillips, R., Randolph, M., and Thorel, L. (2007). "Catalogue of Scaling Laws and Similitude Questions in Geotechnical Centrifuge Modelling." *International Journal of Physical Modelling in Geotechnics*, 7(3), 1-23.

Gazetas, G. (1984). "Seismic response of end-bearing single piles." *International Journal of Soil Dynamics and Earthquake Engineering*, 3(2), 82-93.

Gazetas, G., and Mylonakis, G. (1998). "Seismic Soil-Structure Interaction: New Evidence and Emerging Issues." *Geotechnical Earthquake Engineering and Soil Dynamics III*, P. Dakoulas, ed., ASCE, Seattle, Washington, 1119-1174.

González, L., Abdoun, T., and Dobry, R. (2009). "Effect of Soil Permeability on Centrifuge Modeling of Pile Response to Lateral Spreading." *Journal of Geotechnical and Geoenvironmental Engineering*, 135(1), 62-73.

Hadjian, A. H., Fallgren, R. B., and Tufenkjian, M. R. (1992). "Dynamic Soil-Pile-Structure Interaction—The State-of-Practice." *Piles Under Dynamic Loads*, S. Prakash, ed., ASCE, 1-26.

Han, Y., and Novak, M. (1988). "Dynamic behaviour of single piles under strong harmonic excitation." *Canadian Geotechnical Journal*, 25(3), 523-534.

Hannigan, P. J., Goble, G. G., Likins, G. E., and Rausche, F. (2006). "Design and Construction of Driven Pile Foundations, Reference Manual – Volume I." Federal Highway Administration, Washington, D.C.

Hilber, H. M., Hughes, T. J. R., and Taylor, R. L. (1977). "Improved numerical dissipation for time integration algorithms in structural dynamics." *Earthquake Engineering & Structural Dynamics*, 5(3), 283-292.

Huang, A., Hsueh, C., O'Neill, M., Chern, S., and Chen, C. (2001). "Effects of Construction on Laterally Loaded Pile Groups." *Journal of Geotechnical and Geoenvironmental Engineering*, 127(5), 385-397.

Ilyas, T., Leung, C., Chow, Y., and Budi, S. (2004). "Centrifuge Model Study of Laterally Loaded Pile Groups in Clay." *Journal of Geotechnical and Geoenvironmental Engineering*, 130(3), 274-283.

Jaky, J. (1948). "Pressure in silos." *2nd International Conference on Soil Mechanics and Foundation Engineering*Rotterdam, The Netherland, 103-107.

Japan Road Association (1976). "Road bridge substructure design guide and explanatory notes." *Designing of Pile Foundations*, 144.

Jeremić, B., Jie, G., Preisig, M., and Tafazzoli, N. (2009). "Time domain simulation of soil–foundation–structure interaction in non-uniform soils." *Earthquake Engineering & Structural Dynamics*, 38(5), 699-718.

Kavvadas, M., and Gazetas, G. (1993). "Kinematic seismic response and bending of free-head piles in layered soil." *Géotechnique*, 207-222.

Kawasaki, T., Niina, A., Saitoh, S., Suzuki, Y., and Honjyo, Y. "Deep mixing method using cement hardening agent." *Proc., Proceedings of the Tenth International Conference on Soil Mechanics and Foundation Engineering*.

Kaynia, A. (1982). "Dynamic stiffness and seismic response of pile groups." PhD, Massachusetts Institute of Technology (MIT), Cambridge, MA.

Kaynia, A. M., and Kausel, E. (1991). "Dynamics of piles and pile groups in layered soil media." *Soil Dyn Earthq Eng*, 10(8), 386-401.

Kaynia, A. M., and Novak, M. (1992). "Response of pile foundations to rayleigh waves and obliquely incident body waves." *Earthquake Engineering & Structural Dynamics*, 21(4), 303-318.

Kim, S., and Stewart, J. (2003). "Kinematic Soil-Structure Interaction from Strong Motion Recordings." *Journal of Geotechnical and Geoenvironmental Engineering*, 129(4), 323-335.

Kirupakaran, K., Cerato, A. B., Liu, C., Miller, G. A., Muraleetharan, K. K., Pinilla, J. D., Price, S., and Thompson, Z. M. (2010). "Simulation of a Centrifuge Model

Test of Pile Foundations in CDSM Improved Soft Clays." *Advances in analysis, modeling and design, (GSP 199)*, 1583-1591.

Kitazume, M., and Terashi, M. (2013). *The deep mixing method*, CRC Press/Balkema, London.

Krier, D. (2009). "Modeling of Integral Abutment Bridges Considering Soil-Structure Interaction Effects." University of Oklahoma.

Küçükarslan, S., and Banerjee, P. K. (2003). "Behavior of axially loaded pile group under lateral cyclic loading." *Engineering Structures*, 25(3), 303-311.

Kuhlemeyer, R. L., and Lysmer, J. (1973). "Finite Element Method Accuracy for Wave Propagation Problems." *Journal of the Soil Mechanics and Foundations Division*, 99(5), 421-427.

Kutter, B. L. (1992). "Dynamic Centrifuge Modeling of Geotechnical Structures." *TRANSPORTATION RESEARCH RECORD 1336*, 24-30.

Kutter, B. L. (1995). "Recent advances in centrifuge modeling of seismic shaking." *third international conference on recent advances in geotechnical earthquake engineering and soil dynamics*Rolla, MO, 927–942.

Ladd, C. C., Foott, R., Ishihara, K., Schlosser, F., and Poulos, H. G. (1977). "Stress-deformation and strength characteristics: state of the art report." *9th International Conference on Soil Mechanics and Foundation Engineering*Tokyo, 421-494.

Lemnitzer, A., Khalili-Tehrani, P., Ahlberg, E., Rha, C., Taciroglu, E., Wallace, J., and Stewart, J. (2010). "Nonlinear Efficiency of Bored Pile Group under Lateral

Loading." *Journal of Geotechnical and Geoenvironmental Engineering*, 136(12), 1673-1685.

Lok, M. H. (1999). "Numerical Modeling of Seismic Soil-Pile-Superstructure Interaction in Soft Clay." PhD, University of California, Berkeley.

Lorenzo, G., and Bergado, D. (2006). "Fundamental Characteristics of Cement-Admixed Clay in Deep Mixing." *Journal of Materials in Civil Engineering*, 18(2), 161-174.

Maeso, O., Aznárez, J. J., and García, F. (2005). "Dynamic impedances of piles and groups of piles in saturated soils." *Computers & Structures*, 83(10–11), 769-782.

Maher, A., Douglas, W. S., Jafari, F., and Yang, D. (2006). "In-Situ Solidification of River Sediments Using Cement Deep Soil Mixing (CDSM)." *GeoCongress 2006*, 1-7.

Maheshwari, B. K., Truman, K. Z., El Naggar, M. H., and Gould, P. L. (2004). "Three-dimensional nonlinear analysis for seismic soil–pile-structure interaction." *Soil Dyn Earthq Eng*, 24(4), 343-356.

Maiorano, R. M. S., de Sanctis, L., Aversa, S., and Mandolini, A. (2009). "Kinematic response analysis of piled foundations under seismic excitation." *Canadian Geotechnical Journal*, 46(5), 571-584.

Makris, N. (1994). "Soil–pile interaction during the passage of rayleigh waves: An analytical solution." *Earthquake Engineering & Structural Dynamics*, 23(2), 153-167.

Makris, N., Gazetas, G., and Delis, E. (1996). "Dynamic soil-pile-foundation-structure interaction: records and predictions." *Géotechnique*, 33-50.

Manna, B., and Baidya, D. K. (2010). "Dynamic nonlinear response of pile foundations under vertical vibration—Theory versus experiment." *Soil Dyn Earthq Eng*, 30(6), 456-469.

Mason, H. B., Trombetta, N. W., Chen, Z., Bray, J. D., Hutchinson, T. C., and Kutter, B. L. (2013). "Seismic soil–foundation–structure interaction observed in geotechnical centrifuge experiments." *Soil Dyn Earthq Eng*, 48(0), 162-174.

Massarsch, K. R. (1979). "Lateral Earth Pressure in Normally Consolidated Clay." *7th European Conference on Soil Mechanics and Foundation Engineering*Brighton, 245-249.

Matlock, H. (1970). "Correlations for design of laterally-loaded piles in soft clay." *Second Annual Offshore Technology Conference* OTC, Houston, TX, 577-594.

Matlock, H., Ingram, W. B., Kelley, A. E., and Bogard, D. (1980). "Field tests of the lateral-load behavior of pile groups in soft clay." *12th Annual Offshore Technical Conference*, OTC, Houston, TX, 163–174.

McVay, M., Casper, R., and Shang, T. (1995). "Lateral Response of Three-Row Groups in Loose to Dense Sands at 3D and 5D Pile Spacing." *Journal of Geotechnical Engineering*, 121(5), 436-441.

McVay, M., Zhang, L., Molnit, T., and Lai, P. (1998). "Centrifuge Testing of Large Laterally Loaded Pile Groups in Sands." *Journal of Geotechnical and Geoenvironmental Engineering*, 124(10), 1016-1026.

Meimon, Y., Baguelin, F., and Jezequel, J. F. (1986). "Pile group behavior under long term lateral monotonic and cyclic loading." *3rd International Conference on*

Numerical Methods in Offshore Piling, Inst. Francais Du Petrole, Nantes, France, 286-302.

Meymand, P. (1998). "Shaking Table Scale Model Tests of Nonlinear Soil-Pile-Superstructure Interaction in Soft Clay." Ph.D. Dissertation, University of California, Berkeley.

Meymand, P. J., Riemer, M. F., and Seed, R. B. (2000). "Large scale shaking table tests of seismic soil-pile interaction in soft clay." *12th World Conference on Earthquake Engineering*, Upper Hutt, N.Z. : New Zealand Society for Earthquake Engineering, Auckland, New Zealand, Paper 0915.

Michalowski, R. L. (2005). "Coefficient of Earth Pressure at Rest." *Journal of Geotechnical and Geoenvironmental Engineering*, 131(11), 1429-1433.

Millán, M. A., and Domínguez, J. (2009). "Simplified BEM/FEM model for dynamic analysis of structures on piles and pile groups in viscoelastic and poroelastic soils." *Engineering Analysis with Boundary Elements*, 33(1), 25-34.

Ministero delle Infrastrutture (2008). *Nuove Norme Tecniche per le Costruzioni. DM 14.01.08.*, Gazzetta Ufficiale della Repubblica Italiana.

Mitchell, J. K. (2008). "Mitigation of Liquefaction Potential of Silty Sands." *From Research to Practice in Geotechnical Engineering*, 433-451.

Mitchell, R. J. (1991). "Centrifuge modelling as a consulting tool." *Canadian Geotechnical Journal*, 28(1), 162-167.

Mokwa, R., and Duncan, J. (2005). "Discussion of “Centrifuge Model Study of Laterally Loaded Pile Groups in Clay” by T. Ilyas, C. F. Leung, Y. K. Chow,

and S. S. Budi." *Journal of Geotechnical and Geoenvironmental Engineering*, 131(10), 1305-1308.

Morrison, C., and Reese, L. C. (1988). "Lateral-Load Test of a Full-Scale Pile Group in Sand." FHWA, Washington, D.C.

Muraleetharan, K., Ravichandran, N., and Taylor, L. M. (2003). *TeraDysac: TeraScale dynamic soil analysis code*, School of Civil Engineering and Environmental Science, University of Oklahoma, Norman, Oklahoma.

Muraleetharan, K. K., Deshpande, S., and Adalier, K. (2004). "Dynamic deformations in sand embankments: centrifuge modeling and blind, fully coupled analyses." *Canadian Geotechnical Journal*, 41(1), 48-69.

Muraleetharan, K. K., Mish, K. D., and Arulanandan, K. (1994). "A fully coupled non-linear dynamic analysis procedure and its verification using centrifuge test results." *Int J Numer Anal Met*, 18(5), 305-325.

Mylonakis, G. (2001). "Simplified model for seismic pile bending at soil layer interfaces." *Soils and Foundations*, 41(4), 47-58.

Mylonakis, G., Nikolaou, A., and Gazetas, G. (1997). "Soil–Pile–Bridge Seismic Interaction: Kinematic and Inertial Effects. Part I: Soft Soil." *Earthquake Engineering & Structural Dynamics*, 26(3), 337-359.

Nakagawa, T., Tanaka, M., Fujimori, T., Hatori, T., and Yahata, K. (2000). "Experimental study on the soil–pile–structure interaction by shaking table tests using large-scale laminar box." *Proceedings of the 12th world congress on earthquake engineering*Auckland, New Zealand.

Nikolaou, S., Mylonakis, G., Gazetas, G., and Tazoh, T. (2001). "Kinematic pile bending during earthquakes: analysis and field measurements." *Géotechnique*, 425-440.

Novak, M. (1991). "Piles under dynamic loads." *Second International Conference on Recent Advances in Geotechnical Earthquake Engineering and Soil Dynamics*St. Louis, Missouri.

Novak, M., and Grigg, R. F. (1976). "Dynamic experiments with small pile foundations." *Canadian Geotechnical Journal*, 13(4), 372-385.

Ohtsuka, T., Aramaki, G., and Koga, K. (2004). "Soil improvement of soft ground around pile foundation in earthquake-resistant design." *Lowland Technology International Journal*, 6(1), 42-54.

Ooi, P., and Duncan, J. (1994). "Lateral Load Analysis of Groups of Piles and Drilled Shafts." *Journal of Geotechnical Engineering*, 120(6), 1034-1050.

Padrón, L. A., Aznárez, J. J., and Maeso, O. (2008). "Dynamic analysis of piled foundations in stratified soils by a BEM–FEM model." *Soil Dyn Earthq Eng*, 28(5), 333-346.

Pender, M. J. (1993). "Aseismic pile foundation design analysis." *Bulletin of the New Zealand National Society for Earthquake Engineering*, 26(1), 49-160.

Porbaha, A. (2006). "Recent Advances in Deep Mixing Research and Development in the USA." *Ground Modification and Seismic Mitigation*, ASCE, Shanghai, China, 45-50.

Poulos, H. (1971). "Behavior of Laterally Loaded Piles: II-Pile Groups." *Journal of the Soil Mechanics and Foundations Division*, 97(5), 733-751.

Prakash, S. (1962). "Behavior of Pile groups subjected to lateral loads." PhD thesis, University of Illinois, Urbana, IL.

Puppala, A. J., Madhyannapu, R. S., Nazarian, S., Yuan, D., and Hoyos, L. (2008). "Deep Soil Mixing Technology for Mitigation of Pavement Roughness." *Rep. No. FHWA/TX-08/0-5179-1*.

Rao, S., Ramakrishna, V., and Rao, M. (1998). "Influence of Rigidity on Laterally Loaded Pile Groups in Marine Clay." *Journal of Geotechnical and Geoenvironmental Engineering*, 124(6), 542-549.

Ravichandran, N. (2005). "A framework-based finite element approach for solving large deformation problems in multi-phase porous media." Ph.D., University of Oklahoma, Norman, Oklahoma.

Reese, L. C., Cox, W. R., and Koop, F. D. (1974). "Analysis of laterally loaded piles in sand." *Fifth Annual Offshore Technology Conference* OTC Houston, TX.

Reese, L. C., Cox, W. R., and Koop, F. D. (1975). "Field testing and analysis of laterally loaded piles in stiff clay." *Seventh Offshore Technology Conference* OTC, Houston, TX.

Reese, L. C., and van Impe, W. F. (2011). *Single piles and pile groups under lateral loading*, CRC Press/Balkema, London, UK.

Reese, L. C., Wang, S. T., Arrellaga, J. A., Hendrix, J., and Vasquez, L. (2010). "Computer program GROUP V. 8.0 – A program for the analysis of a group of piles subjected to axial and lateral loading." Ensoft Inc., Austin, Texas.

Reese, L. C., Wang, S. T., Isenhower, W. M., and Arrellaga, J. A. (2004). "LPILE Plus 5.0 for Windows, technical and user manuals." Ensoft Inc., Austin, TX.

Remaud, D., Garnier, J., and Frank, R. (1998). "Laterally loaded piles in dense sand: Group effects." *International Conference Centrifuge 98*, T. Kimura, O. Kusakabe, and J. Takemura, eds., Balkema, Rotterdam, Tokyo, Japan, 533–538.

Rollins, K., and Brown, D. (2011). "Design Guidelines for Increasing the Lateral Resistance of Highway-Bridge Pile Foundations by Improving Weak Soils." *Rep. No. NCHRP 697*.

Rollins, K., Olsen, K., Jensen, D., Garrett, B., Olsen, R., and Egbert, J. (2006). "Pile Spacing Effects on Lateral Pile Group Behavior: Analysis." *Journal of Geotechnical and Geoenvironmental Engineering*, 132(10), 1272-1283.

Rollins, K., Olsen, R., Egbert, J., Jensen, D., Olsen, K., and Garrett, B. (2006). "Pile Spacing Effects on Lateral Pile Group Behavior: Load Tests." *Journal of Geotechnical and Geoenvironmental Engineering*, 132(10), 1262-1271.

Rollins, K., Peterson, K., and Weaver, T. (1998). "Lateral Load Behavior of Full-Scale Pile Group in Clay." *Journal of Geotechnical and Geoenvironmental Engineering*, 124(6), 468-478.

Rollins, K., Snyder, J., and Walsh, J. (2010). "Increased Lateral Resistance of Pile Group in Clay Using Compacted Fill." *GeoFlorida 2010*, 1602-1611.

Rollins, K., and Sparks, A. (2002). "Lateral Resistance of Full-Scale Pile Cap with Gravel Backfill." *Journal of Geotechnical and Geoenvironmental Engineering*, 128(9), 711-723.

Ruesta, P., and Townsend, F. (1997). "Evaluation of Laterally Loaded Pile Group at Roosevelt Bridge." *Journal of Geotechnical and Geoenvironmental Engineering*, 123(12), 1153-1161.

Sadek, M., and Isam, S. (2004). "Three-dimensional finite element analysis of the seismic behavior of inclined micropiles." *Soil Dyn Earthq Eng*, 24(6), 473-485.

Saitoh, M. (2005). "Fixed-Head Pile Bending by Kinematic Interaction and Criteria for Its Minimization at Optimal Pile Radius." *Journal of Geotechnical and Geoenvironmental Engineering*, 131(10), 1243-1251.

Schofield, A. N. (1981). "Dynamic and Earthquake Geotechnical Centrifuge Modelling." *International Conference on Recent Advances in Geotechnical Earthquake Engineering and Soil Dynamics*, Missouri University of Science and Technology, Rolla, MO, 1081–1100.

Sen, R., Davies, T. G., and Banerjee, P. K. (1985). "Dynamic analysis of piles and pile groups embedded in homogeneous soils." *Earthquake Engineering & Structural Dynamics*, 13(1), 53-65.

Sharp, M., Dobry, R., and Abdoun, T. (2003). "Liquefaction Centrifuge Modeling of Sands of Different Permeability." *Journal of Geotechnical and Geoenvironmental Engineering*, 129(12), 1083-1091.

Sharp, M., Dobry, R., and Phillips, R. (2010). "CPT-Based Evaluation of Liquefaction and Lateral Spreading in Centrifuge." *Journal of Geotechnical and Geoenvironmental Engineering*, 136(10), 1334-1346.

Shibazaki, M. (2003). "State of Practice of Jet Grouting." *Grouting and Ground Treatment*, 198-217.

Stewart, J., Seed, R., and Fenves, G. (1999). "Seismic Soil-Structure Interaction in Buildings. II: Empirical Findings." *Journal of Geotechnical and Geoenvironmental Engineering*, 125(1), 38-48.

Taboada-Urtuzuástegui, V., and Dobry, R. (1998). "Centrifuge Modeling of Earthquake-Induced Lateral Spreading in Sand." *Journal of Geotechnical and Geoenvironmental Engineering*, 124(12), 1195-1206.

Taghavi, A., Miller, G., and Muraleetharan, K. (2010). "NEES-pilEs Full-Scale Field Testing in Miami, Oklahoma: Geotechnical Site Investigation Report, Technical Report,." School of Civil Engineering and Environmental Science, University of Oklahoma, Norman, Oklahoma.

Taghavi, A., and Muraleetharan, K. (2012). "Seismic Response of CDSM Improved Soft Clay Sites Supporting Single Piles." *State of the Art and Practice in Geotechnical Engineering (GSP 225)*, 1839-1848.

Taghavi, A., and Muraleetharan, K. (2014). "Simulating Centrifuge Model Tests of Laterally Loaded Pile Groups in CDSM-Improved Soft Clay Using a Nonlinear Winkler Model." *Geo-Characterization and Modeling for Sustainability (GSP 234)*, 1254-1263.

Taghavi, A., and Muraleetharan, K. (2015c). "Analysis of laterally loaded pile groups in improved soft clay." *International Journal of Geomechanics, In review*.

Taghavi, A., Muraleetharan, K., Miller, G., and Cerato, A. (2015a). "Seismic Soil-Pile-Structure Interaction in Improved Soft Clay: Centrifuge Tests." *IFCEE 2015*, ASCE, San Antonio, TX, 1254-1263.

Taghavi, A., Muraleetharan, K. K., and Miller, G. A. (2015d). "Nonlinear Seismic Behavior of Pile Groups in Cement-Improved Soft Clay." *Soil Dynamics and Earthquake Engineering, In preperation*.

Taghavi, A., Muraleetharan, K. K., Miller, G. A., and Cerato, A. B. (2015b). "Centrifuge Modeling of Laterally Loaded Pile Groups in Improved Soft Clay." *Journal of Geotechnical and Geoenvironmental Engineering, In press*, DOI: 10.1061/(ASCE)GT.1943-5606.

Tajimi, H. (1969). "Dynamic Analysis of a Structure Embedded in an Elastic Stratum." *4th World Conferance on Earthquake Engineering*Tokyo, Japan, 53–69.

Tang, L., and Ling, X. (2014). "Response of a RC pile group in liquefiable soil: A shake-table investigation." *Soil Dyn Earthq Eng*, 67(0), 301-315.

Tasiopoulou, P., Gerolymos, N., Tazoh, T., and Gazetas, G. (2013). "Pile-Group Response to Large Soil Displacements and Liquefaction: Centrifuge Experiments versus a Physically Simplified Analysis." *Journal of Geotechnical and Geoenvironmental Engineering*, 139(2), 223-233.

Tazoh, T., Sato, M., Jang, V., Taji, Y., Gazetas, G., and Anastasopoulos, I. (2009). "Kinematic Response of Batter Pile Foundation: Centrifuge Tests." *Proc., 3rd Greece-Japan Workshop "Seismic Design, Observation, and Retrofit of Foundations"*, Y. G. G. Gazetas, and T. Tazoh, ed., 20–35.

Thavaraj, T., Liam Finn, W. D., and Wu, G. (2010). "Seismic Response Analysis of Pile Foundations." *Geotechnical and Geological Engineering*, 28(3), 275-286.

Thompson, Z. M. (2011). "Stress-strain behavior of unimproved and cement-improved soft clays."M.Sc. Thesis, University of Oklahoma, Norman, Oklahoma.

Tokimatsu, k., Mizuno, H., and Kakurai, M. (1996). "Building damage associated with geotechnical problems." *Soils and Foundations*(Special), 219-234.

Tokimatsu, K., Suzuki, H., and Sato, M. (2004). "Effects of inertial and kinematic forces on pile stresses in large shaking table tests." *13th World Conference on Earthquake Engineering*Vancouver, B.C., Canada, Paper No. 1322.

Tokimatsu, K., Tamura, S., Suzuki, H., and Katsumata, K. (2012). "Building damage associated with geotechnical problems in the 2011 Tohoku Pacific Earthquake." *Soils and Foundations*, 52(5), 956-974.

Trifunac, M. D. (1972). "Interaction of a shear wall with the soil for incident plane SH waves." *Bulletin of the Seismological Society of America*, 62(1), 63-83.

US Army (1993). *Design of pile foundations. Technical engineering and design guides No. 1*, US Army Corps of Engineers, Washington, D.C.

Uzuoka, R., Sento, N., Kazama, M., Zhang, F., Yashima, A., and Oka, F. (2007). "Three-dimensional numerical simulation of earthquake damage to group-piles in a liquefied ground." *Soil Dyn Earthq Eng*, 27(5), 395-413.

Van Laak, P. A., Taboada, V. M., Dobry, R., and Elgamal, A.-W. (1994). "Earthquake centrifuge modeling using a laminar box." *Dynamic Geotechnical Testing II (STP 1213)*, ASTM, San Francisco/CA, 370-384.

Wang, S., Kutter, B. L., Chacko, M. J., Wilson, D. W., Boulanger, R. W., and Abghari, A. (1998). "Nonlinear Seismic Soil-Pile Structure Interaction." *Earthq Spectra*, 14(2), 377-396.

Wang, S., and Reese, L. (1993). "COM624P, Laterally Loaded Pile Analysis for the Microcomputer, Version 2.0, Report No. FHWA-SA-91-048." FHWA Office of Technology Applications.

Weaver, T., Ashford, S., and Rollins, K. (2005). "Response of 0.6 m Cast-in-Steel-Shell Pile in Liquefied Soil under Lateral Loading." *Journal of Geotechnical and Geoenvironmental Engineering*, 131(1), 94-102.

Whitman, R. V., and Lambe, P. C. (1986). "Effect of Boundary Conditions Upon Centrifuge Experiments Using Ground Motion Simulation." *Geotechnical Testing Journal*, 9(2), 61-71.

Wilson, D., Boulanger, R., and Kutter, B. (2000). "Observed Seismic Lateral Resistance of Liquefying Sand." *Journal of Geotechnical and Geoenvironmental Engineering*, 126(10), 898-906.

Wilson, D. W. (1998). "Soil-Pile-Superstructure Interaction in Liquefying Sand and Soft Clay." Ph.D. Dissertation, University of California at Davis.

Wolf, J. P. (1985). *Dynamic soil–structure interaction*, Prentice-Hall, Inc., Upper Saddle River, NJ.

Wroth, C. P. (1984). "The interpretation of in situ soil tests." *Géotechnique*, 34(4), 449-489.

Wu, G., and Finn, W. D. L. (1997). "Dynamic nonlinear analysis of pile foundations using finite element method in the time domain." *Canadian Geotechnical Journal*, 34(1), 44-52.

Yamashita, K., Hamada, J., Onimaru, S., and Higashino, M. (2012). "Seismic behavior of piled raft with ground improvement supporting a base-isolated building on soft ground in Tokyo." *Soils and Foundations*, 52(5), 1000-1015.

Yasuda, S., Ishihara, K., Morimoto, I., Orense, R., Ikeda, M., and S., T. (2000). "Large-scale shaking table tests on pile foundations in liquefied ground." *Proceedings*

of the 12th world congress on earthquake engineering, New Zealand Society for Earthquake Engineering, Auckland, New Zealand.

Yoshida, H. (2012). "Recent Developments in Jet Grouting." *Grouting and Deep Mixing 2012*, 1548-1561.

Zeng, X., and Schofield, A. N. (1996). "Design and performance of an equivalent-shear-beam container for earthquake centrifuge modelling." *Géotechnique*, 83-102.

Zhang, C., White, D., and Randolph, M. (2011). "Centrifuge Modeling of the Cyclic Lateral Response of a Rigid Pile in Soft Clay." *Journal of Geotechnical and Geoenvironmental Engineering*, 137(7), 717-729.

Zhang, L., McVay, M., and Lai, P. (1999). "Numerical Analysis of Laterally Loaded 3 × 3 to 7 × 3 Pile Groups in Sands." *Journal of Geotechnical and Geoenvironmental Engineering*, 125(11), 936-946.

Zhang, Y., Conte, J. P., Yang, Z., Elgamal, A., Bielak, J., and Acero, G. (2008). "Two-Dimensional Nonlinear Earthquake Response Analysis of a Bridge-Foundation-Ground System." *Earthq Spectra*, 24(2), 343-386.

Appendix A: Detailed Instrumentation Layout

The detailed instrumentation layout of the second series of centrifuge tests is presented in Figure A.1. The type and coordinates of the instruments are provided in Table A.1.

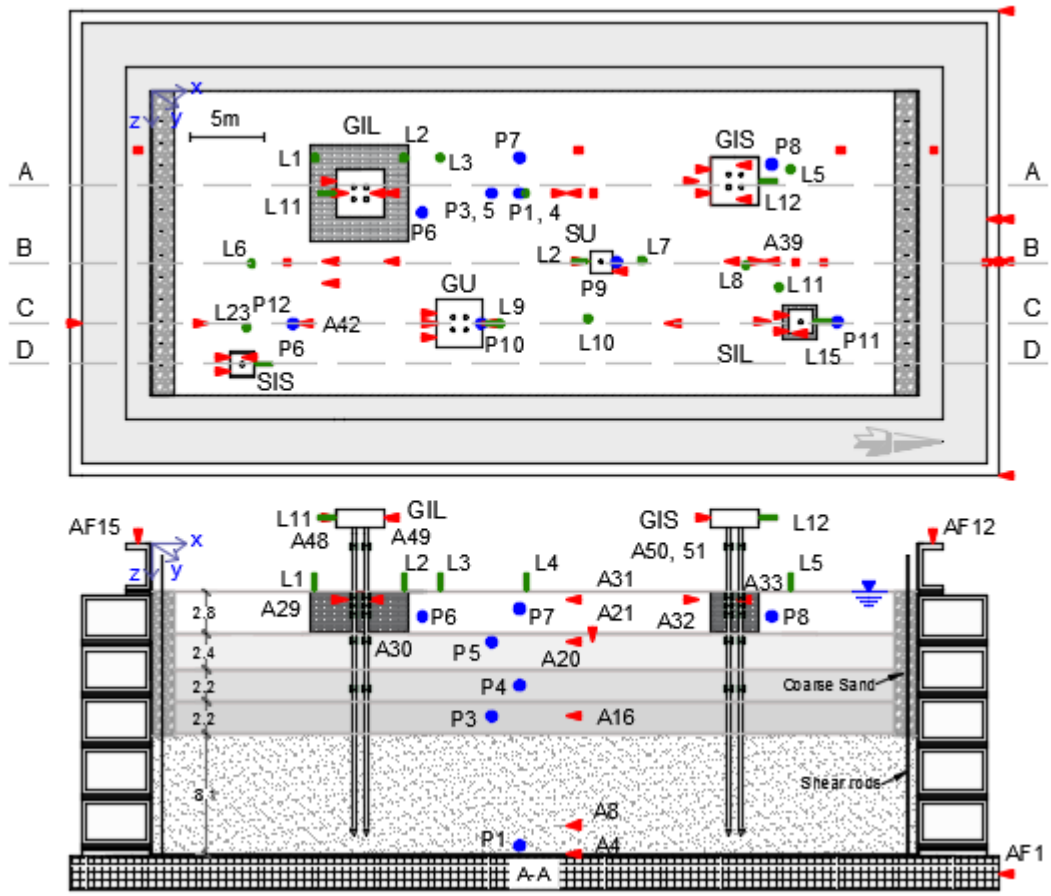

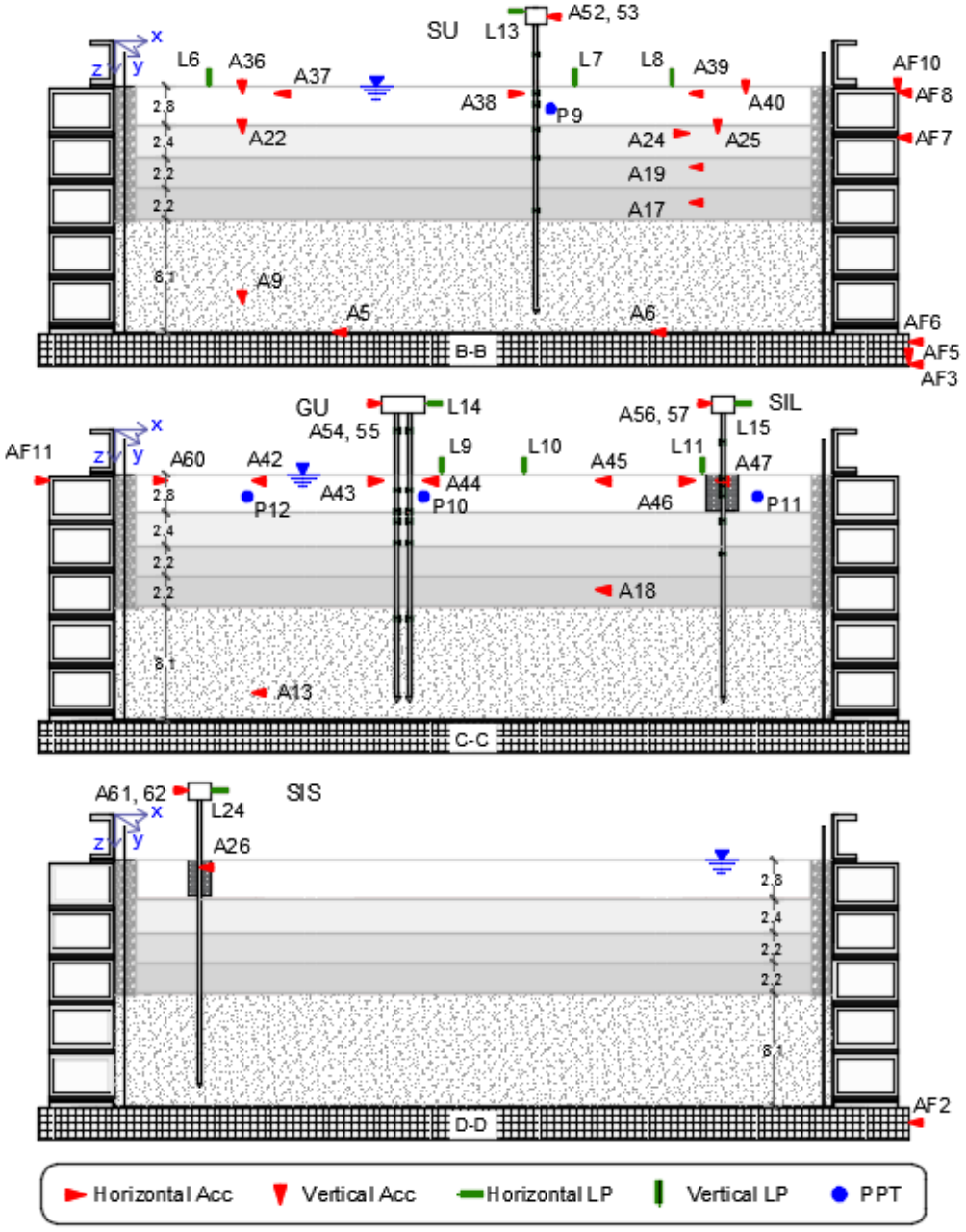

Figure A-1. Detailed Cross Sections and Plan View of the Centrifuge Model Set-Up for Single Piles and 2×2 Pile Groups with 3D Spacing (All Dimensions are in m)

Table A-1. Coordinates of the Instruments

Instrument	Type	Position			Units
		x	y	z	
AF1	ICP Accelerometer	1896.7	-182.8	736.94	mm
AF2	ICP Accelerometer	1896.7	860.2	736.94	mm
AF3	ICP Accelerometer	1896.7	380.7	769.31	mm
A4	ICP Accelerometer	928.65	226.71	697	mm
A5	ICP Accelerometer	519.89	380.7	697	mm
A6	ICP Accelerometer	1283.45	380.7	697	mm
A61	ICP Accelerometer	1768.9	583.51	-56.24	mm
A8	ICP Accelerometer	928.65	226.71	626.7	mm
A9	ICP Accelerometer	304.3	380.7	626.7	mm
AF4	ICP Accelerometer	1896.7	380.7	769.31	mm
A13	ICP Accelerometer	328.71	518.46	626.7	mm
A16	ICP Accelerometer	928.65	226.71	384.2	mm
A17	ICP Accelerometer	1371.1	380.7	384.2	mm
A18	ICP Accelerometer	1150.05	518.46	384.2	mm
A19	ICP Accelerometer	1371.1	380.7	301.2	mm
A20	ICP Accelerometer	928.65	226.71	218.2	mm
A21	ICP Accelerometer	988.65	226.71	218.2	mm
A22	ICP Accelerometer	304.3	380.7	218.2	mm
A24	ICP Accelerometer	1371.1	380.7	218.2	mm
A25	ICP Accelerometer	1441.1	380.7	218.2	mm
A26	ICP Accelerometer	202.43	593.43	218.2	mm
AF5	ICP Accelerometer	1896.7	380.7	769.31	mm
AF6	ICP Accelerometer	1896.7	284.73	715.14	mm
A29	ICP Accelerometer	466.71	226.71	123.7	mm
A30	ICP Accelerometer	466.71	226.71	123.7	mm
A31	ICP Accelerometer	928.65	226.71	123.7	mm
A32	ICP Accelerometer	1223.81	199.26	123.7	mm
A33	ICP Accelerometer	1306.2	199.26	123.7	mm
A34	ICP Accelerometer	1306.2	199.26	123.7	mm
AF7	ICP Accelerometer	1870.2	284.73	230.33	mm
A36	ICP Accelerometer	304.3	380.7	123.7	mm
A37	ICP Accelerometer	384.3	427.4	123.7	mm
A38	ICP Accelerometer	976.94	380.7	123.7	mm
A39	ICP Accelerometer	1371.1	380.7	123.7	mm
A40	ICP Accelerometer	1505.4	380.7	123.7	mm
AF8	ICP Accelerometer	1870.2	380.7	122.91	mm
A42	ICP Accelerometer	328.71	518.46	123.7	mm
A43	ICP Accelerometer	640.09	518.46	123.76	mm

A44	ICP Accelerometer	737.99	518.46	123.76	mm
A45	ICP Accelerometer	1150.05	518.46	123.7	mm
A46	ICP Accelerometer	1384.41	514.51	123.7	mm
A47	ICP Accelerometer	1433.74	514.51	123.7	mm
AF9	ICP Accelerometer	1870.2	380.7	122.91	mm
A49	ICP Accelerometer	414.21	226.71	-56.24	mm
AF10	ICP Accelerometer	1870.2	380.7	122.91	mm
A51	ICP Accelerometer	1358.7	199.26	-56.3	mm
A52	ICP Accelerometer	980.7	380.7	-56.3	mm
A53	ICP Accelerometer	980.7	380.7	-56.3	mm
AF11	ICP Accelerometer	1870.2	284.73	122.91	mm
A55	ICP Accelerometer	636.7	532.49	-56.24	mm
A56	ICP Accelerometer	1478.51	514.51	-56.3	mm
A57	ICP Accelerometer	1478.51	514.51	-56.3	mm
AF12	ICP Accelerometer	1749.75	131.41	0	mm
AF13	ICP Accelerometer	1543.16	131.41	-55	mm
A60	ICP Accelerometer	127	614.4	124	mm
A61	ICP Accelerometer	1012.4	353.4	124	mm
AF14	ICP Accelerometer	955.82	131.41	-55	mm
AF15	ICP Accelerometer	-29.85	131.41	0	mm
A62	ICP Accelerometer	176.89	626.75	-56.24	mm
L13	Linear Potentiometer	980.65	380.7	-56.3	mm
L9	Linear Potentiometer	780	512.4	-93.7	mm
L2	Linear Potentiometer	565	147	-93.7	mm
L11	Linear Potentiometer	414.21	226.71	-56.3	mm
L3	Linear Potentiometer	620	143	-93.7	mm
L4	Linear Potentiometer	837	236	-93.7	mm
L6	Linear Potentiometer	226	384	-93.7	mm
L5	Linear Potentiometer	1430	200	-93.7	mm
L7	Linear Potentiometer	1098	377.4	-93.7	mm
L8	Linear Potentiometer	388	1280	-93.7	mm
L12	Linear Potentiometer	1358.7	199.26	-56.3	mm
L15	Linear Potentiometer	1481.81	162.83	-56.3	mm
L10	Linear Potentiometer	977	507.4	-93.7	mm
L14	Linear Potentiometer	741.7	518.4	-56.3	mm
L24	Linear Potentiometer	228.89	71.19	-56.3	mm
L1	Linear Potentiometer	383	137	-93.7	mm
TSS01-Ch0	Strain Gage	452.43	212.43	3.64	mm
TSS01-Ch1	Strain Gage	452.43	212.43	116.64	mm
TSS01-Ch2	Strain Gage	452.43	212.43	136.64	mm
TSS01-Ch3	Strain Gage	452.43	212.43	156.64	mm

TSS01-Ch4	Strain Gage	452.43	212.43	216.64	mm
TSS01-Ch5	Strain Gage	452.43	212.43	323.64	mm
TSS01-Ch6	Strain Gage	481	212.43	3.64	mm
TSS01-Ch7	Strain Gage	481	212.43	116.64	mm
TSS02-Ch0	Strain Gage	481	212.43	136.64	mm
TSS02-Ch1	Strain Gage	481	212.43	156.64	mm
TSS02-Ch2	Strain Gage	481	212.43	216.64	mm
TSS02-Ch3	Strain Gage	481	212.43	323.64	mm
TSS02-Ch4	Strain Gage	452.43	241	3.64	mm
TSS02-Ch5	Strain Gage	452.43	241	116.64	mm
TSS02-Ch6	Strain Gage	452.43	241	136.64	mm
TSS02-Ch7	Strain Gage	452.43	241	156.64	mm
TSS03-Ch0	Strain Gage	452.43	241	216.64	mm
TSS03-Ch1	Strain Gage	452.43	241	323.64	mm
TSS03-Ch2	Strain Gage	481	241	3.64	mm
TSS03-Ch3	Strain Gage	481	241	116.64	mm
TSS03-Ch4	Strain Gage	481	241	136.64	mm
TSS03-Ch5	Strain Gage	481	241	156.64	mm
TSS03-Ch6	Strain Gage	481	241	216.64	mm
TSS03-Ch7	Strain Gage	481	241	323.64	mm
TSS10-Ch4	Strain Gage	1452.51	514.51	217.7	mm
TSS10-Ch5	Strain Gage	1452.51	514.51	297.7	mm
TSS10-Ch6	Strain Gage	1001.94	380.7	30.7	mm
TSS10-Ch7	Strain Gage	1001.94	380.7	123.7	mm
TSS11-Ch0	Strain Gage	1001.94	380.7	150.7	mm
TSS11-Ch1	Strain Gage	1001.94	380.7	210.7	mm
TSS11-Ch2	Strain Gage	1001.94	380.7	277.7	mm
TSS11-Ch3	Strain Gage	1001.94	380.7	403.7	mm
P9	Pore Pressure Transducer	1041.53	380.7	143.7	mm
P10	Pore Pressure Transducer	687	560.4	143.7	mm
P11	Pore Pressure Transducer	1535.34	514.34	143.7	mm
TSS07-Ch1	Strain Gage	674.91	503.91	145.64	mm
TSS07-Ch2	Strain Gage	674.91	503.91	195.64	mm
TSS07-Ch3	Strain Gage	674.91	503.91	220.64	mm
TSS07-Ch4	Strain Gage	674.91	503.91	270.64	mm
TSS07-Ch5	Strain Gage	674.91	503.91	450.64	mm
TSS07-Ch6	Strain Gage	703.49	503.91	3.64	mm
TSS07-Ch7	Strain Gage	703.49	503.91	145.64	mm
TSS08-Ch0	Strain Gage	703.49	503.91	195.64	mm
TSS08-Ch1	Strain Gage	703.49	503.91	220.64	mm
TSS08-Ch2	Strain Gage	703.49	503.91	270.64	mm

TSS08-Ch3	Strain Gage	703.49	532.49	450.64	mm
TSS08-Ch4	Strain Gage	674.91	532.49	3.64	mm
TSS08-Ch6	Strain Gage	674.91	532.49	195.64	mm
TSS08-Ch7	Strain Gage	674.91	532.49	220.64	mm
TSS09-Ch0	Strain Gage	674.91	532.49	270.64	mm
TSS09-Ch1	Strain Gage	674.91	532.49	450.64	mm
TSS09-Ch2	Strain Gage	703.49	532.49	3.64	mm
TSS09-Ch3	Strain Gage	703.49	532.49	145.64	mm
TSS09-Ch4	Strain Gage	703.49	532.49	195.64	mm
TSS09-Ch5	Strain Gage	703.49	532.49	220.64	mm
TSS09-Ch6	Strain Gage	703.49	532.49	270.64	mm
TSS09-Ch7	Strain Gage	703.49	532.49	450.64	mm
TSS10-Ch0	Strain Gage	1452.51	514.51	30.7	mm
TSS10-Ch1	Strain Gage	1452.51	514.51	117.7	mm
TSS10-Ch2	Strain Gage	1452.51	514.51	137.7	mm
TSS10-Ch3	Strain Gage	1452.51	514.51	157.7	mm
P1	Pore Pressure Transducer	824.02	226.65	673.7	mm
A48	MEMS Accelerometer	414.21	212.43	-56.24	mm
A50	MEMS Accelerometer	1358.59	199.08	-56.24	mm
P4	Pore Pressure Transducer	824.02	226.65	301.2	mm
A54	MEMS Accelerometer	636.7	503.91	-56.24	mm
P6	Pore Pressure Transducer	606.21	270	143.7	mm
P7	Pore Pressure Transducer	823.98	147	143.7	mm
P8	Pore Pressure Transducer	1388.65	161.94	143.7	mm
TSS04-Ch0	Strain Gage	1291.91	184.91	3.64	mm
TSS04-Ch1	Strain Gage	1291.91	184.91	116.64	mm
TSS04-Ch2	Strain Gage	1291.91	184.91	136.64	mm
TSS04-Ch3	Strain Gage	1291.91	184.91	156.64	mm
TSS04-Ch4	Strain Gage	1291.91	184.91	216.64	mm
TSS04-Ch5	Strain Gage	1291.91	184.91	323.64	mm
TSS04-Ch6	Strain Gage	1320.49	184.91	3.64	mm
TSS04-Ch7	Strain Gage	1320.49	184.91	116.64	mm
TSS05-Ch0	Strain Gage	1320.49	184.91	136.64	mm
TSS05-Ch1	Strain Gage	1320.49	184.91	156.64	mm
TSS05-Ch2	Strain Gage	1320.49	184.91	216.64	mm
TSS05-Ch3	Strain Gage	1320.49	184.91	323.64	mm
TSS05-Ch4	Strain Gage	1291.91	213.49	3.64	mm
TSS05-Ch5	Strain Gage	1291.91	213.49	116.64	mm
TSS05-Ch6	Strain Gage	1291.91	213.49	136.64	mm
TSS05-Ch7	Strain Gage	1291.91	213.49	156.64	mm
TSS06-Ch0	Strain Gage	1291.91	213.49	216.64	mm

TSS06-Ch1	Strain Gage	1291.91	213.49	323.64	mm
TSS06-Ch2	Strain Gage	1320.49	213.49	3.64	mm
TSS06-Ch3	Strain Gage	1320.49	213.49	116.64	mm
TSS06-Ch4	Strain Gage	1320.49	213.49	136.64	mm
TSS06-Ch5	Strain Gage	1320.49	213.49	156.64	mm
TSS06-Ch6	Strain Gage	1320.49	213.49	216.64	mm
TSS06-Ch7	Strain Gage	1320.49	213.49	323.64	mm